論文 / 著書情報
Article / Book Information

題目(和文)	
Title(English)	Efficient Fabrication Process of a Metallic Nano Dot Array on a Plastic Substrate by the Nano-Plastic Forming Assisted Thermal Dewetting Method
著者(和文)	TRUONGDUCPHUC
Author(English)	Truong Duc Phuc
出典(和文)	学位:博士(学術), 学位授与機関:東京工業大学, 報告番号:甲第9568号, 授与年月日:2014年3月26日, 学位の種別:課程博士, 審査員:吉野　雅彦,井上　裕嗣,山本　貴富喜,山崎　敬久,平田　敦
Citation(English)	Degree:Doctor (Academic), Conferring organization: Tokyo Institute of Technology, Report number:甲第9568号, Conferred date:2014/3/26, Degree Type:Course doctor, Examiner:,,,,
学位種別(和文)	博士論文
Type(English)	Doctoral Thesis

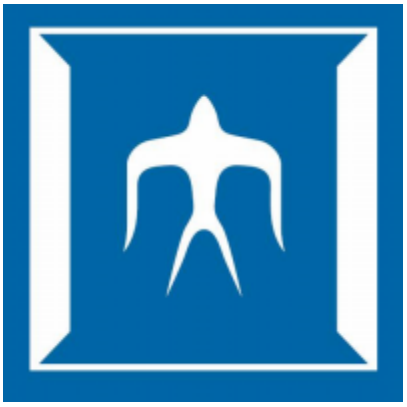

Tokyo Institute of Technology

Graduate School of Science and Engineering

Department of Mechanical and Control Engineering

Efficient Fabrication Process of a Metallic Nano Dot Array on a Plastic Substrate by the Nano-Plastic Forming Assisted Thermal Dewetting Method

by

Truong Duc Phuc

Submitted to the Department of Mechanical and Control Engineering

In Partial Fulfillment of the Requirements for the Degree of

Doctor of Philosophy in Mechanical and Control Engineering

at the

Tokyo Institute of Technology

Supervisor: Prof. Masahiko Yoshino

Advisor: Assoc. Prof. Takatoki Yamamoto

December 2013

Abstract

In this thesis, firstly, technical and social backgrounds of nano dot arrays are studied, and requirements to efficient fabrication processes of nano dot arrays are discussed. Then, a new fabrication process of a metallic nano dot array is proposed. The process consists of three steps, i.e. sputter coating of a metal film on a substrate, thermal dewetting, and the dot transferring to a plastic film. The process for fabrication of a random metallic nano dot array on a plastic film by thermal dewetting on a flat substrate and dot transfer technique is first proposed. The feasibility of the proposed process is demonstrated through the experiments. In addition, the effects of process condition on the morphology and optical property of nano dot arrays and on the nano dot transfer ratio will be studied. Then, the proposed process is extended to fabrication of an ordered metallic nano dot array on a plastic film by nano-plastic forming assisted thermal dewetting on pattened substrate and dot transfer technique. The feasibility of the extended process is investigated. In addition, the effect of process conditions on the morphology of nano dot array aggregated on a patterned substrate by thermal dewetting and transferring of an ordered nano dot array to a plastic film will be studied.

For the first proposed process, the experiment results show that the morphology of random nano dot array strongly depends on the annealing temperature, annealing time, substrate material, and gold film thickness: Mean diameter and corresponding standard deviation of the nano dots increase with the increase in the gold film thickness, but decrease with the increase in the annealing temperature; the nano dots aggregated on a quartz glass substrate are large and sparse, while the nano dots aggregated on a silicon substrate are small and dense; the contact angle of the nano dots both on a quartz glass substrate and a silicon substrate increases with the increase in the annealing temperature; the circularity of nano dots increases with the increase in the annealing time, but becomes saturated to a certain value that depends on the annealing temperature. In addition, it is found that the localized surface plasmon resonance (LSPR) property of a nano dot array strongly depends on the morphology of the nano dot array, especially the circularity of the nano dot array. It is also found that the transfer ratio is strongly influenced by the substrate materials, the plastic materials, and the annealing temperature: The silicon substrate shows slightly higher transfer ratio than the quartz glass substrate; Araldite rapid epoxy decreases

the transfer ratio while the SpeciFix-20 epoxy increases transfer ratio when the annealing temperature becomes higher.
Furthermore, the nano dot transfer mechanism based on the total free energy theory is established to explain the experimental results.

For the second proposed process, the experimental results show that under proper conditions, patterning on a substrate by nano plastic forming improves the uniformity and regularity of nano dot array through thermal dewetting process. It is found that the uniformity and regularity of nano dot array strongly depends on the gold film thickness, the annealing temperature, and the indentation load. These parameters are studied and optimized in order to obtain an ordered nano dot array of good uniformity and regularity. The ordered nano dot array is then transferred to a plastic film to evaluate the feasibility of the process. The experimental results show that ordered nano dot arrays were successfully fabricated both on Araldite rapid epoxy film and SpeciFix-20 epoxy film by the proposed process. In addition, the re-usability of the patterned substrate is demonstrated for obtaining high throughput.

Acknowledgements

First of all, I would like to express my deepest thankfulness to my academic supervisor, **Prof. Masahiko Yoshino** for all of his continuous helps, instructions, and encouragements throughout my research work at Tokyo Institute of Technology. His uninterrupted helps and guidance not only help me to attain achievements, success in the research work, and lead to this dissertation, but also provide me useful direction to develop my professional in the future. In my achievements throughout my study at Tokyo Institute of Technology, a large part is based on his helps and guidance. He is not only an excellent supervisor for science research but also a friendly professor who introduces and tells me about Japanese culture and society. I owe a debt of gratitude for his helps and guidance forever.

I would like to express my special thanks to **Assoc. Prof. Takatoki Yamamoto, Assoc. Prof. Akinori Yamanaka, and Asst. Prof. Terano Motoki** for all their helps and supports during my research work in Yoshino & Yamamoto laboratory. Their helps and supports are essential useful for my research work.

I would like to thank all the members of Yoshino & Yamamoto laboratory for their kindness and their helps to order experimental materials. Also, I would like to thank them for providing a friendly and enjoyable environment throughout the time I worked with them in Yoshino & Yamamoto laboratory.

I would like to acknowledge **Japan International Cooperation Agency (JICA)** for providing me a scholarship during my research at Tokyo Institute of Technology. Their financial support is very useful for my study in Japan.

Finally, I also would like to express my most sincere gratitude to my parents, my brothers and sisters for all of their love and supports over the years. They always stay behind me to encourage and support me in my life. Their love and emotional support have helped me to have stronger will to overcome the difficulties in the life. Without their love and emotional supports, I don’t know whether I can complete this research work or not.

Table of Contents

List of Figures

List of Tables

List of Abbreviations

NPs	:	Nanoparticles
CNTs	:	Carbon nanotubes
OLEDs	:	Organics light-emitting diodes
NNI	:	National Nanotechnology Initiative
AFM	:	Atomic force microscopy
DC	:	Direct current
DOF	:	Depth of focus
EBL	:	Electron beam lithography
XRL	:	X-ray lithography
FE-SEM	:	Field emission scanning electron microscopy
FIB	:	Focused ion beam
IC	:	Integrated circuit
NA	:	Numerical aperture
NGL	:	Next generation lithography
NIL	:	Nanoimprint lithography
NPF	:	Nano plastic forming
RIE	:	Reactive ion etching
SEM	:	Scanning electron microscopy
SPM	:	Scanning probe microscopy
STM	:	Scanning tunneling microscopy
T-NIL	:	Thermal nanoimprint lithography
UV-NIL	:	Ultraviolet curable nanoimprint lithography
3D	:	Three dimensional
PAC	:	Photoactive compound

LCD	:	Liquid crystal display
DUVL	:	Deep ultraviolet lithography
EUVL	:	Extreme ultraviolet lithography
NSL	:	Nanosphere lithography
PAMD	:	Porous alumina mask deposition
ALD	:	Atomic layer deposition
ITO	:	Indium-tin oxide
SERS	:	Surface enhanced Raman scattering
LSPR	:	Localize surface plasmon resonance
SPR	:	Surface plasmon resonance
HDD	:	Hard disk drive
SRS	:	Synchrotron radiation source
RAE	:	Relative arrangement error

CHAPTER 1

Introduction

In this chapter, firstly, a brief background of nanotechnology including applications, history, future trench, and brief introduction of nanofabrication are presented. Then, the motivation and objectives of this study is presented, respectively.

1.1 Background

Nanotechnology is an advanced technology that has been attracting a lot of attention and interests of the global community over past few decades. Up to now, it has been one of the hottest fields in academy, industry and business. It is a rapidly evolving and potentially transformative technology which has potential to improve many aspects of human life greatly. Nanotechnology is promising to create stronger and lighter materials, novel and safer energy sources, more nutritious, healthy and longer-lasting foods, more efficacious pharmaceuticals, etc. It has capability to address recent environmental problems, energy problems, medical problems and economy problems.

Nanotechnology is art and science of manipulating atoms and molecules to create new systems, new materials, devices which provides many benefits to various aspects of entire spectrum of industry. Tremendous advances in many fields of the human life such as engery, medicine, nano-biotechnology, optical engineering, nanodevices, defense, etc. which are fruits of nanotechnology have been reported. Figure 1.1 shows the applications nanotechnology to some fields which are briefly introduced as follows:

In aerospace, the strength and lightness of carbon nanotubes makes them great materials for the aerospace industry. Carbon composites and nano-coating are used for the bodies of aircraft and in aerospace components instead of aluminum alloy to make the bodies of aircraft stronger and lighter. In addition, these nano-modified composite materials improve the mechanical property; and enhance the resistance to flammability and solvent.

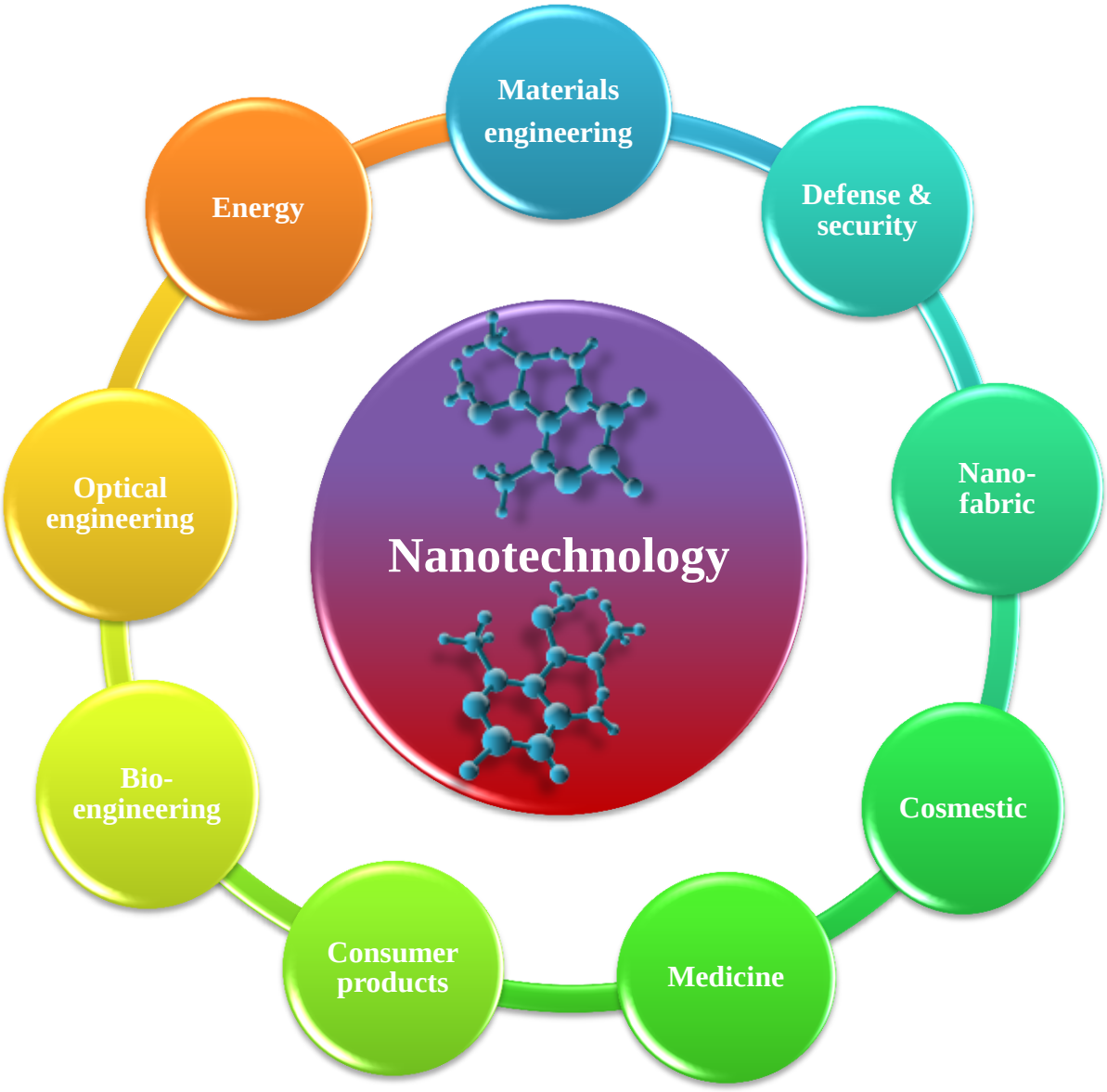

Figure 1. 1 Applications of nanotechnology

In automobile industry, nanostructured surfaces were utilized to improve paint adhesion and color durability. New kinds of car paints developed by nanotechnology are applied to improve the self-cleaning, scratch resistant, dirt repellent and self-healing properties. Nanostructure materials are being utilized to make the chassis and the body of the car stronger and lighter. Thus, reduce the consumption of fuel and enhance the economic efficiency.

In electronics, nanoscale transistors are grown together on a silicon wafer. This obviously reduces the size of the circuit board and provides more functions. The carbon nanotubes (CNT) are used in transistors as conducting channels and have clearly shown

possibility of high speed operation of CNT transistors. Nanomaterials are employed to improve the resolution of CRTs. Organic flexible displays based on organics light-emitting diodes (OLEDs) are available on the markets and provide more advantages such as higher resolution, brighter, and wider viewable angles. The displays are thinner and of lighter weight than traditional liquid crystal display (LCD) displays. This makes them ideally suited to mobile electronics such as digital cameras, cellular phones, etc.

In medicine and pharmacy, some antibacterial cleansers utilize nano-emulsion technology to kill pathogens. These cleansers have ability to kill bacterial and tuberculosis while remaining nontoxic, noncorrosive and nonflammable. Nano-engineered gels and other materials are used in replacement of lost tissue or providing structures for the regeneration of natural tissue. Silver nanoparticles are used in medical bandages for treatment for wounds and burns. They provide antimicrobial barrier protection and help skin to heal by preventing infections during treatment.

In sport goods, special nanoparticles (NPs) and carbon nanotubes (CNTs) are utilized to stiffen areas of the racquet head and shaft. CNTs doped composites have been used in many goods such as hockey stick, tennis and badminton racquets, etc. to make them more durable, stronger and lighter. Tennis ball coated with nano-size membrane slows down the pressure drain and increase the lifetime of ball. The list of applications of nanotechnology is going on. Figure 1.2 shows the applications and products of nanotechnology expected to become commercially in near future.

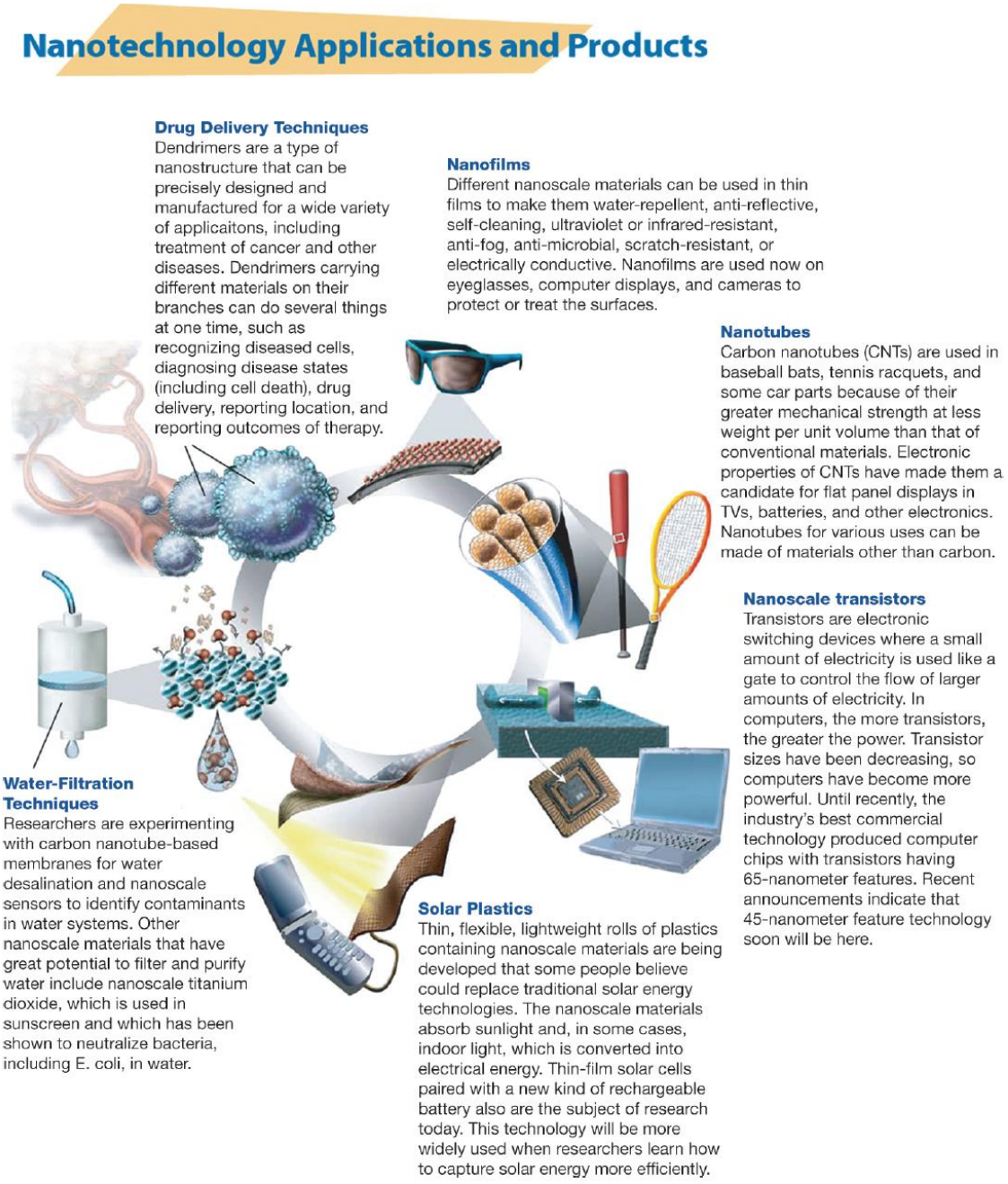

Figure 1. 2 Applications and products of nanotechnology already on market or expected to become commercially in near future

(*Figure copied from Ref. [1]*)

Figure 1.3 shows the timeline of history of nanotechnology. Historically, the term "nanotechnology" has been traced to 1974. It was first introduced by Norio Taniguchi from Tokyo University of Science in his paper entitled "On the Basic Concept of 'Nano-Technology" [2]. In his paper, Taniguchi described nanotechnology as a technology that manipulates the engineering materials at nanometer level. He outlined his prediction of

atom-by-atom or molecule-by-molecule manipulation of matter for the semiconductor industry.

However, the history of nanotechnology was actually initiated earlier. The origins of nanotechnology are traced back to a lecture given by Richard Feynman at an American Physical Society meeting at Caltech on December 29, 1959 entitled "There's Plenty of Room at the Bottom." [3] In this talk, Feynman questioned that: "*Why cannot we write the entire 24 volumes of the Encyclopedia Brittanica on the head of a pin?*" and then he provided the evidences to prove that it is possible to write the entire 24 volumes of the Encyclopaedia Britannica on the head of a pin. As he spoke: "*The principles of physics, as far as I can see, do not speak against the possibility of manoeuvring things atom by atom. It is not an attempt to violate any law; it is something, in principle, that can be done; but in practice, it has not been done because we are too big"*, He explained the principles of miniaturization and making small things at atomic-level precision and how these concepts do not against any known law of physics.

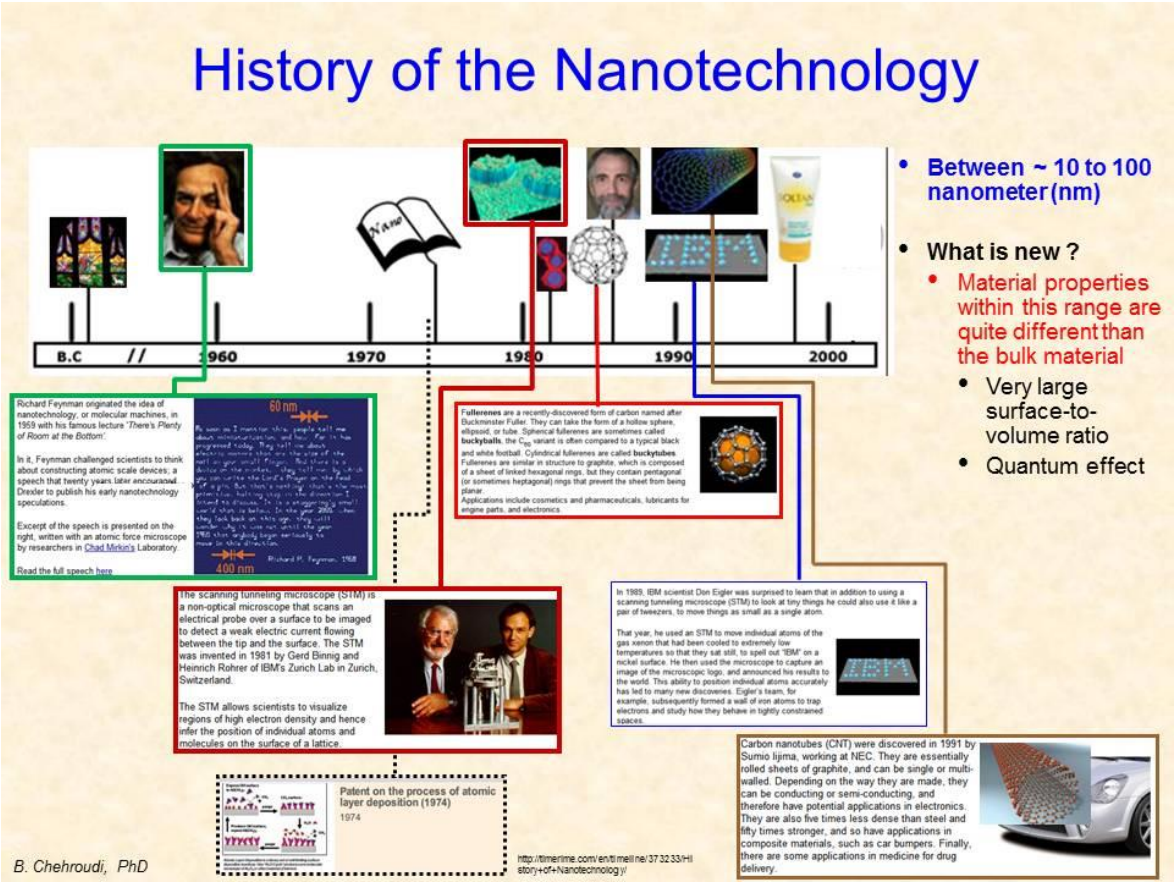

(Source*: http://www.advtechconsultants.com/NanotechnologyHistory.jpg*)

Figure 1. 3 Timeline of history of nanotechnology

In 1987, K. Eric Drexler published a book named "*Engines of Creation:The Coming Era of Nanotechnology*" [4]. He explained new kind of technology based on "*assemblers*" of molecular which enables to "place atoms in almost any reasonable arrangement" and thereby allows people to "build almost anything that the laws of nature allow to exist." That is a fanciful and fantastical idea which marked a distinct jumping off point for the development of nanotechnology.

With the discovery of novel materials on the nanoscale notably began with the buckyball in 1985 by Robert Curl, Harold Kroto and Richard Smalley, and carbon nanotubes in 1991 by Sumio Iijima of NEC, the nanoscale materials have been focusing intensively in both academic community and industry up to date.

In 2000, the National Nanotechnology Initiative (NNI) was founded by the US government in order to manage funding and develop nanotechnology as the major research in the twenty first century. According to the NNI, *"Nanotechnology is the understanding and control of matter at dimensions between approximately 1 and 100 nanometers, where unique phenomena enable novel applications. Encompassing nanoscale science, engineering, and technology, nanotechnology involves imaging, measuring, modeling, and manipulating matter at this length scale."*

The advances of nanotechnology have great improvements on the various aspects of human life and society. There have been more and more nanotechnology products are now available on the market. According to the estimation of National Science Foundation (NSF) of the United States, the world market for nanotechnology products will reach over of 1 trillion US Dollars by 2015 in which $340 billion for materials, $300 billion for electronics and communication, $180 billion for pharmaceuticals, $100 billion in chemical manufacturing, $70 billion for aerospace, $45 billion for sustainable process, $30 for healthcare, and $22 billion for tools and instrumentation [5]. Figure 1.4 shows the forecast for the world market of nanotechnology from European Commission. By 2020, the annual global economic impact of nanotechnology is estimated approximately $3 trillion US dollars [6]. It implies that a great potential in the market for nanotechnology products. That is the reason why nanotechnology has been investing more and more by the governments in both developed and developing countries and industrial investors. It is now recognized as the future of technological development.

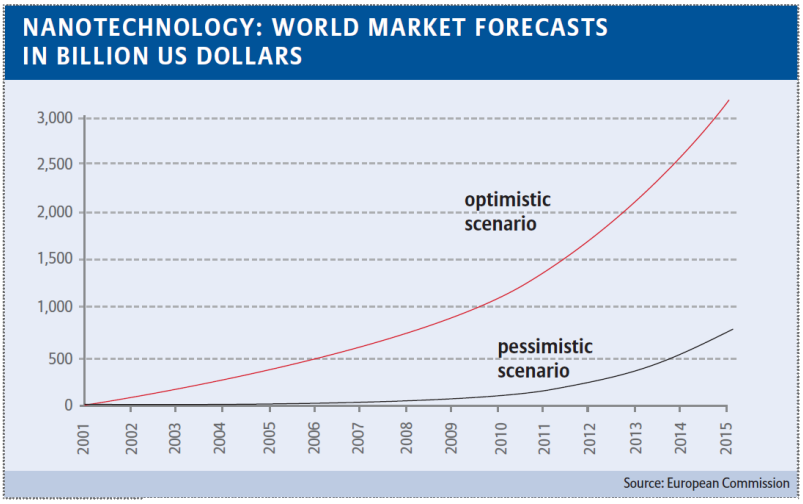

(Source*: European Comission*)

Figure 1. 4 World market forecast for nanotechnology

In the development of nanotechnology, nanofabrication plays a very important role because it is the art of designing and manufacturing in nanoscale, and it is the tool box that enables us to manipulate the materials at the nanoscale. It includes the set of techniques to grow, pattern, form and remove material with near nanometer control, repeatability and precision. The goal of nanofabrication is to create structures at the nanoscale which can be utilized as components, devices, or systems, in large quantity at potentially low costs. It provides a lot of advantages and benefits such as minimizing the consumption of material and energy, enhancement of resolution and sensitivity, reduction the burden of waste and environment, enabling high throughput and cost effective production which is vital for industrializing and commercializing.

Nanofabrication represents a wide range of techniques and methods which can be classified into either top-down approaches or bottom-up approaches for fabricating nanostructures and nanomaterials. The top-down approaches refer to methods which start with a macroscopically dimensioned material, then reduce the size of structures generally by employing physical techniques such as machining, lithography, etc. On the other hand, the bottom-up approaches refer to methods which use atomic or molecular precursors to build up nanostructures. Figure 1.5 shows the two nanofabrication approaches and the methods or techniques belonged to each approach.

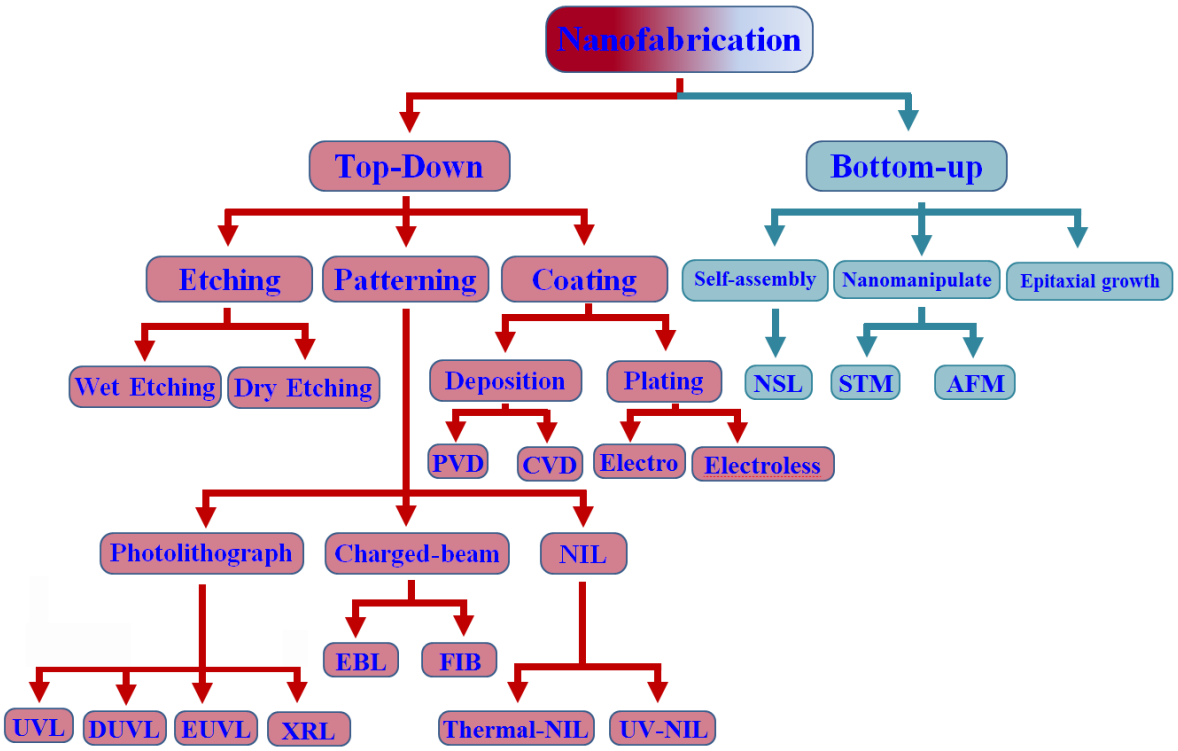

Figure 1. 5 Nanofabrication category

Plenty nanofabrication methods and techniques have been developed to fabricate nanostructures and nanomaterials with the enhancement of resolution or reduction of smallest attainable feature size by the time as shown in figure 1.5. Besides the advantages, each method or technique has its own weakness such as either limitation of smallest attainable feature size, or expensive equipment cost and running equipment cost, or stringent in control, etc. For instance, photolithography, or optical lithography, has been the workhorse for microfabrication and now nanofabrication in the semiconductor industry since its invention nearly half century ago. It is the most common used to fabricate patterned relief structures with submicron feature size on the surface of a planar substrate [7-9]. This process has advantage of high throughput which is suitable for mass production. However, its resolution is limited by exposure wavelength of light source (diffraction of light), the equipment (numerical aperture of projected lens) which is governed by the well-known Rayleigh's equation [10, 11]. In addition, the performance of photoresist also influences the resolution of photolithography. In order to improve the resolution of photolithography system, various resolution enhancement strategies such as using short wavelength light sources (deep UV excimer laser), high numerical aperture optics and immersion lenses, phase shifting mask, optical proximity correction and double pattering,

were implemented [10-12]. As a result, conventional photolithography has moved well into the nanoscale and new generations of photolithography with more advances have been established such as deep ultraviolet lithography, extreme ultraviolet lithography, and X-ray lithography.

Deep ultraviolet lithography (DUVL) utilized the light source from excimer laser which has higher photon energy and shorter wavelength than light source (from mercury lamp) used in conventional photolithography. The excimer laser with the wavelength of 193 nm (Argon fluoride excimer laser) was used as the illumination sources for DUVL which can achieve smallest feature size down to 45 nm ~ 32 nm [10, 14]. However, the resolution of DUVL is also limited. This is because the decrease of wavelength of illumination source in DUV lithography causes extremely difficult technical issues such as materials for making optical lenses, transparent and radiation durable of protected film for mask, and material for the resist.

Extreme ultraviolet lithography (EUVL) utilized the laser source wavelength of 13 nm as the illumination source. EUVL can achieve smallest feature size down to 32 nm ~ 22 nm or below [10, 13] because of its much shorter wavelength of illumination source. However, it is difficult to create EUV source with high output power to provide high throughput. The projection optics in EUVL is very complicated. Moreover, the EUVL system is very expensive and can cost up to $50 M.

X-ray lithography (XRL) utilized the ultimate short wavelength photon radiation from 1 nm (soft X-ray) to 0.1nm (hard X-ray). The basic difference between X-ray wave and optical wave is that X-ray can penetrate the most of materials except high atomic number materials. X-ray cannot be focused because all the materials have same refractive index to X-ray. Therefore, XRL can only exposure mask image to the resist with a ratio of 1:1 with a proximity gap between them. XRL can fabricate smallest feature size of 30 nm or even smaller [14, 15]. However, XRL requires extremely stringent in control proximity gap between the mask and the resist. Since the resolution of X-ray depends on the resolution of the exposure mask, it is very difficult to fabricate the mask with high resolution. In addition, the cost for XRL system is extremely expensive (more than $1 billion [10]).

Electron beam lithography (EBL) and focus ion beam (FIB) lithography are similar to photolithography except that the charged beams are used as exposure sources in EBL and FIB other than the light source. EBL and FIB utilize electron beam and focus ion beam to directly machine the resist coated on substrate in a writing manner to make the patterns.

The beam size plays a key role in the resolution of EBL and FIB. It has been demonstrated that fabrication of nanostructures with feature size smaller than 10 nm by EBL [16-18] and smaller than 50 nm by FIB [19, 20]. However, the throughput of EBL and FIB is very low because they are serial operation process. Also, EBL system and FIB system are also costly.

Nanoimprint lithography (NIL) is a replicated process which was first proposed by Stephen Chou in 1995 for fabrication of micro/nanostructures. It was proposed to replace the costly photolithography or EBL for fabrication of high resolution at high throughput but at a fraction of cost [21-27]. Though NIL is simple and high resolution and is regarded as one of the next generation lithography candidates (NGL). It has some limitations and technological issues. Firstly, the mold used in NIL contains predefined structures which are generally fabricated by photolithography or EBL or FIB [21, 23, 27-29]. Therefore, the smallest attainable feature size is limited by the resolution of those processes. In addition, the processing time and cost will be added up by utilizing those processes for making the mold. Secondly, in conventional NIL (thermal NIL) requires relatively high temperature to soften the polymer and relatively high pressure to press the stamp into the polymer. It takes time to heat up and cool down the polymer so that undesirable for high throughput manufacturing. High pressure during pressing the stamp into the polymer may increase the wear of stamp which results in defects in the replicated patterns. Finally, UV-cured nanoimprinting (UV-NIL) utilizes liquid polymers instead of solid polymers. The polymer is molded into shapes and solidified by photopolymerization (UV curing). Hence, UV-NIL can be operated at low temperature without the need of high pressure as in thermal NIL. However, the mold used in UV-NIL is generally coated with a thin anti-stick layer to prevent or reduce the pattern defects generated due to sticking of polymer material to the mold [30-32]. It requires stringent control of uniformity of the anti-stick layer thickness over the whole patterned area of the mold. The non-uniform thickness of anti-stick layer affects the feature size and results in defects of replicated patterns. Moreover, the anti-stick layer degrades after several uses [33] which results in infidelity and defects in replicated patterns.

On the other hand, the bottom up methods such as nanosphere lithography (NSL), and epitaxial growth offer high throughout fabrication of nanostructures at lower cost [34]. How it is very difficult to control the uniformity and regularity or the order-ness of the nanostructures fabricated by these methods. Scanning probe lithography (SPL) has capability of manipulate materials to create nanostructures at high resolution at low cost by

employing simple facilities, thus a scanning tunnel microscope (STM) or an atomic force microscope (AFM) [35]. However, the throughput of SPL is very low and the patterned area is very small which is not suitable for large scale nanofabrication.

Recently, together with the rapid development of material science, abundant of advanced materials with outstanding property have been created. One of them is plastic semiconductor or polymer semiconductor [36, 37]. They possess important advantages when compared to conventional semiconductor materials because they are lightweight, flexible and very cheap to produce. The plastic semiconductors are more and more used in the electronic devices which are called organic electronics [38-42]. Figure 1.6 illustrates a photograph of a foldable OLED made of organic semiconductor on plastic film. In order to integrate nanostructures/nanomaterials into organic electronic devices to improve their performances, fabrication techniques to create nanostructures/nanomaterials on plastic films play a key role. However, there is a critical issue that lacking of a cost effective, high throughput, less stringent in operation and environment friendly manufacturing process to fabricate nanostructures/nanomaterials on plastic films.

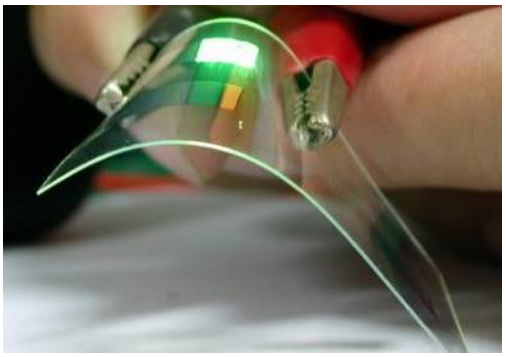

(Source: *http://www.egi.eu/case-studies/eng_tech/semiconductor.html*)

Figure 1. 6 A foldable organic light emitting diode (OLED)

It is very difficult to fabricate nanostructures/nano dot array on plastic films by the aforementioned methods because the high processing temperature or the organic solutions or the etching process may damage the plastic films. Moreover, the plastic film is very soft so that difficult to be handled and fixed on the stage for exposing in photolithography or EBL. In addition, the plastic film easily bends and form curve surface which results in defects of exposure pattern when utilizing photolithography or EBL. So far, ink-jet printing and nanoimprinting lithography (also called micro contact printing) are widely utilized to fabricate metallic micro/nanostructures such as nano dot array, line pattern, etc. on plastic

films. Ink-jet printing [43, 44] injects metal ink through a nozzle to a plastic film in the writing manner such that various micro/nano metal patterns formed on a plastic film. However, the resolution of this method is limited due to the size of the nozzle. It is very difficult to fabricate feature size smaller than 1 μm by ink-jet printing [45]. Moreover, the throughput of this method is very low because it is a serial process. On the other hand, NIL uses an elastomer stamp or a hard stamp with nano/micro features to transfer metal pattern to a plastic film in the printing manner [45-50]. This method enables us to fabricate micro/nano patterns on plastic films at very high throughput. However, this technique has a serious problem that is the edge roughness or the residual at the edge of the pattern feature. In addition, the master mold for replicating the elastomer stamp or the hard stamp is usually fabricated by EBL or FIB or other lithography techniques. Therefore, the overall throughput is limited and facility cost is high. Therefore, alternative methods with low facility cost, high throughput, less stringent in operation to fabricate nanostructures/nano dot arrays on plastics film are highly desired.

This research work aims to develop an efficient nanofabrication process to fabricate a sub-100 nm nano dot array on a plastic film at high throughput and low facility cost [51-54]. This process utilizes the formation of nano dot array on a both flat substrates and patterned substrates by thermal dewetting and transferring of the nano dot array from a substrate to a plastic film. Since, the nano dot array formed on the substrate by thermal dewetting which is a simple process with low facility cost. In addition, the patterns on the substrate are conducted by using NPF technique which is a precise nanoscale plastic-forming by merely mechanical indentation. This process is expected to achieve high throughput, high accuracy, low facility cost. Also, it is environment friendly because no toxic gas or chemical is used.

1.2 Motivation

The motivations for developing process to fabricate a nano dot array on a plastic film are: (1) to fabricate random and ordered metal nano dot arrays with sub-100 nm in diameter on plastic films using a simple technique, (2) to study the effects of the process conditions on the morphology of nano dot array aggregated on both flat substrate and patterned substrate, (3) to study the effects of the process conditions on the transfer ratio of

nano dot from a substrate to a plastic film and on the optical property of nano dot array, (4) to establish the nano dot transfer mechanism, (5) to verify the feasibility of fabrication of a nano dot array in large area on a plastic film, and (6) to lower the fabrication cost.

1.3 Objectives

The objectives of this research work are summarized as below:

1. Establishing the concept of fabrication process to fabricate a random nano dot array on a plastic film.
2. Demonstrating the feasibility of proposed process
3. Study nano dot aggregation process and effects of the process conditions on the transfer ratio of nano dot array to a plastic film and on the optical property of nano dot array
4. Demonstrating the feasibility of fabrication of large area nano dot array on a plastic film
5. Studying nano dot transfer mechanism
6. Establishing the concept of fabrication process to fabricate an ordered nano dot array on a plastic film
7. Optimizing the process condition to achieve high uniformity and regularity of nano dot arrays
8. Verifying the feasibility of using the patterned substrate to transfer an ordered nano dot array to a plastic film.

1.4 Outline of the thesis

The thesis is presented in five chapters as follows:

Chapter 1: INTRODUCTION

Firstly, this chapter covers the research background which relates to nanotechnology and nanofabrication. The applications of nanotechnology and its improvements to human life are briefly presented; and the history of nanotechnology is introduced as well. In addition,

this chapter overviews the nanofabrication with the focuses on the advantages, disadvantages of each technique. Finally, the motivation and the objective of this research work are presented.

Chapter 2: LITERATURE REVIEW

This chapter overviews the state of the art of applications, fabrications of nanostructures and nano dot array. The future trends in fabrications and applications of nanostructures and nano dot array are also introduced. The scope of this research work is presented. Finally, some remarks of this chapter are summarized.

Chapter 3: FABRICATION OF A RANDOM NANO DOT ARRAY ON A PLASTIC FILM

In this chapter, firstly, the concept of the method to fabricate a random nano dot array on a plastic film is introduced. Then, the experimental methods, apparatus, procedures and experimental conditions are presented. The effects of process conditions such as substrate materials, coating thickness, and annealing conditions on the morphology and optical property of nano dot array are presented and discussed. Then, the effects of process conditions on the transfer ratio of nano dot are presented and discussed. Finally, the nano dot transfer mechanism is presented and compared with the experimental results.

Chapter 4: FABRICATION OF AN ORDERED NANO DOT ARRAY ON A PLASTIC FILM

In this chapter, firstly, the concept of the method to fabricate an ordered nano dot array on a plastic film is presented. Then, the equipment and working principle of nano-plastic forming are presented. The effects of nano-plastic forming conditions, coating thickness and annealing condition on the morphology of nano dot array aggregated on a patterned substrate are presented and discussed. Finally, the transfer of an ordered nano dot array from a patterned substrate to a plastic film is presented.

Chapter 5: CONCLUSION

This chapter presents the summary and conclusion of this research work. Also, some suggestions for future work are described.

CHAPTER 2

Literature Review

In this chapter, firstly, the state of the art of applications of nanoparticles/nano dot array to various fields such as bio-sensing, bio-imaging, and electrical/electronic devices will be described. The future trend of applications of nanoparticles/nano dot array will also be presented. Then, various nanofabrication techniques for fabricating of nanoparticles/nano dot array will be described. For each nanofabrication techniques, the discussions focus on the overview of the technique, the advantages and limitations, and some examples of nanoparticles/nano dot array fabricated by that technique reported in literature. Then the scope of this research will be presented. Finally, summary of this chapter is presented.

2.1 State of the art and future trends of applications of nanoparticle/nano dot array

Recently, metallic nanoparticle/nano dot arrays have been attracting interest because of their unique optical properties such as localize surface plasmon resonance (LSPR), LSPR is a collective oscillation of the conduction electrons on the surface of nanoparticles/nano dots when they are excited by incident light of specific wavelengths [55, 56]. Plasmon resonance on the surface of the nanoparticles/nano dots takes place in the form of either radiated light (scattering) or conversion into heat (absorption). Large electromagnetic field enhancement at the LSPR frequency [55, 56] on the surface of metallic nanoparticles/nano dots induces very strong absorption and scattering of the light. This makes metallic nanoparticles/nano dots very auspicious to be applied to several fields such as plasmonic bio-sensing [57-59], bio-imaging [60-62], photo-thermal therapy [62-64], plasmonic solar cells [56, 65-68] and some electrical/electronic devices [69-71]. In this section, the applications of metallic nanoparticles/nano dots to several fields will be presented.

2.1.1 Applications of metallic nanoparticle/nano dot array in bio-sensing, bio-imaging and photo-thermal therapy

In the field of bio-sensing, noble metals such as gold (Au) and silver (Ag) are studied intensively due to their strong surface plasmon resonances (SPRs) in the visible wavelength range [55, 56, 72]. It is known that the LSPR property depends on the shape, size, arrangement of the nanoparticles/nano dots, and the dielectric constant of medium surrounding the nanoparticles/nano dots [62, 63, 73-76]. The later property is exploited intensively in plasmonic bio-sensing devices [57-59, 77]. This is because adding molecules or bio species such as proteins, anti-bodies, etc. on the surface of nanoparticles/nano dots array causes the shift of LSPR peak. The change of molecules or bio species on nanoparticles/nano dots array can be detected by measuring the shift of the LSPR peak. Furthermore, the plasmonic sensitivity can be enhanced greatly by tuning the shape, size and arrangement of nanoparticles/nano dots array. Figure 2.1 illustrates the experimental setup of nanostructure plamonic bio-sensing device for detection of bio molecules binding on the nanostructure through the measurement of LSPR peak shift.

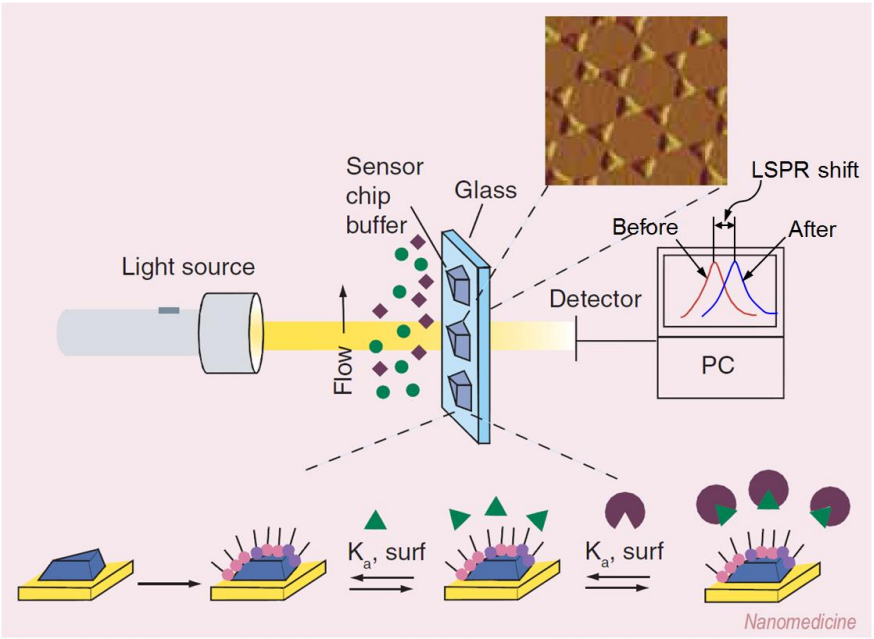

Figure 2. 1 Illustration of nanostructure plasmonic bio-sensing device to detect molecules through measurement of LSPR shift

(*Figure copied from Ref. [77]*)

In order to evaluate the sensing performance of plasmonic sensing devices based on LSPR band shift, three important parameters were introduced. The first parameter is sensitivity (refractive index sensitivity-*RIS*), which is defined as the ratio of the resonance wavelength shift ($\Delta\lambda_{\text{resonant}}$) to the variation of the refractive index of the surrounding medium ($\Delta n_{\text{surrounding}}$) as in equation (2.1).

$$RIS = \frac{\Delta\lambda_{\text{resonant}}}{\Delta n_{\text{surrounding}}} = \frac{|\lambda_{\text{after}} - \lambda_{\text{before}}|}{|n_{\text{after}} - n_{\text{before}}|} \qquad (nm/RIU) \tag{2.1}$$

Where, RIU refers to the refractive index unit.

The second parameter is figure of merit (FOM) - a dimensionless parameter, which is defined as the ratio of refractive index sensitivity (RIS) to the full width at haft maxima (FWHM) of the LSPR band as in equation (2.2).

$$FOM = \frac{RIS}{FWHM} \tag{2.2}$$

The final parameter is the resolution which means that the minimum detection limit of the device. Each LSPR-based sensor has its own resolution for detecting of the signal which can be improved by the shape, size and arrangement of the nanoparticles/nano dots

Tremendous efforts of scientists and researchers have been put into developing of particle synthesis processes and fabrication techniques to attempt high sensitivity plasmonic bio-sensing devices by changing the shape, size and the arrangement of the nanoparticles/nano dots array. Various shapes and sizes of nanoparticles/nano dots were studied to enhance the sensitivity of plasmonic bio-sensing devices such as nanosphere, nanocube, nanobranch, nanopyramid, nanorod, nanodisk, nanotriangle, nanoring and nanopillar [75, 76, 78-82] as shown in the figure 2.2. Plenty of researches have reported the sensitivity of different shapes and sizes of nanoparticles utilized in plasmonic biosensors. The subsequence paragraphs give the summary some achieved sensitivity in the literature.

Nanospheres exhibit one surface plasmon peak. Gold nanospheres with the diameter of 30 nm show modest sensitivity of 70 nm/RIU [83]. In the meantime, gold nanospheres with the diameters increase from 60 nm to 100 nm, they offer higher sensitivity from 99 nm/RIU to 181 nm/RIU [83]. The explanation for the increase of sensitivity with the

increase of diameter of nanosphere is attributed to the radiative damping and retardation [83]. Other researches have reported the sensitivity of 70.9 nm/RIU, 60 nm/RIU and 44 nm/RIU for gold nanospheres with diameter of 30 nm, 50 nm and 15 nm, respectively [75, 84]. A FOM of 0.6 was reported for gold nanospheres of 15 nm in diameter [75].

Nanocubes also exhibit one surface plasmon peak. It was reported that gold nanocubes with the size of 40nm have the sensitivity of 83 nm/RIU and FOM of 1.5 [75]. Silver nanocubes with the size of 100nm show the sensitivity of 165 nm/RIU [85]. Another study reported that the silver nanocubes with the size of 40nm aggregated within a cylindrical pores offer sensitivity up to 770 nm/RIU [86].

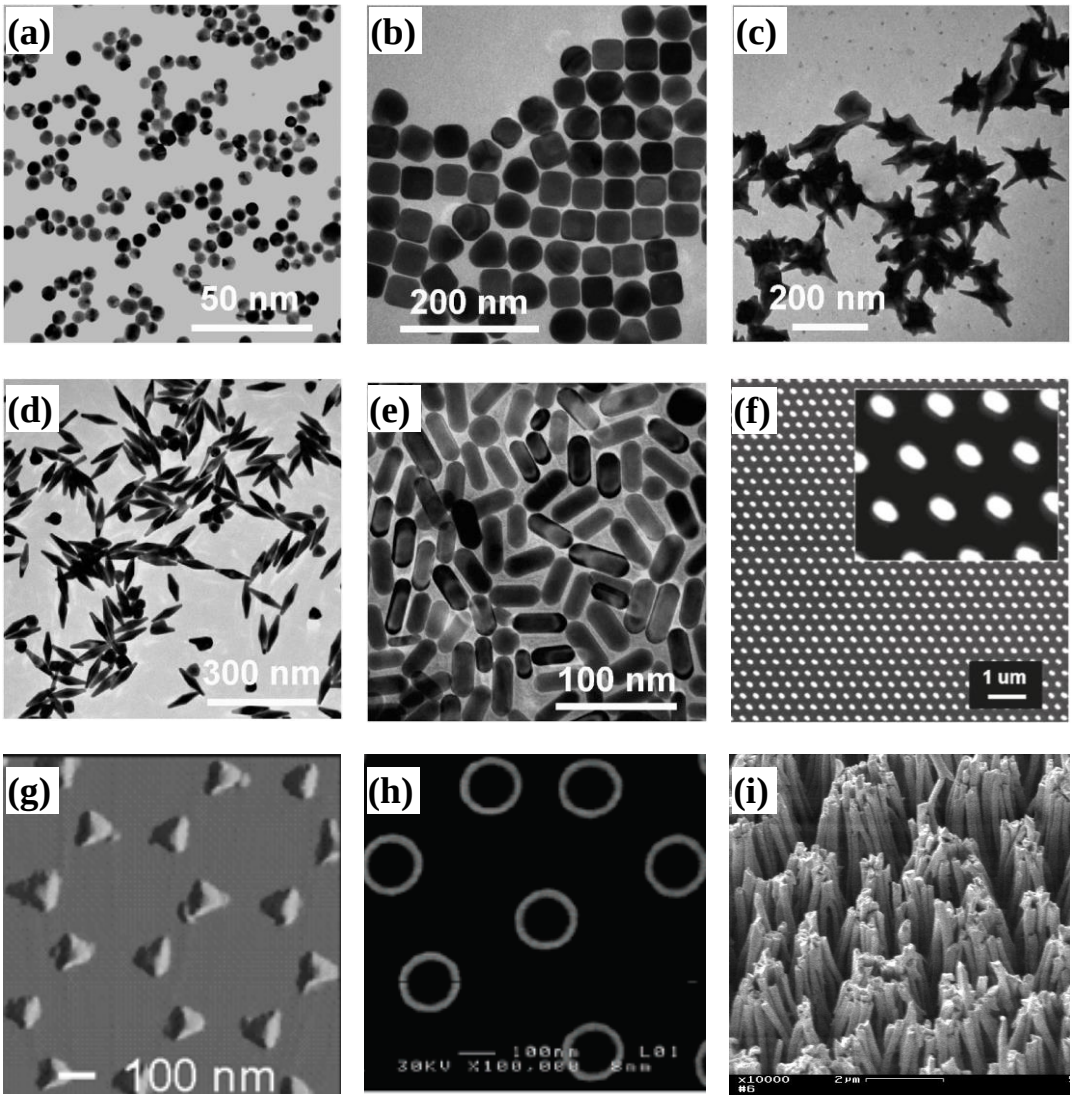

Figure 2. 2 Typical shapes of nanoparticle utilized for plasmonic bio-sensing: (a) nanosphere, (b) nanocube, (c) nanobranch, (d) nanopyramid, (e) nanorod, (f) nanodisk, (g) nanotriangle, (h) nanoring and (i) nanopillar

(*Figure copied from Ref. [75, 79-82]*)

Nanorods exhibit two surface plasmon peaks. One is associated to the oscillation of electrons along the transversal direction (short axis) and the other is associated to the oscillation of electrons along the longitudinal direction (long axis) [75]. The aspect ratio of nanorod which defined as the ratio of the length of long axis to the length of the short axis influences the wavelength of the surface plasmon peaks. Generally, the short axis surface plasmon peaks are almost constant for different aspect ratio while the long axis surface plasmon peaks shift to red side (longer wavelengths side) with the increase in aspect ratio of nanorods [75, 76]. In plasmonic bio-sensing, the shift of the long axis surface plasmon peak is frequently used because it is much more prevail than the shift of short axis surface plasmon peak. It was reported that gold nanorods have sensitivity of 195 nm/RIU, 224 nm/RIU and 288 nm/RIU for the nanorods with the aspect ratio of 2.4 (rod diameter ~ 17 nm), 3.4 (rod diameter ~ 16 nm) and 4.6 (rod diameter ~ 17 nm), respectively [75]. In addition, the FOM of the nanorods were 2.6, 2.1 and 1.7 for those aspect ratios, respectively [75]. Other research reported that the gold nanorods have sensitivity of 491.4 nm/RIU for the nanorods with the aspect ratio of 3.4 (rod diameter ~ 40 nm) [87]. Silver nanorods offer sensitivity of 235 nm/RIU for the nanorods with the aspect ratio of 3.4 (rod diameter ~ 35 nm).

Nanopyramids, similar to nanorods, also have two surface plasmon peaks, (i.e. short axis surface plasmon peak and long axis surface plasmon peak) [75]. The shift of long axis surface plasmon peak is also frequently used in plasmonic sensing. It was reported that the gold nanopyramids have sensitivity of 150 nm/RIU, 212 nm/RIU, 392 nm/RIU and 540 nm/RIU for the nanopyramids with the aspect ratio of 1.5 (pyramid diameter ~ 19 nm), 2.7 (pyramid diameter ~ 18 nm), 3.9 (pyramid diameter ~ 26 nm) and 4.7 (pyramid diameter ~ 40 nm), respectively [75]. Moreover, the FOM of the nanopyramids were 1.7, 2.8, 4.2 and 4.5 for those aspect ratios, respectively [75]. Another research reported that the sensitivity of the nanopyramid array fabricated by template of 320 nm silica spheres is 239 nm/RIU [88].

Nanobranches (also call nanostars), nanocrescents, nanorices offer very high sensitivity due to their sharp tips. Generally, the index sensitivity increase when the apexes or tips become sharper [75]. It was reported that the nanobranches with the core size of about 80 nm have a sensitivity of 703 nm/RIU [75]. Another research reported that the nanobranches with the core size of 30-50 nm and the conical tip size of 10-60 nm have a sensitivity of 218 nm/RIU [89]. Some other shapes of nanoparticles used in plasmonic

sensing also studied and reported. For instance, the nanorings with the diameter of 75 – 150 nm offer sensitivity up to 880 nm/RIU [81]. Gold nanocrescents was reported a sensitivity up to 879 nm/RIU [90]. Nanorices was reported a sensitivity up to 802 nm/RIU [91].

The arrangement of the nanoparticles/nano dots also plays an important role in the enhancement of the sensitivity of the plasmonic bio-sensing. This is because the array form or the ordered arrangement of nanoparticles/nano dots and the intrinsic LSPR properties of the individual nanoparticle/nano dot both influence on the optical properties of the nanopatterns [92-96]. It has been theoretically studied and experimentally verified that the small gaps between sharp corners or sharp tips of noble metals nanoparticles/nano dots are essential to exciting the localized surface plasmons. [95-99]. Many patterns or arrays of nanoparticles/nano dots with different shapes and sizes used in plasmonic sensors have been reported. For instances, ordered elliptical Au nanodisk array fabricated by thermal NIL was used as LSPR sensing substrate to detect clinical immunoassay [80]. The result showed that a strong enhancement in the sensitivity for the detection of the prostate-specific antigen (PSA). The sensitivity reaches femtomolar detection limit which is far under the diagnostic level of 4-10 ng mL^{-1} [80]. Highly ordered periodic silver nano dot arrays with diameter of 100 nm fabricated by platinum assisted nanoimprint lithography were used to detect Cy3-labeled target DNA; and an enhancement of 15.8 times higher in fluorescence signal was observed for 200 nm period silver nano dot array [92]. An ordered gold nano dot array with the dot diameter of ~ 60 nm fabricated on ITO glass substrates by using porous alumina masks was used to detect HeLa cells. The results showed that gold nano dot array improves the sensitivity and enhances the contrast of the confocal imaging of the cell [93].

Besides applications in LSPR shifted-based plasmonic bio-sensing, another application of nanoparticles/nano dots in bio-sensing which also attracted tremendous interests from scientists and researchers is surface enhanced Raman scattering (also called as surface enhanced Raman spectroscopy – SERS) [100]. SERS consists of utilizing the large local field enhancements which may exist at metallic surfaces under specific conditions to boost the signal of Raman scattering of molecules at the metal surface or very close to the metal surface. It is a well-established technique which has capability to detect organic molecules adsorbed onto the metal substrates at ultralow molecule concentration. SERS is a technique which enhances the Raman scattering signal intensity up to several orders of magnitude. It

is developed to surmount the traditional drawback of Raman scattering, that is weakness of scattering signal. Enhancement of SERS has been demonstrated as high as 10^{14} to 10^{15} [101-104] which enables the detection of even single molecule using Raman [103-107].

The large enhancement of SERS scattering intensity has been explained by means of two mechanisms: one is an electromagnetic (EM) field enhancement associated with large local field caused by surface plasmon resonance on the metal surface, and the other is chemical enhancement associated to short distance effects due to the charge transfer between the adsorbed molecule and the metal surface [108-110]. The enhancement of SERS is mainly resulted from the combination of these two effects. In most cases, the EM field enhancement contributes dominantly to the Raman enhancement. Especially, the EM field enhancement effect is particularly pronounced in noble metal coupled structures with nano-gap, nano-tips and sharp corners. These features result in extraordinary enhancement of EM field so called "hot spot".

One of the most important aspects of SERS is to evaluate how much the signal can be enhanced. That is the enhancement factor (EF) which characterizes the enhancement obtained under SERS conditions with respect to the one obtained under non-SERS conditions for the same molecule. There have been several definitions of the enhancement factor [108]. However, the most widely used definition of the enhancement factor is presented as in the equation (2.3) [108, 111, 112], which is considered to provide the best estimation of average SERS EF for a given SERS substrate.

$$EF = \frac{I_{\mathrm{SERS}}/N_{\mathrm{Surf}}}{I_{\mathrm{RS}}/N_{\mathrm{Vol}}} \tag{2.3}$$

In the above equation, I_{SERS} is the intensity of the special band of the spectra of probe molecules which absorb on the SERS substrate. I_{RS} is the intensity of the same band of the spectra of probe molecules in the Raman measurement (non-SERS condition). N_{Vol} is the average number of molecules in the scattering volume of Raman measurement (non-SERS condition). N_{Surf} is the average number of adsorbed molecules in the same volume for SERS measurement.

Gold and silver are the two metals most used for SERS and plasmonic sensing because they provide large EM enhancement [113, 114]. In addition, their plasmon resonance occur in the visible/near-infrared region [55, 56, 72, 114] (wavelength of ~ 400 - 1000 nm) which is the typical wavelength range for molecular Raman scattering measurement. A wide

variety of substrates has been used as SERS substrates which can be classified into two major categories. One is from metallic particles in solution (or colloidal solution of noble metal nanoparticles) and the other is planar metallic structure (nanostructure supported by a "planar" substrate).

The metallic particles with various shapes such as nanospheres, nanotriangles, nanocubes, nanorods, nanowires, etc. in solution (colloids) have been widely used for SERS substrates [115, 116]. Because they offer large Raman enhancement; and the synthesis of the colloids is quite straightforward and well established. However, the utility of colloids as SERS substrate is limited. This is because the nanoparticles are randomly distributed in solution which often produces unpredictable signal enhancements. In addition, the reproducibility in the SERS enhancement of these kinds of substrates is very poor. The aggregated colloids on a planar substrate and roughened metallic surface have also been intensively used in SERS [103, 117, 118]. However, they have the same drawbacks as the particles in solution due to the randomness of the aggregated particles or the roughened surface.

In order to overcome the limitations of the nanoparticle colloids and roughened surface, various noble metal nanostructures have been developed for SERS substrates, including ordered nanoparticle/nano dot arrays, metal islands array, metal coated nanosphere, metal coated nanopillars, metal dot on nanopillar structures [119-123]. It has been theoretically studied and experimentally demonstrated that the magnitude of Raman signal enhancement is strongly dependent on the morphology of nanostructured metal surface, i.e. nanoparticle shape, size and distance (gap) between the nanoparticles. Especially, for the nanostructured metal surfaces comprise of coupled structures with nano-gap, nano-tips and sharp corners [102, 122, 123].

Recently, with the advances of the nanofabrication techniques, many metal nanostructures have been fabricated and used in SERS studies. For instant, highly ordered array of particle-in-bowl structures fabricated by the combination of self-assembly of polystyrene spheres and atomic layer deposition (ALD) was used as SERS substrate to probe Rhodmaine 6G molecules [124]. The result showed that the spatially averaged SERS enhancement factor was 3.8×10^7 [124]. Silver nanostructures arrays with sub 5 nm gaps fabricated by anodic aluminum oxide (AAO) templates and e-beam evaporation were used as SERS substrate to probe Rhodmaine 6G molecules [125]. The result showed that an enhancement factor up to 4.14×10^7 was achieved [125]. Ordered gold coated silicon

dioxide nanopillars array fabricated by holographic interference lithography (HIL) and ALD was used as SERS substrate to probe 1,2 bis-(4-pyridyl)-ethylene (BPE) molecules [126]. It was reported that an enhancement factor of over 0.5 x 10^9 was achieved [126]. Ordered multi-segment of Ag/SiO_2/Au nanopillars array fabricated on silicon wafer by soft NIL was used as SERS substrate to probe Rhodamine 6G (R6G) molecules [127]. The result showed that an enhancement factor of 1.2×10^6 was achieved [127]. Figure 2.3 shows some nanostructures used for SERS substrates reported in literature.

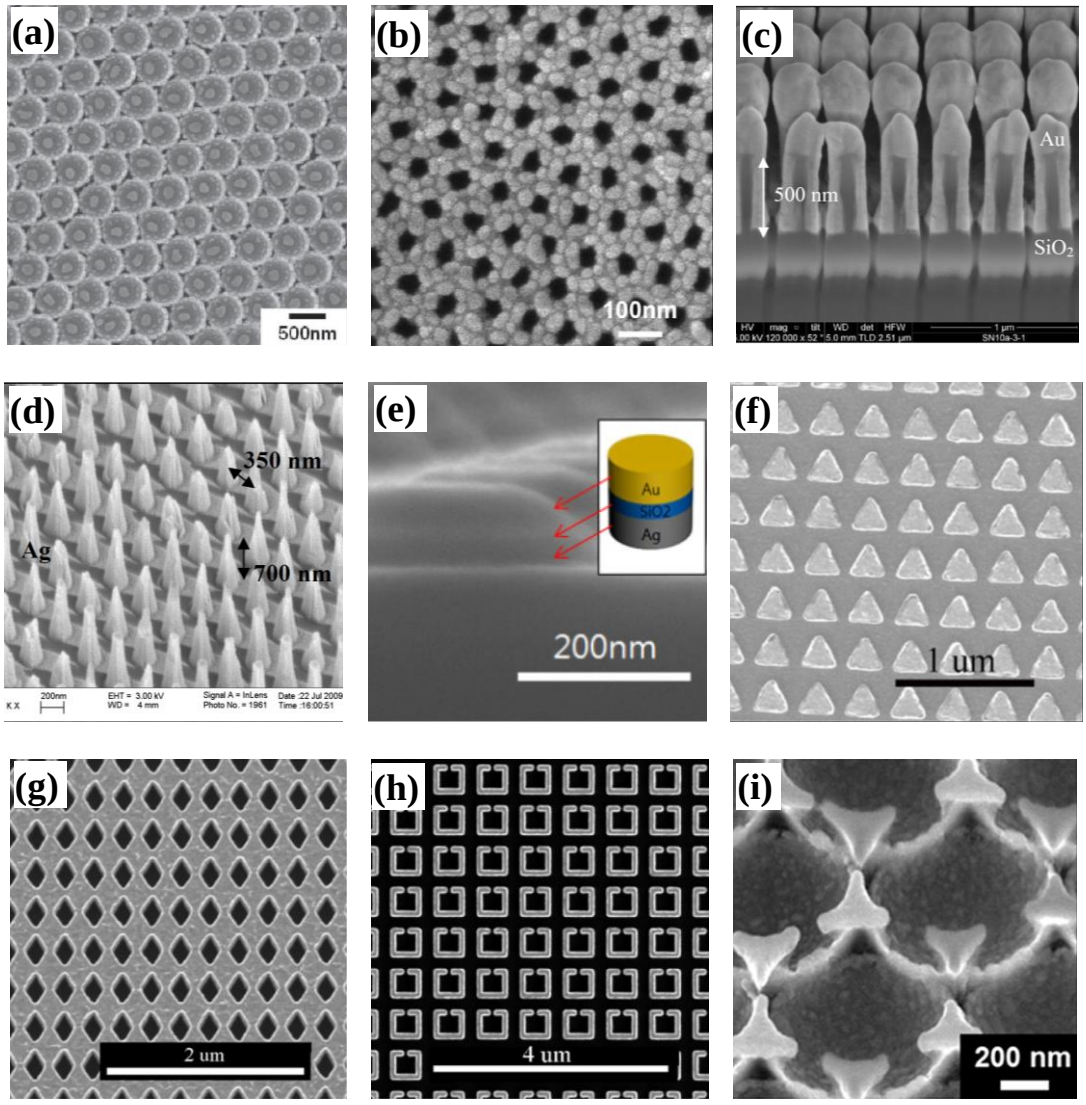

Figure 2. 3 Some nanostructures used for SERS substrates: (a) Particle-in-Bowl structures, (b) Silver nanostructures arrays, (c) Gold coated silicon dioxide nanopillars array, (d) Silver coated silicon dioxide nanopillars array, (e) Multi-segment of Ag/SiO_2/Au nanopillars array, (f) Gold nanotriangle array, (g) Gold rhombus nanoholes structure, (h Gold split-ring resonators array and (i) Silver nanotriangle on top nanopillar array

(*Figure copied from Ref. [124-129]*)

Besides applications in the bio-sensing, noble metal nanoparticles/nano dot also have potential application in bio-imaging and cancer cell diagnostic. This is because the strongly enhanced LSPR at the surface of nanoparticle/nano dot results in very strong scattering of light at the LSPR frequency. It was reported that a gold nanoparticle with the diameter of 80 nm offers scattering 5 orders of magnitude higher than the light emission from a fluorescing dye [130]. Plasmonic nanoparticles can have optical cross sections up to 10 times larger than their physical cross sections [131, 132], allowing individual nanoparticles to be imaged using dark field microscopy [60-62, 133]. Figure 2.4 show the dark field imaging photograph of nanospheres and nanorods. It is obvious that the optical cross section is much larger than its physical size and seen in the dark field imaging photograph and the TEM micrograph. This property is very useful bio-imaging since the highly enhanced cross sections provide more sensitive and highly contrasted imaging.

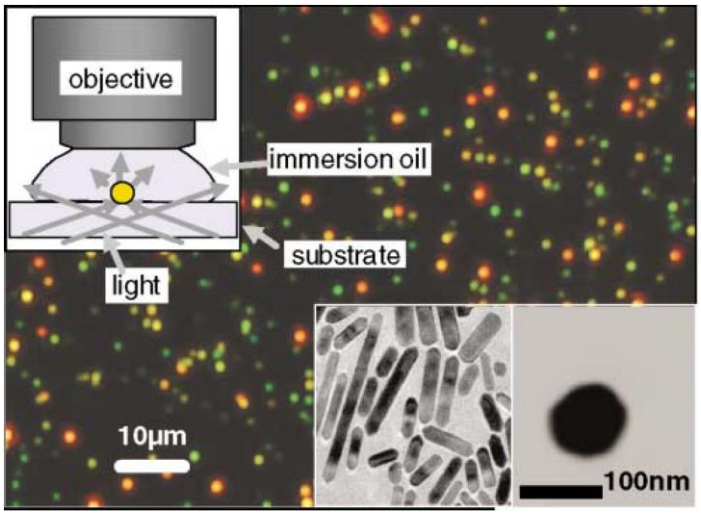

Figure 2. 4 Dark field imaging photograph of gold nanorods (red) and 60 nm nanospheres (green). The inset is the TEM images of a dense ensemble of nanorods and a single nanosphere

(*Figure copied from Ref. [133]*)

Strong scattering of the light makes noble metal nanoparticles/nano dots also very useful to be applied in cancer cell diagnostic. It was reported that gold nanoparticles conjugated with anti-EGFR antibody were very effective to distinguish the cancer cells from the healthy cells [62]. Figure 2.5 shows the dark field micrographs of HaCaT healthy cell and the HSC cancer cell integrated with EGFR antibody conjugated with the with gold nanospheres (figure 2.5 (a) & (b)), and nanorods (figure 2.5 (c) & (d)). In the case of healthy cells the nanospheres and nanorods randomly distributed due to non-specific binding as seen in the figure 2.5 (a) and (c). On the other hand, strong LSPR scattering occurs on the surface of cancer cell due to the gold

nanoparticles bound specifically to the EGFR antibody on the cancer cells. As a result, the cancer cell is easily distinguished from the healthy cell as seen in the figure 2.5 (b) and (d). This technique finds great potential applications in the oral cancer diagnostic [62]. Recently, it has been reported that ordered gold nano dot array fabricated on indium-tin-oxide (ITO) by thermal evaporation through nanoporous alumina mask considerably enhanced the contrast of the confocal image of the HeLa cells [93].

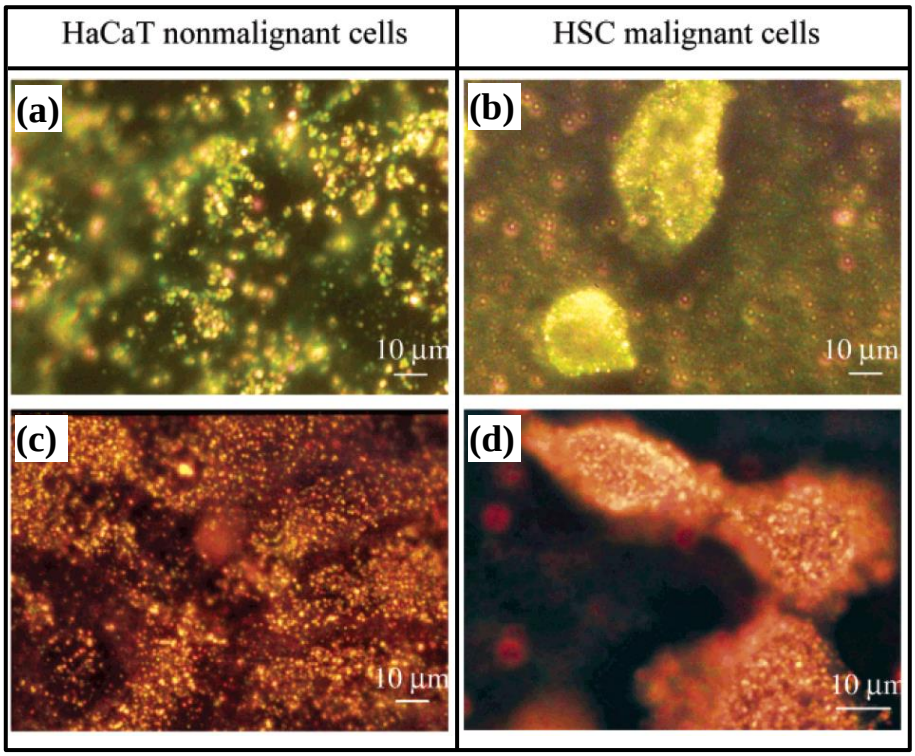

Figure 2. 5 Dark field imaging photographs of (a) Healthy HaCaT cell integrated with gold nanospheres and EGFR antibody (b) HSC cancer cell integrated with gold nanospheres and EGFR antibody (c) Healthy HaCaT cell integrated with gold nanorods and EGFR antibody (d) HSC cancer cell integrated with gold nanorods and EGFR antibody

(*Figure copied from Ref. [62]*)

2.1.2 Applications of noble metal nanoparticle/nano dot array in electrical/electronic devices

One of the most attracting interest applications of surface plasmon resonance (SPR) on the surface of nanoparticle/nano dot in the electrical/electronic applications is in photovoltaic field. Photovoltaic or solar cells are devices which produce electrical energy

(direct current electric - DC electric) by converting the sunlight into electrical power. In photovoltaic industry, crystalline silicon wafer has been used the most for the active absorbing layer. Conventionally, solar cells consist of a thick absorbing layer (made of crystalline silicon, thickness of hundreds of nanometers) to have sufficient optical thickness for effectively converting sunlight to electric power. The cost of a solar cell is mainly attributed to the cost of silicon material and the processing cost. In order to reduce the cost of solar cell, reducing the material cost by using thinner the absorbing layer is necessary. However, merely decrease of the thickness of absorbing layer results in a decrease in the optical length thus decreases the solar cell efficiency. Light trapping technique by utilizing pyramid texture on the surface of the solar cell was introduced to increase the scattering of light into the solar cell thus increase effective optical path length. However, it is desirable to further reduce the thickness of the absorbing layer to few micrometers which is called as thin film solar cell, and the pyramid texture structure surface is not appropriate because the height of the pyramid exceeds the film thickness. Fortunately, utilizing of the surface plasmon of nanoparticle/nano dot properly doped in thin film solar cell will increase the absorption of sunlight in to the solar cell thus results in an increase of efficiency. Figure 2.6 illustrates a typical plasmonic solar cell doped with the nanoparticles on its top surface to increase the absorption of the sunlight.

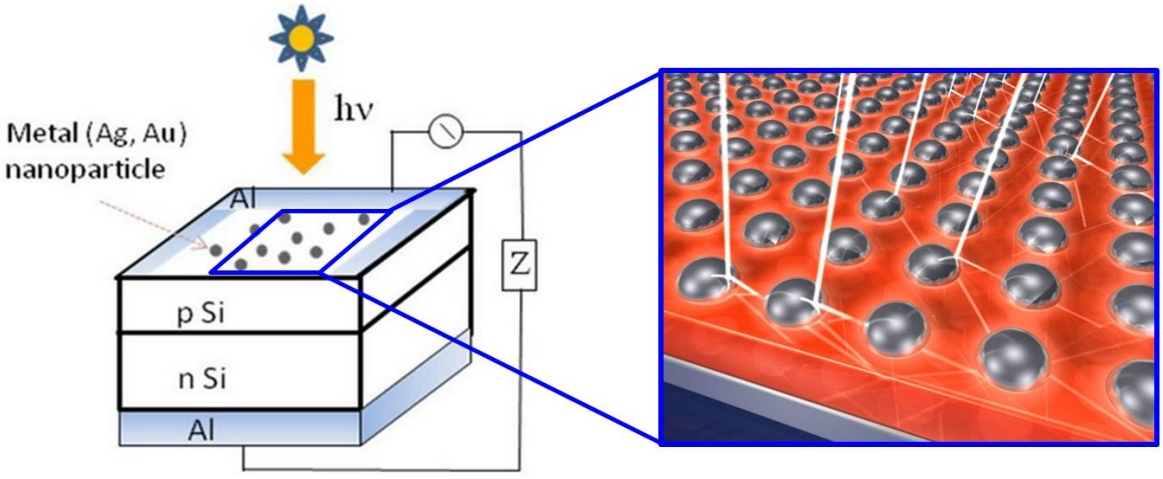

Figure 2. 6 Schematic illustration of plasmonic solar cell

(*Figure copied from Ref. [134-135]*)

Several strategies have been introduced to utilize the surface plasmon of the nanoparticle/nano dot and nanostructures to increase the efficiency of thin film solar cells

[136-138]. Figure 2.7 illustrates two typical light trapping methods utilizing the plasmonic on the surface of nanoparticles/nano dots. In figure 2.7 (a), the metal nanoparticles/nano dots are decorated at the surface of the solar cell. The incident light is scattered by the metal nanoparticles at the surface of the solar cell and then the light is trapped into the semiconductor absorbing layer by multiple and high angle scattering [136]. It results in an increase of the effective optical path length in the cell thus increase the absorption efficiency. In figure 2.7 (b), the metal nanoparticles/nano dots are embedded in the semiconductor. The incident light is excited by the nanoparticles/nano dots causing LSPR on the surface of the nanoparticles/nano dots. The LSPR on the nanoparticles increases the creation of electron–hole pairs in the semiconductor thus increases photocurrent of the colar cell [136].

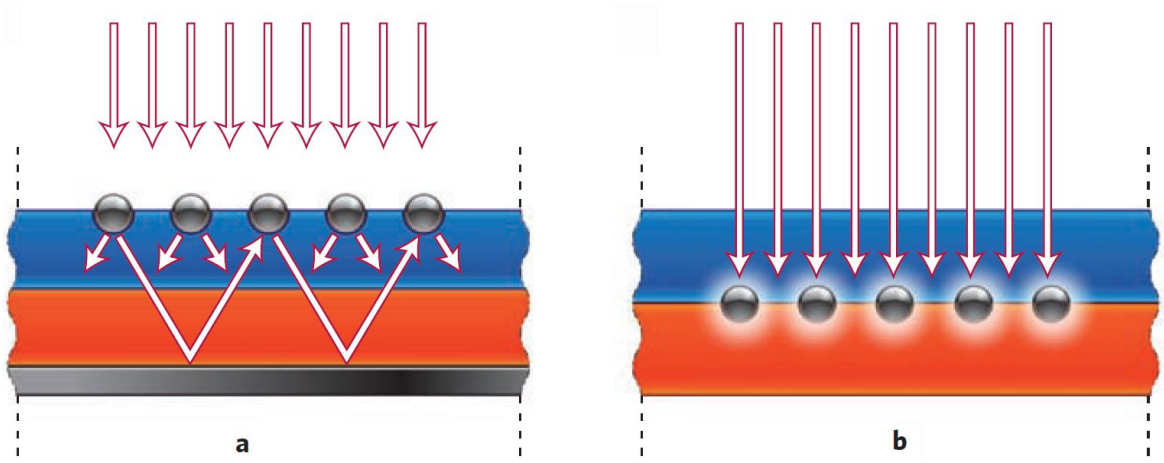

Figure 2. 7 Light trapping by plasmonic nanoparticle/nano dots: (a) nanoparticles/nano dot at the surface of solar cell and (b) nanoparticles/nano dots embedded in solar cell [136]

(*Figure copied from Ref. [136]*)

The aforementioned light trapping techniques from the plasmonic nanoparticles/nano dots have been widely utilized in thin film solar cells to increase its efficiency. For instant, silver nanospheres of 40 nm in diameter were emerged into the photoactive layer of an organic solar cell to increase the light absorption [139]. Adding silver nanospheres into photoactive layer results in a 50% enhancement of light absorption for bulk hetero-junction layer of the organic solar cell [139]. The enhancement of light absorption is attributed to strong scattering of light by the particles inside the hetero-junction. Another study reported that adding gold nanospheres with average diameter of around 20 nm into photoactive layer of a polymer–fullerene bulk hetero junction photovoltaic devices results in a 140% increase in its efficiency

[140]. The enhancement of the efficiency is attributed to the improvement of short circuit current due to an enhanced absorption of the photoactive layer caused by LSPR on the gold nanoparticles [140]. It was reported that ordered silver nanoparticles deposited on GaAs solar cells by porous aluminum mask effectively increase the light scattering and the optical path of the light in the absorbing layer [66]. The deposition of dense and high aspect ratio silver particle results in an 8% increase in short circuit current density and around 9% increase in the efficiency of the cell [66].

Another application of nanoparticle/nano dot arrays in electrical/electronic devices is patterned media and ultrahigh density data storage devices [141-144]. These applications are very promising to address the demands of increasing of storage capacity of the devices to store more and more data and high quality, high resolution entertainment media. Application of ultrahigh density magnetic nano dot arrays in the storage devices is realized and available on the market now. For instant, Hitachi Corporation recently has reported a new patterned media utilized ordered magnetic nano dot array to increase the storage capacity as shown in the figure 2. 8.

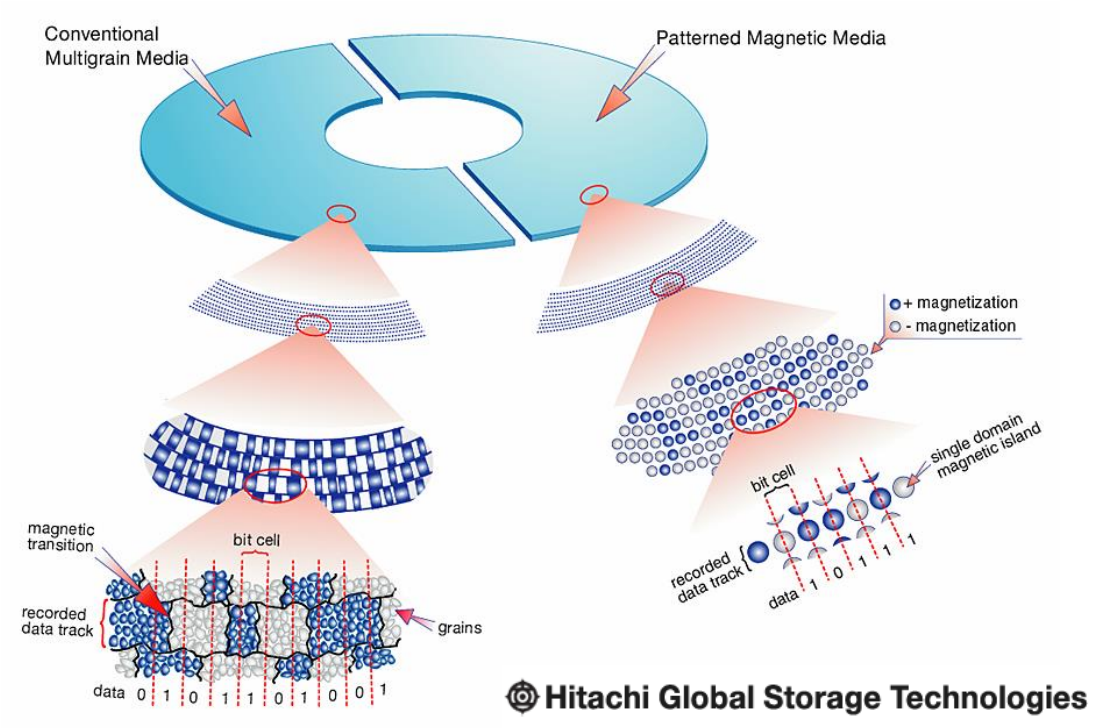

Figure 2. 8 New patterned media versus the conventional multigrain media

(*Figure copied from Ref. [141]*)

The left-hand side of figure 2.8 is the conventional media whose the magnetic recording layer is a thin film of a magnetic alloy. Naturally, this magnetic alloy film forms random

pattern of grains of nanometers in size, and each grain behaves as independent magnetic elements. Many of these random grains are used to store one recorded bit. As a result, the area of the magnetic film requires to store a bit is large. Therefore, the storage capacity of conventional storage device is low. On the other hand, the right-hand side of figure 2.8 shows the new patterned media whose the magnetic layer is created as an ordered, high uniform magnetic nano dot array. Each magnetic dot is capable of storing an individual bit. Since the advances and development of nanofabrication techniques provide the capability to fabricate more and more densed, ordered and uniform magnetic nano dot array. As a result, the storage capacity of the storage devices is increase considerably. In addition, the cost for storing one unit of data is cheaper and cheaper. At this moment, Hitachi Corporation and many PC component manufacturers offer 3.5 inch hard disk drive (HDD) with the storage capacity up to 4 TB to the market.

Other applications of nanoparticles/nano dot array for other electrical/electronic devices such as in photonics devices [145] are studied in the laboratories or in research and development center. These devices will be realized in the near future.

2.1.3 Future trend of application of nanoparticle/nano dot array

In the previous sections, a broad range of applications of nanoparticles/nano dots such as in bio-sensing, bio imaging, cancer diagnostics, electrical and electronic devices etc. were presented. The applications of nanoparticles/nano dots also showed a broad range of the shapes, sizes and materials of the nanoparticles/nano dots. The nanoparticles/nano dots found in the applications can be in the form of colloids, randomly distributed on substrates and orderly arranged in the substrates. Generally, in most applications, it is believed that the order or pattern form of uniformed shape and size of the nanoparticles/nano dots provides better properties and better performances. Therefore, the future trend of applications of nanoparticles/nano dots show great demands for fabrication of arrays or patterns of nanoparticles/nano dots with good uniformity in shape, size and well aligned in desired arrangements. In addition, fabrication of these nanoparticles/nano dots arrays in large area is also very important to realize their application to commercial devices. It is also desirable to extend the fabrication of nanoparticle/nano dot arrays with good controllability of shape, size and arrangement from two dimensions to three dimensions. Furthermore, with the great demands for the portable devices which may require light-

weight, flexible and low production cost. Therefore, fabrication of nanoparticle/nano dot arrays on polymer or plastic substrates is also highly desired.

2.2 Development of nanoparticle/nano dot array fabrication

Nanofabrication methods can be classified into two categories, namely the top-down methods and the bottom-up methods. The top-down methods start with a bulk or thin film material and removes selective regions in order to fabricate nanostructures. This approach is mainly derived from standard lithography and micromachining techniques. On the other hand, the bottom up methods exploit the molecular recognition and self-assembly to build nanostructures from smaller blocks such as molecules, colloids, and atom, etc. This approach strongly depends on chemical engineering and material science and based on fundamentally different principles.

Nano dot arays can be fabricated by the several methods which belong to the either top-down approaches or bottom-up approaches or hybrid of these two approaches. In top-down approaches, the most popular and widely used methods for fabrication of nano dot array consist of photolithography, X-ray lithography, E-beam lithography, focus ion beam, and nanoimprinting lithography. In the bottom-up approaches, on the other hand, the most popular and widely used methods for fabrication of nano dot array consist of nanosphere lithography, porous alumina mask deposition, scanning probe microscopy (SPM), ink-jet printing, epitaxial growth, and thermal annealing. In addition, the hybrid methods for fabrication of nano dot arrays consist of template thermal dewetting, patterning assisted thermal dewetting.

In this section, the major nanofabrication methods for fabrication of nano dot arrays will be presented. For each method, the overview of the method will be introduced first. The advantages and disadvantages of the method are then discussed. Finally, some achievements in fabrication of nano dot array by that method are presented. The sequence in this section starts first from top-down methods, then the bottom-up methods.

2.2.1 Photolithography

Photolithography (also called as optical lithography) is a process utilizing light to transfer pre-defined patterns on a mask to a light sensitive polymer (also called as photoresist) coated on a substrate. The light is focused onto the photoresist causing the cross-linking or scission of the polymer chain which changes the solubility of the exposed area of photoresist. The patterns on the photoresist are then developed to form 3D relief images on a substrate. Depends on the application, the substrate is then etched to remove substrate material to create micro/nanostructures or the substrate is coated with some material (usually coated with metal) to create protrusion micro/nanostructures on the substrate. In semiconductor industry, it also very often used the pattern on photoresist coated on substrate for selectively doping material into the silicon substrate to create p-n junction or

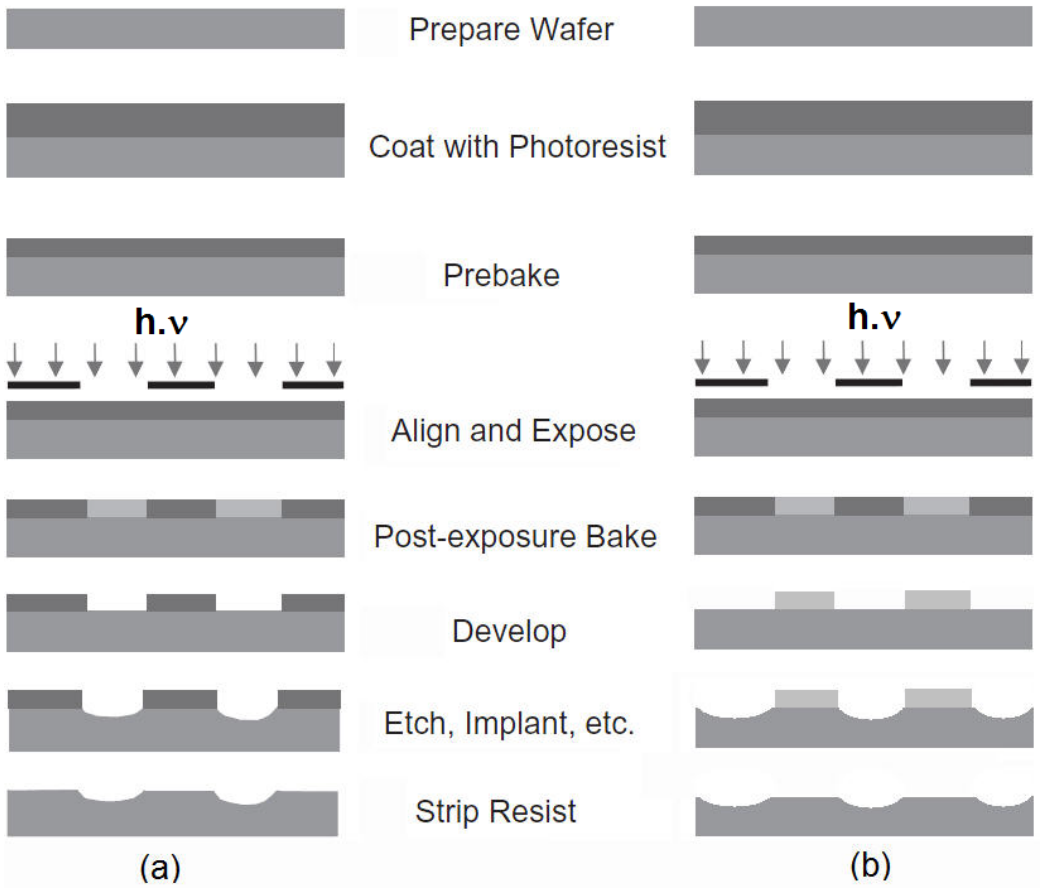

Figure 2. 9 Illustration of photolithography processing steps: (a) for positive photoresist, (b) for negative photoresist

(*Figure copied from Ref. [146]*)

other electrical component. Finally, the photoresist is removed from the substrate, and leave the micro/nanostructures on the substrate. This method is widely used to fabricate micro/nanostructures with the features size in the range from micron to submicron meters. It has been the workhorse for the semiconductor industry during since it was invented nearly half of century ago. Figure 2.9 shows a typical photolithography process for the (a) positive photoresist and (b) negative photoresist. Generally, fabrication of micro/nanostructures by photolithography consists of following processing steps: substrate preparation, photoresist spin coating, pre-bake, exposure, post-exposure bake, development, post bake, etching/implanting, and finally removing the photoresist.

Two kinds of photoresist materials are utilized in photolithography: positive photoresist and negative photoresist as shown in the figure 2.10. Upon exposing the light source, the cross-linking or scission of the polymer chain occurs in the exposed areas, and changes solubility of those exposed areas. In positive photoresist, the areas exposed to the light are soluble and washed away in the developer solution, while the unexposed areas are remained. Oppositely, in negative photoresist, the areas exposed to the light are insoluble and remained in the developer solution, while the unexposed areas are washed away.

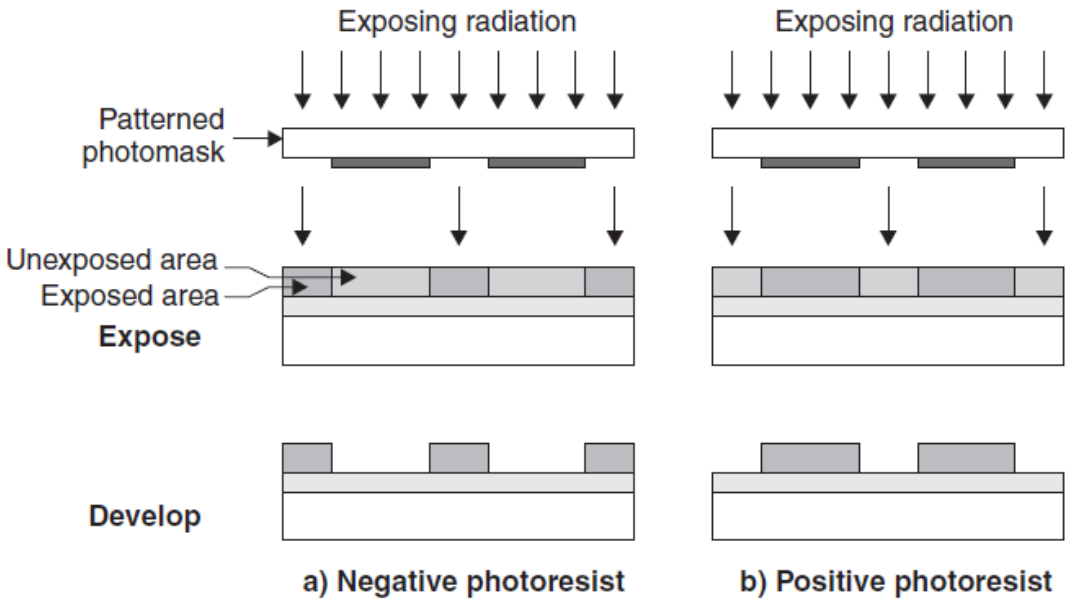

Figure 2. 10 Behaviour of positive photoresist and negative photoresist

(*Figure copied from Ref. [147]*)

In early days, the contact mode of exposure system was used in photolithography in which an optical mask is directly contacted with the photoresist-coated substrate. The

disadvantage of this exposure system is that the photomask is easily damaged due to directly contacting with the photoresist. This system was then replaced by the proximity gap exposure system in which the photomask is at a very narrow gap from the photoresist-coated substrate. This narrow gap improves the lifetime of the photomask due to non-contact with the photoresist. In both the contact and proximity exposure systems, the features on the photomask are imaged onto the photoresist in only ratio of 1:1 without any reduction. Therefore, their resolution is limited, and depends on the resolution of the photomask. Later, the projection exposure system was used in photolithography. This system is much more advanced than the contact and proximity ones because it can project the feature on photomask onto photoresist with demagnification ratio of 5:1 or 10:1. This allows fabrication of much smaller feature size. Figure 2.11 illustrates the three exposure systems used photolithography.

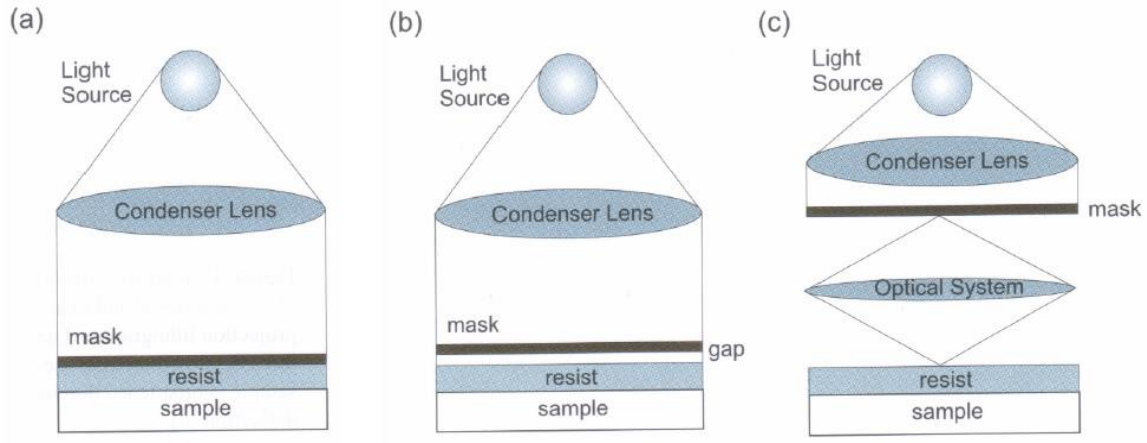

Figure 2. 11 Exposure systems in photolithography

(*Figure copied from Ref. [148]*)

The projection photolithography has been widely used in the semiconductor industry since the mid of 1970s. A typical projection photolithorapgy system is shown in figure 2.12. In projection photolithography, the features on the photomask are projected onto the photoresist through the optical systems (lens system) as seen in Figure 2.11. The light source passes through the features on the photomask (transparent windows or uncovered windows) and then goes into the lens system. A transparent feature (transparent window) on the photomask can act as a narrow slit. When the light passes through a narrow slit, the light diffraction phenomenon will occur, and this diffraction phenomenon is followed the

Huygen's principle. After passing the slit, the light is diffracted and spreads out on the image plane, and the diffracted light is more spread on the image plane when the width of the slit is narrower or the wavelength of light source is longer. Since, the photomask consists of many features, and each feature acts as a narrow slit. If two slits are too closed to each other, the diffracted light from these two slits may be overlapping on the image plane (photoresist plane). If this occurs, two features on the photomask will have an overlapping (or same position) exposed area on the photoresist. This causes a defect in the fabricated pattern on the photoresist in the development process. Therefore, the minimum distance between features on the photomask is limited. On the other hand, if the features on the photomask are too narrow or small, the exposed areas from two adjacent features on

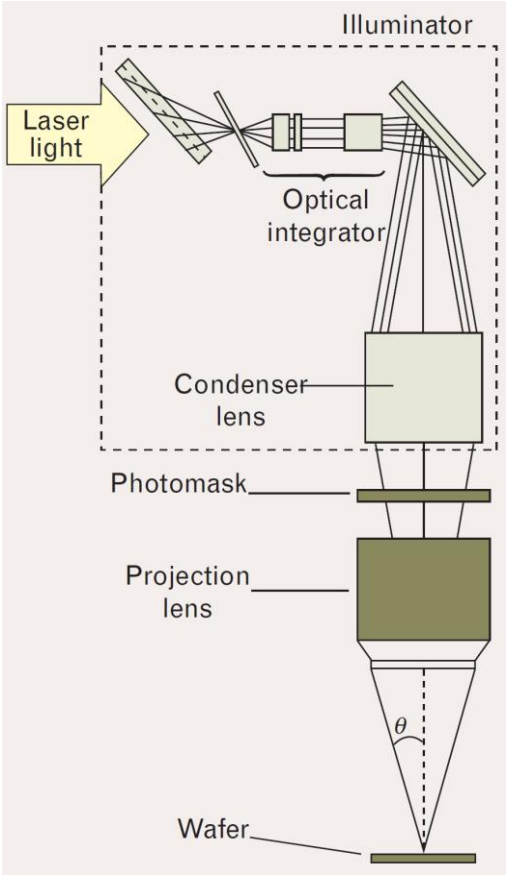

Figure 2. 12 Reduction projection lithography system

(*Figure copied from Ref. [9]*)

the photoresist may be overlapping. This also results in defects in the patterns on the photoresist in the development process. Therefore, the minimum feature size on the photomask is also limited. Overall, the light diffraction phenomenon limits the attainable

resolution of photolithography (limitations in feature size and distance between the features). The resolution of projection lithography is determined as the equation (2.4) [9-12]:

$$R = k_1 \frac{\lambda}{NA} \tag{2.4}$$

Where, λ is the illumination wavelength, and *NA* is the numerical aperture of the imaging optical system, k_1 is a coefficient depends on the imaging process ($k_1 < 1$). It was reported that $k_1 = 0.61$ for the system used in reference [10]. From equation (2.4), it is obvious that the resolution of projection photolithography can be improved if using shorter wavelengths light source or using higher numerical aperture of the imaging optical system.

In early days, the light source with wavelength of 436 nm (G-line) from a mercury lamp was first used for illumination source in photolithography. Then it was replaced by the light source with wavelength of 365 nm (I-line) for the smaller feature size. For further decrease in feature size, the shorter wavelengths of excimer laser were used as the illumination source in photolithography: deep ultraviolet (DUV) with the wavelengths of 248 nm (KrF), 193nm (ArF), 157 nm (F_2) and extreme ultraviolet (EUV) with the wavelength of 13 nm. This marked the come out DUV-lithography and EUV-lithography in the semiconductor industry. Figure 2.13 shows the reduction of the feature size and the wavelength of illumination source in projection photolithography over the time.

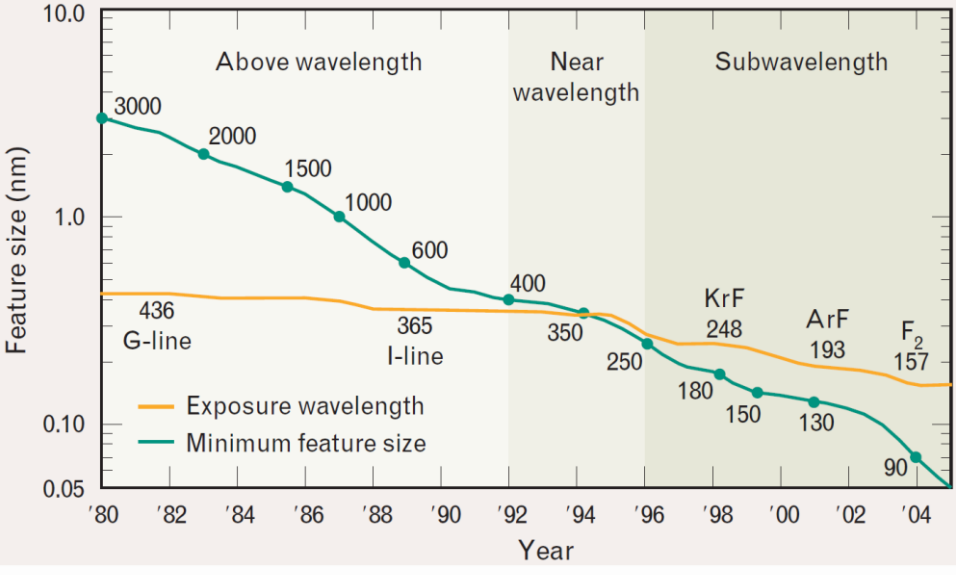

Figure 2. 13 Reduction of feature size and wavelength of illumination source over time

(*Figure copied from Ref. [9]*)

From figure 2.13, it is obvious that the attainable feature size decrease together with the decrease in the wavelength of the illumination source. However, the decrease in wavelength of illumination source obviously results in increase in technical difficulties or issues. The technical difficulty is attributed to the high absorption of photon of material at short wavelengths. It causes technical issues for finding the materials for the projected lens system, materials for photomask and materials for the photoresist.

From equation (2.4), another approach to increase resolution (decrease *R* value) of the projection lithography is to increase the numerical aperture of optical lens, *NA*, which is gorvenrned by the equation (2.5) [146].

$$NA = n\sin\theta \tag{2.5}$$

Where, *n* is the refractive index of the medium between the lens and an image plane (photoresist), θ is the haft-angle of the maximum cone of the light enters or exits the lens. From equation (2.5), there are two way to increase the numerical aperture, *NA*, by increasing in either the half-angle of maximum cone,θ, or refractive index, *n*. The first method is achieved by increasing in the diameter of the lens in optical projection system. However, the increase of *NA* by increase the lens diameter has limitation since higher oblique incidence angle of light from air to the photoresist increases the reflection of the light on photoresist surface. It results in poor contrast of image and low image intensity. In addition, the increases in lens diameter mean that the system is bigger, heavier, and obviously more expensive.

The second method to increase the numerical aperture, *NA*, is to increase the refractive index, *n*, by filling the liquid between the projection lens and the photoresist. This is system in known as immersion photolithography. In immersion photolithography, it allows using numerical aperture *NA* > 1. So it offers much more improvement in the resolution by simply utilizing liquid medium between the optical lens and the photoresist. A typical immersion photolithography system is shown in the figure 2.14. However, immersion optical lithography also causes some technical issues. The first one is that bubbles may appears in the liquid during it is dispensed into the photoresist. This causes the distortion of the projection light which results in defected patterns on photoresist. The other issue is that the contamination of the lens due to direct contact with liquid medium. It reduces the

lifetime of the optical system. Also, the water marks may appear on the surface of the lens and photoresist which may cause the defects on the fabricated patterns.

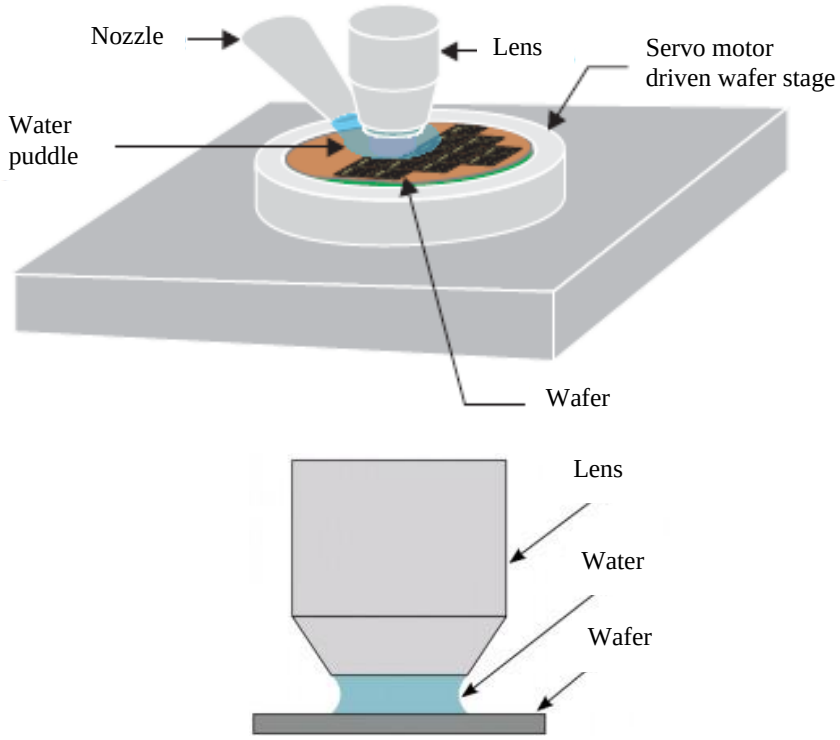

Figure 2. 14 Schematic of immersion lithography

(*Figure copied from Ref. [149]*)

An increase in numerical aperture, *NA*, results in an enhancement of resolution of projection photolithography. However, it also causes detrimental effect which is the decrease in the depth of focus (also called as depth of field), *DOF*, which is governed by the equation (2.6) [9-12].

$$DOF = k_2 \frac{\lambda}{NA^2} \tag{2.6}$$

Where, k_2 is a constant ($k_2 < 1$). Generally, for high throughput manufacturing process in semiconductor industry, in one batch, many integrated circuits (ICs) are fabricated on a large silicon wafer with the size from 6 to 12 in. Since, large silicon wafer is impossibly perfect flat and also has surface roughness. The decrease in *DOF* means that the range of the objects on the image planes in focus is narrower. It results in the height of objects on the silicon wafer in focus is in narrower range. It causes some parts of materials on the

silicon wafer being processed is out of focus due to the wafer bowing. Consequently, it causes defects in the fabricated patterns.

Further decrease in wavelength of the exposure source was in X-ray lithography (XRL) which used ultimate short wavelength from 1 nm (soft X-ray) to 0.1 nm (hard X-ray). A typical XRL system is illustrated in Figure 2.15. In XRL, the patterns on a mask are transferred to the surface of the X-ray sensitive resist coated on the substrate (usually is silicon wafer) through the use collimated X-rays. Since, X-ray is different from the light source that used in photolithography due to the fact that X-ray can penetrates into most of materials except high atomic number materials. Unlike UV light, X-rays cannot be focused through a lens because all the materials have same refractive index to X-ray. Therefore, X-ray lithography can only exposure mask image to the resist with a ratio of 1:1. In addition, the masks used in X-ray lithography are designed with unique materials due to property of X-ray, and generally thinner than those used in the optical lithography. An X-ray mask typically consists of membranes made of low atomic numbers materials and the patterns made of high atomic number materials. The areas of the membrane covered with high atomic number materials will block or absorb X-ray, while other areas are transparent to X-ray. Since, the X-ray mask is very thin and fragile, it is necessary to have small gap or proximity gap between the mask and resist surface.

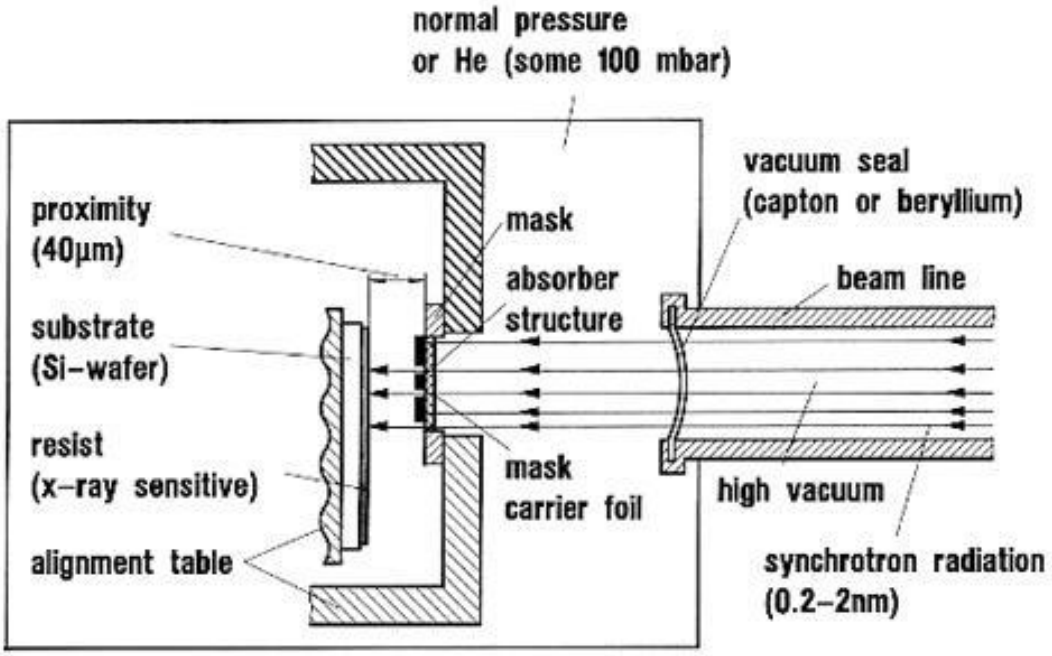

Figure 2. 15 Schematic of X-ray lithography

(*Figure copied from Ref. [150]*)

Because of the ultimate short wavelength of X-ray, The obvious advantage of X-ray lithography is higher resolution and more precise. It offers capability for fabrication of smaller and denser patterned structures on the substrate. In addition, diffraction issues which is the limitation in photolithography, does not occur in XRL. However, the biggest obstacle of X-ray lithography is fabrication of the mask. This is because X-ray lithography can only exposure pattern on the mask image to the resist with a ratio of 1:1.

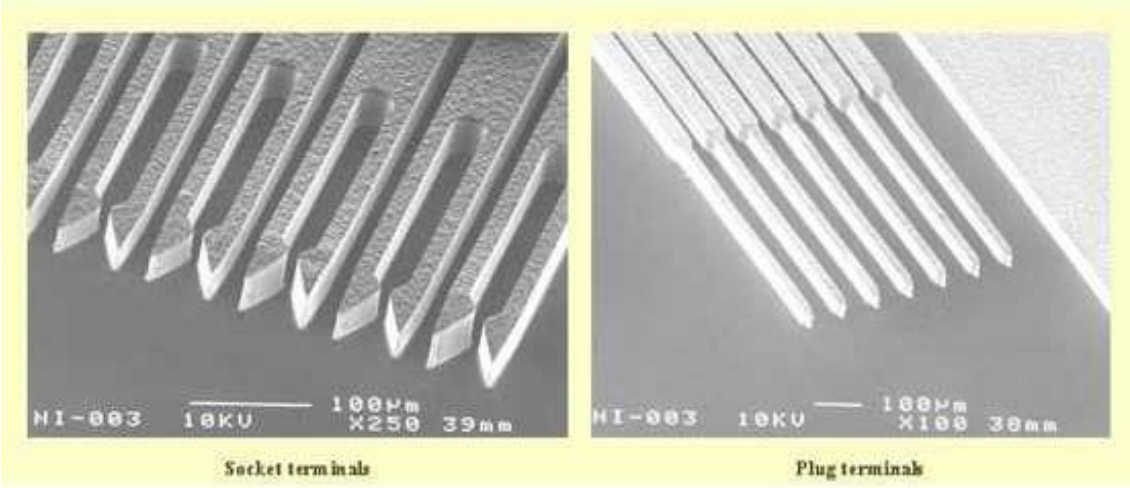

(a) Micro socket and plug terminals

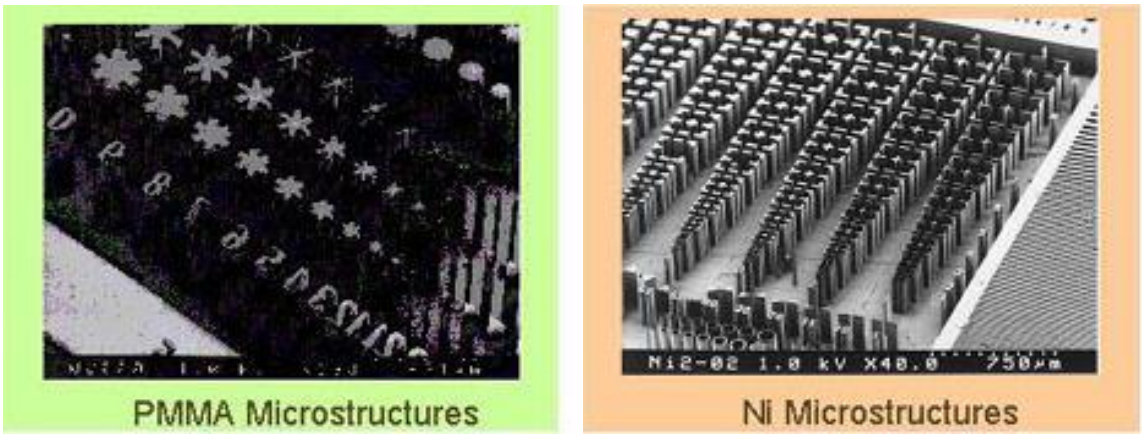

(b) Microstructure mold

Figure 2. 16 Micro/Nanostrucures fabricated by photolithophy

(*Figure copied from Ref. [151]*)

This means that the size of designs on the mask and size of the designs on the wafer must be the same. It considerably increases the difficulty in fabrication of the mask when the features size shrinks. This is because the mask is very thin, and the internal stress may

cause the distortion of the X-ray absorber pattern. Furthermore, X-ray source is generally produced by the synchrotron radiation source (SRS) which requires very expensive equipment and facility. Over the technical issues, the biggest hurdle in X-ray lithography is very costly equipments and facilities. Figure 2.16 illustrates some micro/nanostructures fabricated by photolithography.

2.2.2 Electron beam lithography

Electron Beam Lithography (EBL) is a maskless lithography method which employs an accelerated focused beam of electrons to create patterns on an electron-sensitive resist-coated substrate in the writing or drawing manner. A schematic diagram of EBL system is shown in figure 2.17. Typically, an EBL system consists of the following parts: an electron source that supplies the electrons; an electron column that focuses the electron beam; mechanical stage for setting and positioning the wafer, wafer handling system, and a computer system for controlling the equipment.

Similar to photolithography, two kinds of electron-sensitive resists (called e-beam resist) are employed in EBL: positive and negative e-beam resist. For positive e-beam resists, the e-beam exposed patterns are the same as the fabricated on substrate, while for negative ones, the e-beam exposed patterns are the reverse of the fabricated one on substrate. In the development step, the exposed areas of a positive resist and unexposed areas of a negative resist will be dissolved and washed away.

Because of employing high energy range of 10-100 keV electron beam which possesses ultimate short wavelength (0.1 ~ 0.01 nm), EBL offers higher resolution than photolithography. EBL has been demonstrated the capability to achieve sub-10 nm resolution [16-18, 153]. Figure 2.18 shows some nanostructures fabricated by EBL.

However, EBL also have several disadvantages. First of all is low throughput because it is a serial process. The patterns are fabricated in point-to-point writing manner. This makes EBL unsuitable for mass production. In addition, although EBL has capability for high resolution fabrication, its resolution is limited by other factors, such as scattering of electron in the resist material, the swelling of resist in the developer solution, and by various aberrations in its electron optics. Finally, EBL is rather expensive, an EBL system costs above $2 M.

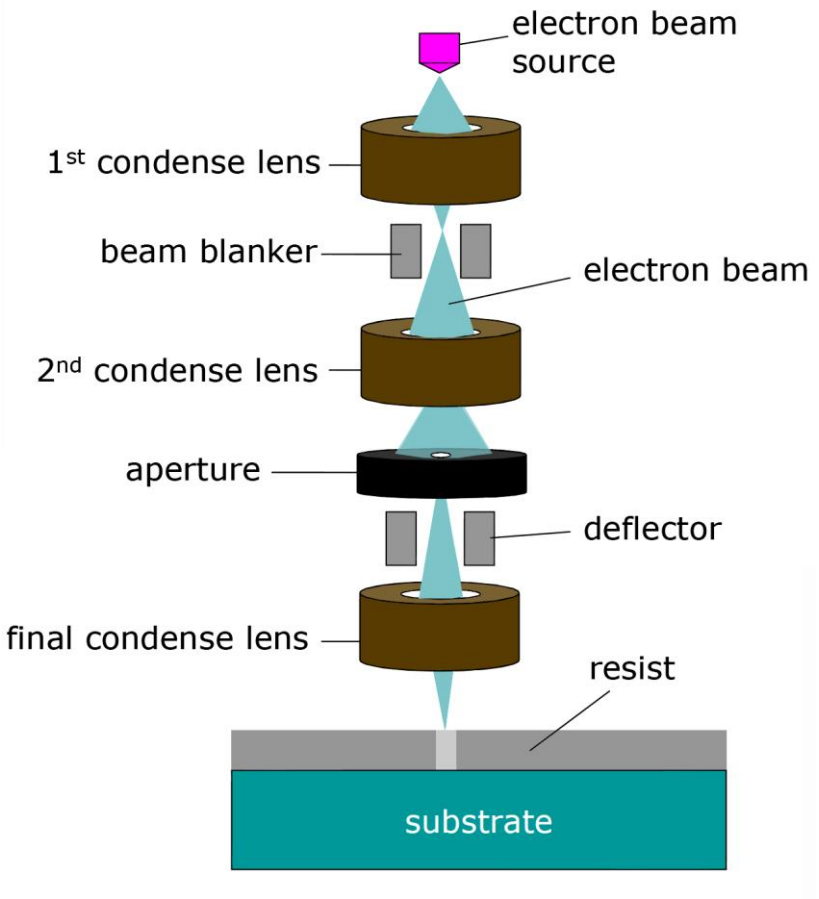

Figure 2. 17 Schematic diagram of EBL system

(*Figure copied from Ref. [152]*)

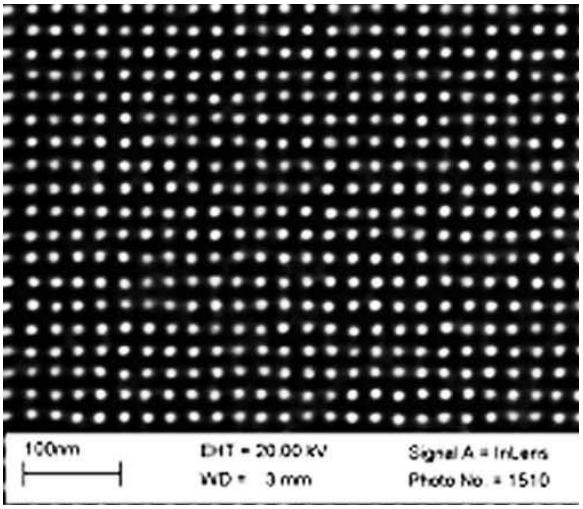

(a) Nano dot array

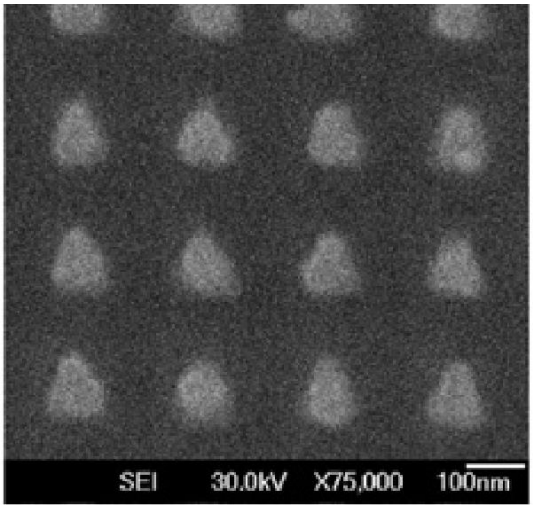

(b) Nanotriangle array

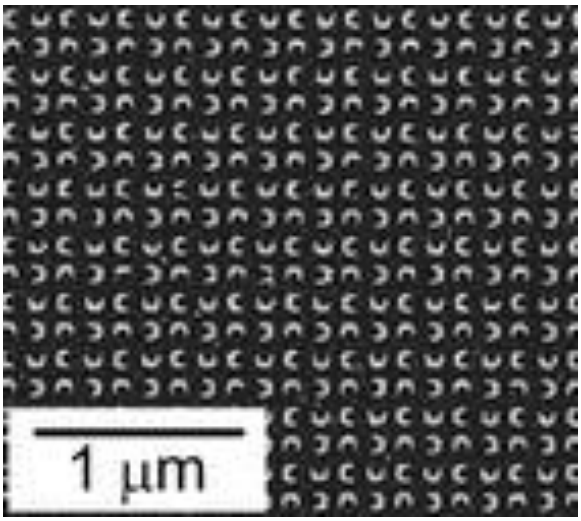

(c) Split resonance ring array

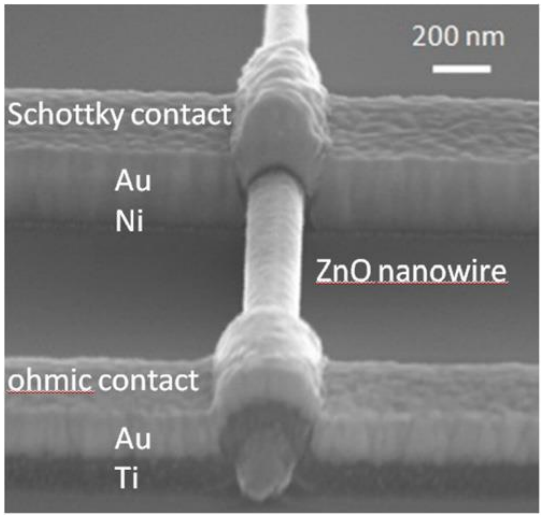

(d) Ohmic contact nanostructure

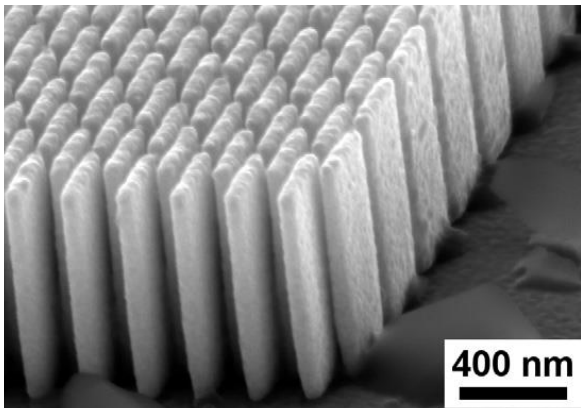

(e) PMMA nanostructure mold

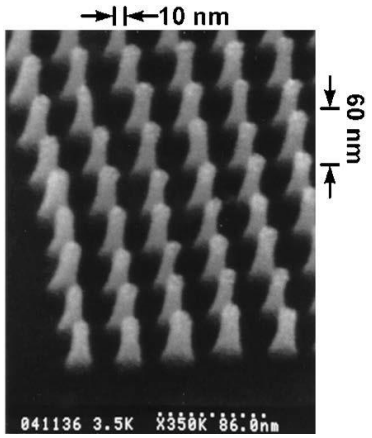

(f) Nanopillar structure mold

Figure 2. 18 Nanostructures fabricated by EBL

(*Figure copied from Ref. [23, 94, 142,154-156]*)

2.2.3 Focus Ion Beam

Focused ion beam (FIB) systems employs an accelerated, finely stream of high energy ionized atoms of a relatively massive element to focus onto the sample for several purposes such as etching, deposition, implantation, and imaging. The FIB instrument is similar to a scanning electron microscope (SEM). A typical FIB system is shown in figure 2.19. A typical FIB system generally consists of following parts: liquid ion source that produces ion stream, an ion column that directs and focuses the ion beam by an electric field, vacuum system and chamber, a sample stage which allows positioning of sample, detectors for imaging purpose, gas delivery system. The FIB system is operated under the control of a computer. Gallium (Ga^{+}) ion is most widely used for the ion source in FIB system. This is because of its low melting point temperature, low volatility at melting point. In addition, its mass is heavy enough for capability of etching or milling heavier elements.

Figure 2. 19 Focus ion beam system
(*Figure copied from Ref. [157]*)

A FIB system and an electron beam (EB) system are based on the same principle except that the difference in the charged beam source. Both FIB and EB systems utilized finely, accelerated charged beam and focus the beam onto the sample for several purpose: etching, deposition, and imaging. The major difference is of FIB and EB is from the beam characteristic. Ion is much heavier and larger than electron. Therefore, ion beam has more energy to bombard the sample surface, result in higher productivity for fabrication structure than EBL. While, EBL is suitable for etching or machining soft materials, FIB

has capability of etching both soft and hard material. However, due to the heavier mass, ion travel more slowly compare with electron. Therefore, it requires the ion column having greater fields to accelerate, direct and focus the ion beam. A typical ion column in a FIB system is shown in figure 2.20. Similar to EBL, FIB virtually does not suffer from diffraction limitation, greater apertures of ion column can also allow for a high resolution fabrication. Figure 2.21illustrates some micro/nanostructures fabricated by FIB.

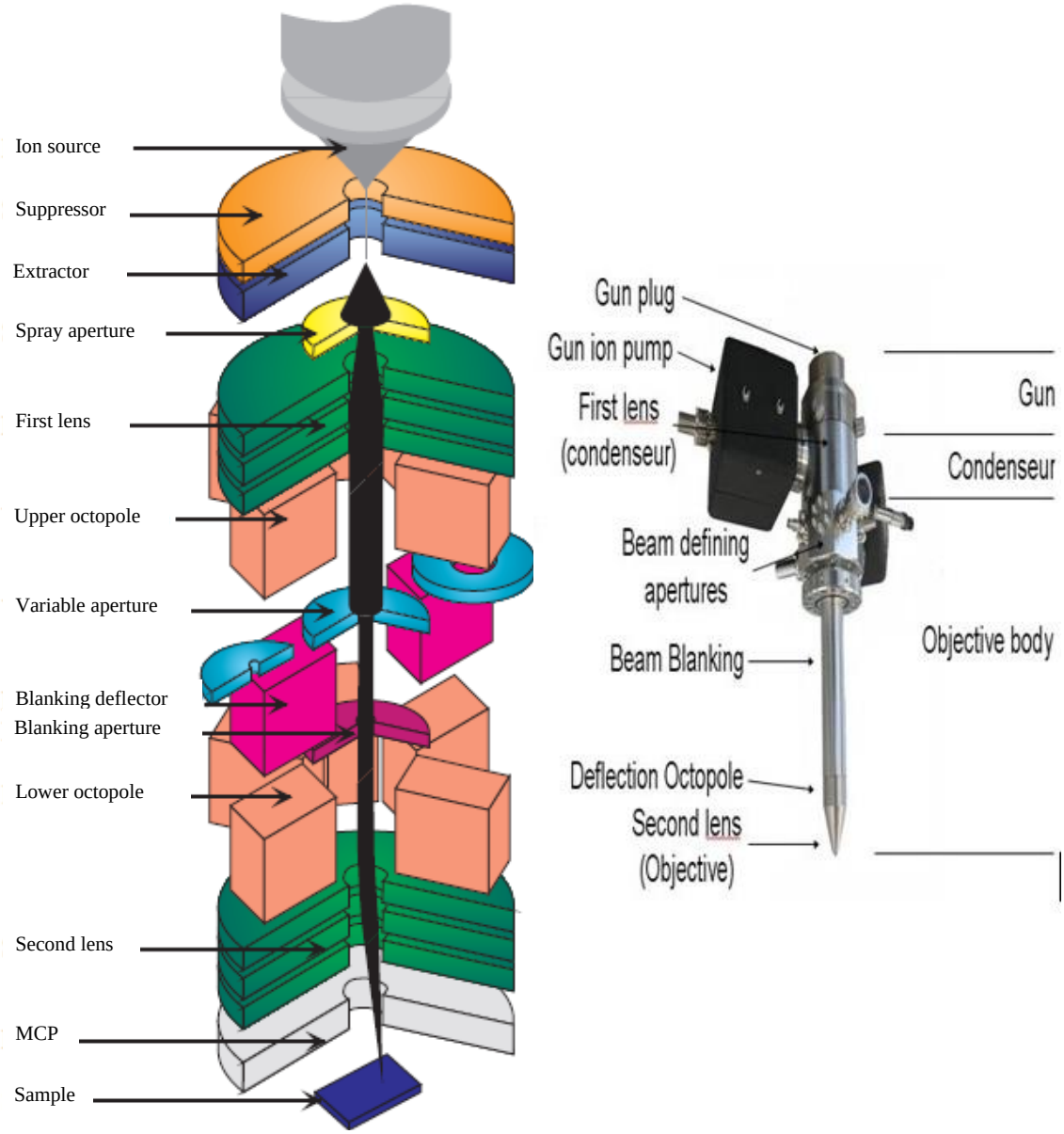

Figure 2. 20 Schematic diagram of FIB ion column

(Diagram is copied from Ref. [158],
Photograph of FIB column is copied from http://en.wikipedia.org/wiki/Focused_ion_beam)

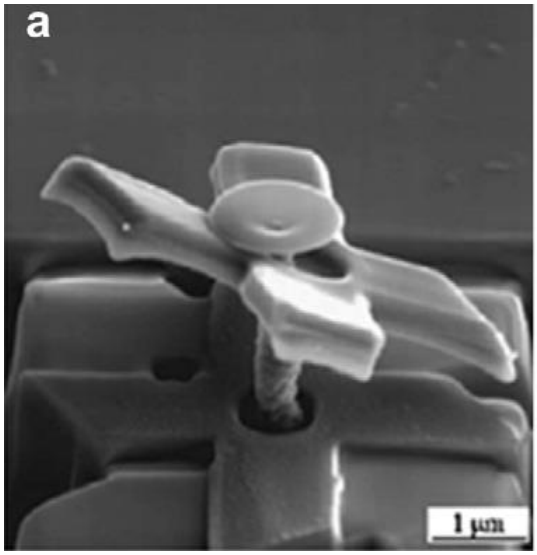

(a) Nano-rotor

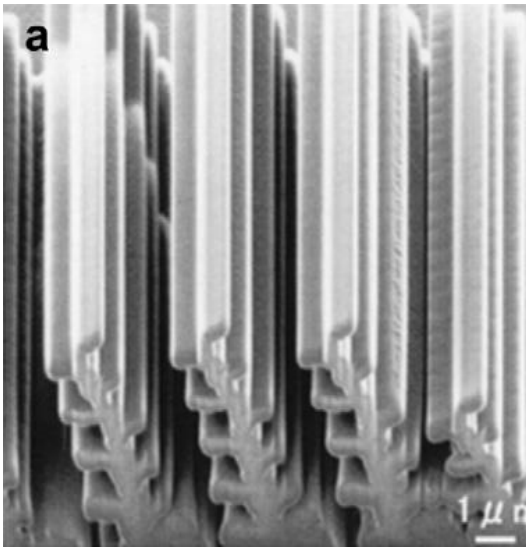

(b) filtering tool

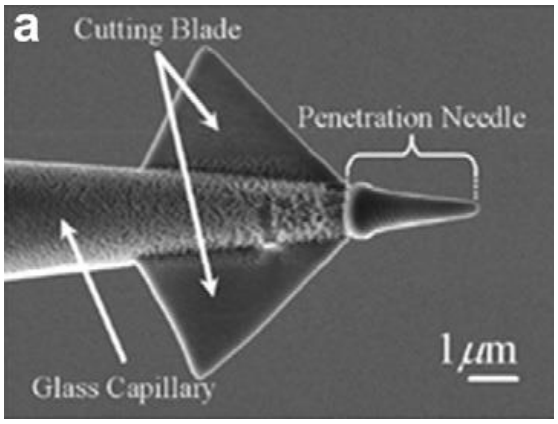

(c) Cell wall cutting tool

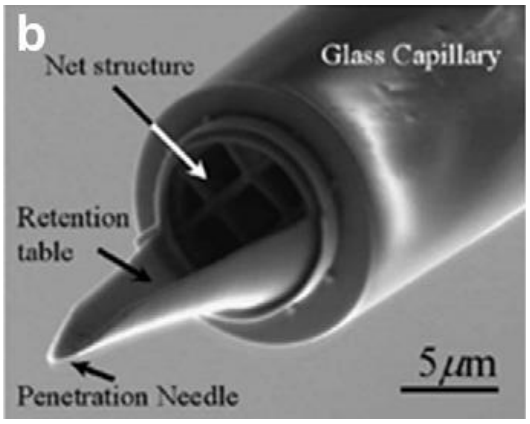

(d) Filtering tool

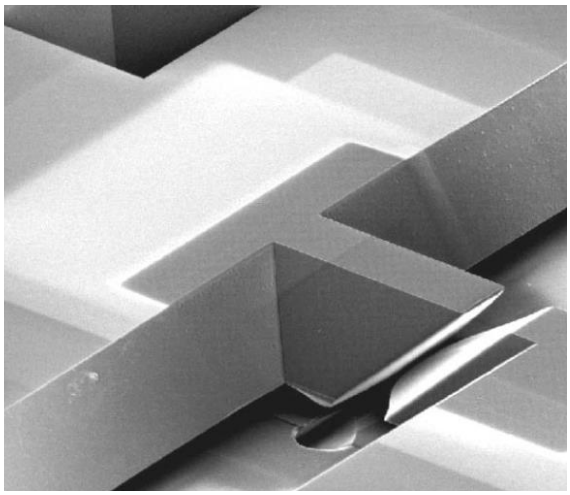

(e) Readout gap milled by FIB

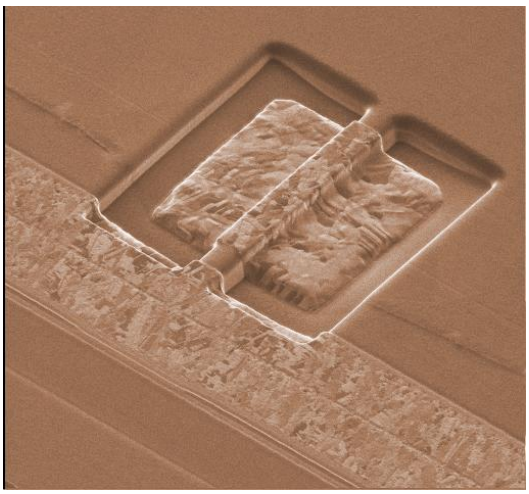

(f) FIB trimmed thin-film magnetic head

Figure 2. 21 Nanostrucures fabricated by FIB

(*Figure copied from Ref. [158, 159]*)

2.2.4 Nanoimprint lithography

Nanoimprint lithography (NIL) creates micro/nanopatterns on a resist coated-substrate by a simple replicated process which was first proposed by Stephen Chou in 1995. It is an alternative method proposed to replace the costly photolithography or EBL for fabrication of sub-100 nm resolution at high throughput but at lower cost [21-27]. A typical NIL process is shown in figure 2.22.

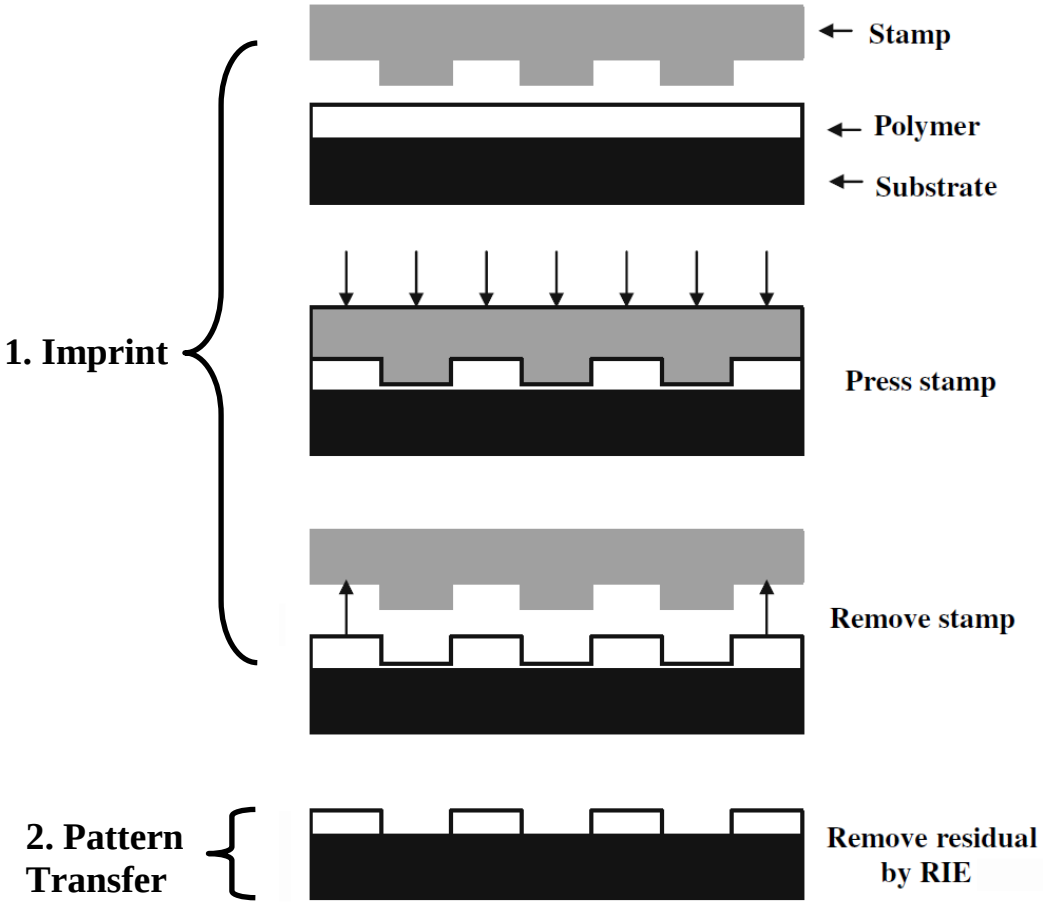

Figure 2. 22 Schematic of nanoimprint lithography process

(*Figure copied from Ref. [13]*)

NIL consists of two steps: imprint to create patterns on a resist-coated substrate and pattern transfer by removing the residual layer of photoresist material. In the first step, a master mold or stamp whose pre-defined micro/nanostructures is pressed or imprinted onto the soft/softened resist coated on the substrate to create reverse micro/nanostructures on the resist. The second step is to remove the residual layer of resist material between the top of

protrusion features of the master mold and the substrate. These two steps of NIL produce micro/nano patterns on the resist-coated substrate which are the same as the ones fabricated by photolithography of EBL after development step. But NIL employs simple replication technique. After removing the residual layer, the remaining resist pattern can serve as a masking layer which can be used for further etching or deposition steps.

Since it was introduced in 1995, NIL has been attracting tremendously interest from nanofabrication community. Up to date, various offshoots of NIL process have been developed and reported. However, they are mainly classified into two categories, namely thermal NIL and UV curable NIL as shown in figure 2.23.

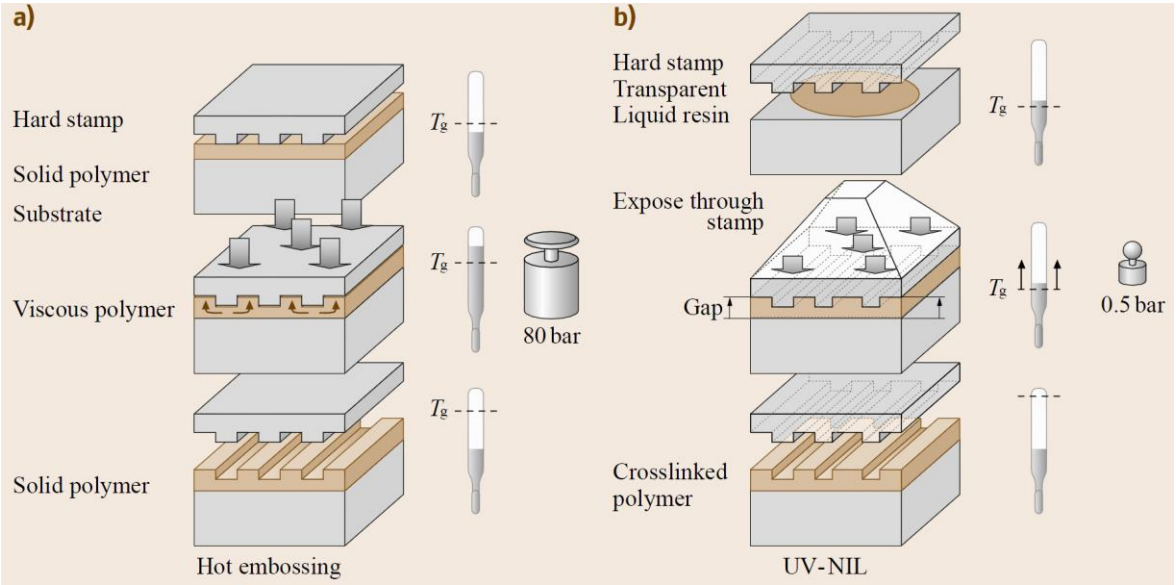

Figure 2. 23 Schematic of NIL process: (a) thermal NIL (hot embossing) and (b) UV-NIL
(*Figure copied from Ref. [160]*)

In thermal NIL (also called as hot embossing, figure 2.23 (a)), firstly the resist layer (thickness of several nanometers) is heated to above the glass transition temperature (Tg) so that it is softened. A mold or stamp with defined micro/nanostructures is pressed into the softened thin polymer layer at pressure around 40 - 120 bars pressure, depending on the mold size, viscosity of softened polymer. To avoid any damages of the mold caused by indirect contact with the hard substrate, the imprint depth is slightly less than the polymer layer thickness. Then, the stamp is retracted (demolded, separated) from the polymer layer while it is still soft. After demolding the stamp, an inverse structure of the mold structure is

left in the resist layer. Finally, the residual polymer layer inside the imprinted pattern areas is removed by an etching process such as reactive ion etching (RIE) or plasma etching.

In UV-NIL (in figure 2.23 (b)), it is performed at room temperature and at much lower pressure than thermal NIL. The UV-NIL process is similar to thermal NIL except the key difference is that UV-NIL employs a transparent stamp and UV-curable polymer. The UV-curable polymer in liquid form at room temperature (viscosity of polymer is ranging from 40 mPa.s to 250 mPa.s) is dispensed onto the substrate. Then, the stamp is press onto the liquid polymer with a little of pressure (<1 bar, depending on the viscosity of polymer) to fill the polymer into the cavities on the stamp. The liquid polymer is then solidified by UV illumination through the transparent stamp. After solidification of the polymer, the stamp is demolded and the residual layer is removed by etching process same as in thermal NIL. For the ease of demolding the stamp without any damages, the elastic polymers or silicone rubbers are frequently used in UV-NIL. Figure 2.24 shows some nanostructures fabricated by NIL.

Although NIL is simple and high throughput nanofabrication process which has capability for fabrication of sub 100 nm feature size or even 10 nm feature size structure [21-27]. However, NIL has some limitations. Firstly, the nanostructured stamps used in NIL are generally fabricated EUVL or EBL [21, 23, 27-29]. Therefore, the minimum feature size of NIL is limited by those processes. Fabrication of the stamp is time consuming and expensive. Secondly, thermal NIL operates at relatively high temperature and relatively high pressure. Therefore, it takes time to heat up and cool down the polymer so that decrease the throughput of the process. The stamp is easily damaged under high pressure pressing into the polymer. Finally, in UV-NIL, the stamp is usually coated with a thin anti-stick layer for the ease of demolding [30-32]. It is stringent to produce a uniformity thickness of the anti-stick coating over the whole nanostructure area of the stamp.

In the previous sections, several typical top-down nanofabrication methods have been described with the discussion focused on the principle, the advantages and disadvantages, and the nanostructures fabricated by those processes reported in literatures. In following sections, the discussion is focused on some typical bottom-up nanofabrication methods.

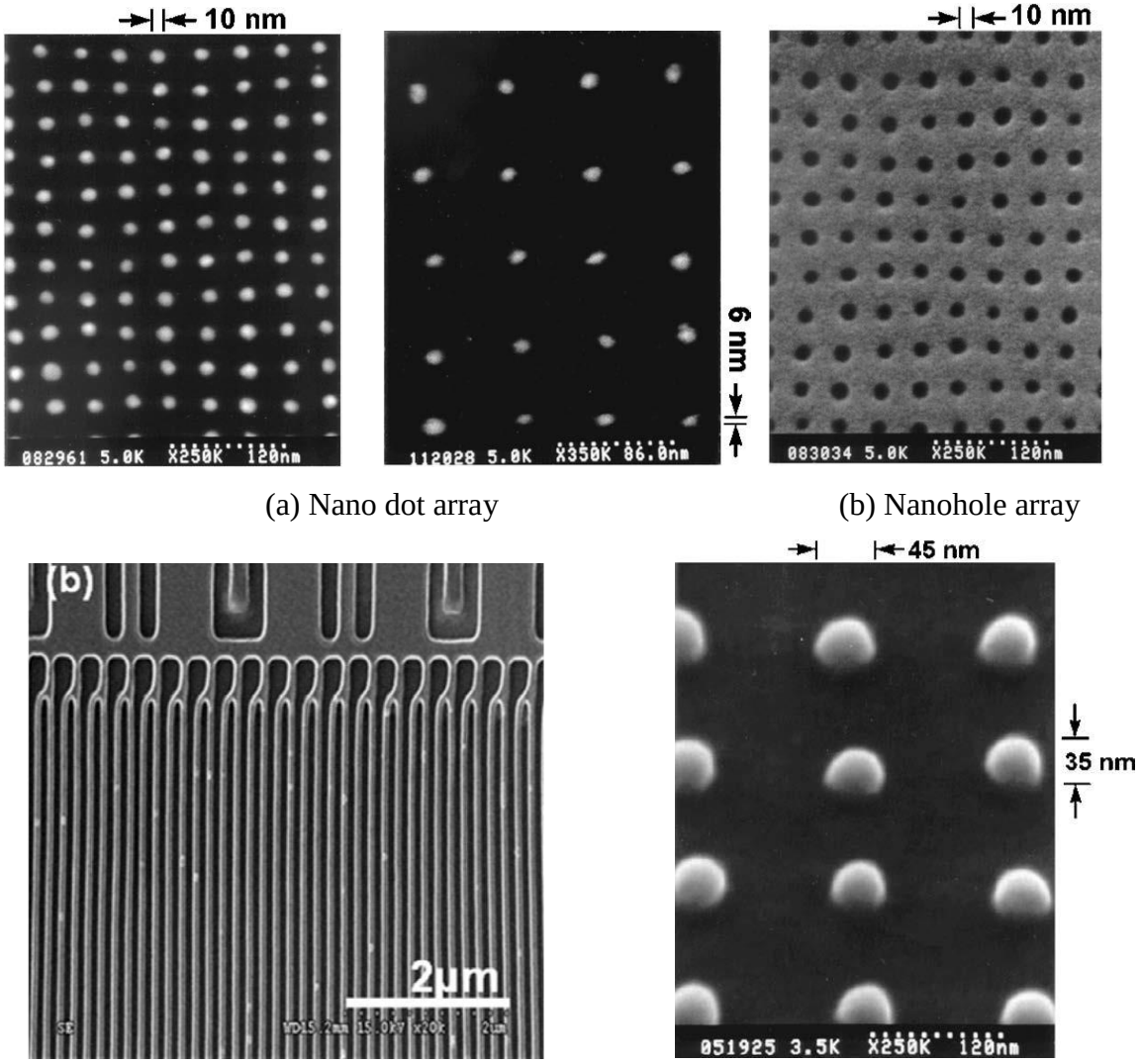

(a) Nano dot array (b) Nanohole array

(c) Line pattern (d) Nanopillar array

Figure 2. 24 Nanostrucures fabricated by nanoimprint lithography

(*Figure copied from Ref. [23, 47, 50]*)

2.2.5 Nanosphere lithography

Nanosphere lithography (NSL) is expected as a low production cost technique for fabrication of regular and uniform arrays of nanoparticles/nano dots. The size of the nanoparticles/nano dots can be controlled by adjusting the size of the nanospheres. Figure 2.25 illustrates a typical NSL process for fabrication of nano dot array.

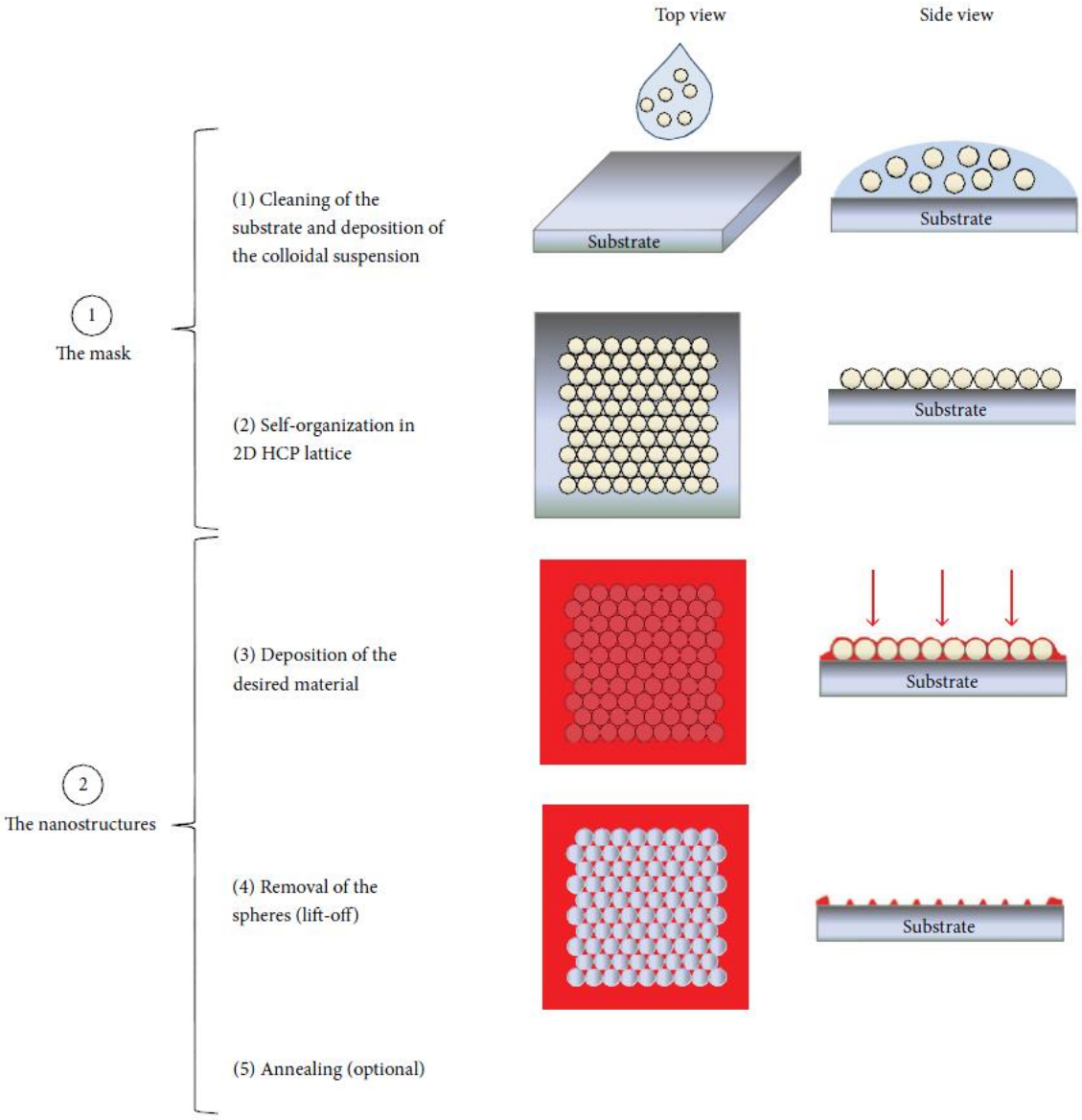

Figure 2. 25 Nanosphere lithography process

(*Figure copied from Ref. [34]*)

NSL process consists of two steps: mask preparation and using the mask for fabrication of nanostructures. Firstly, a flat substrate is coated with a solution of spherical colloids (usually polystyrene nanosphere). After drying process, a hexagonal-close-packed monolayer or bilayer of nanospheres is formed on the substrate. The mask is then utilized as an etching mask or to create a pattern on substrate by deposition through interstices. Finally, the nanosphere mask is removed from the substrate by an adequate solvent. Figure 2.26 illustrates some nanostructures fabricated by NSL.

This method combines the advantages of both top-down and bottom-up approaches that offer capability for fabrication of ordered nanoparticles/nano dot array in relative large area.

However, it has some limitation in the arrangement and shape of the particle/dot. Only the hexagonal-close-packed arrangement of nano dot can be fabricated. Generally, the triangle dots are fabricated on the substrate without other additional process.

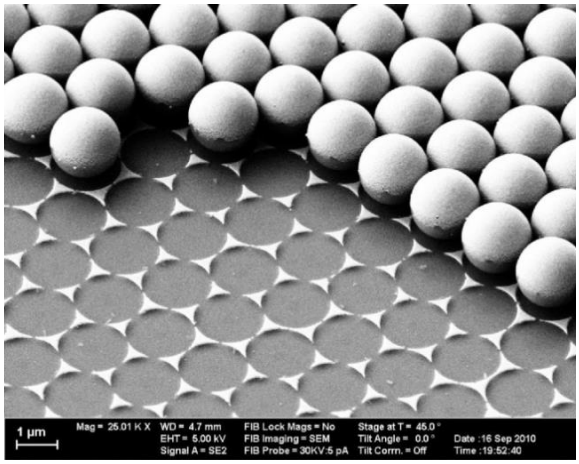

(a) Nanotriangle array

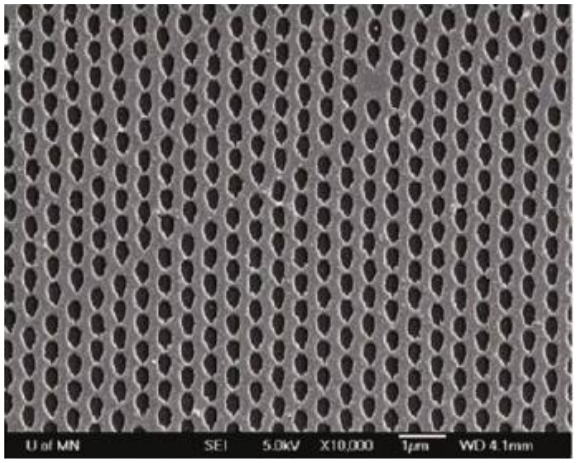

(b) Elliptical silver porous ordered arrays

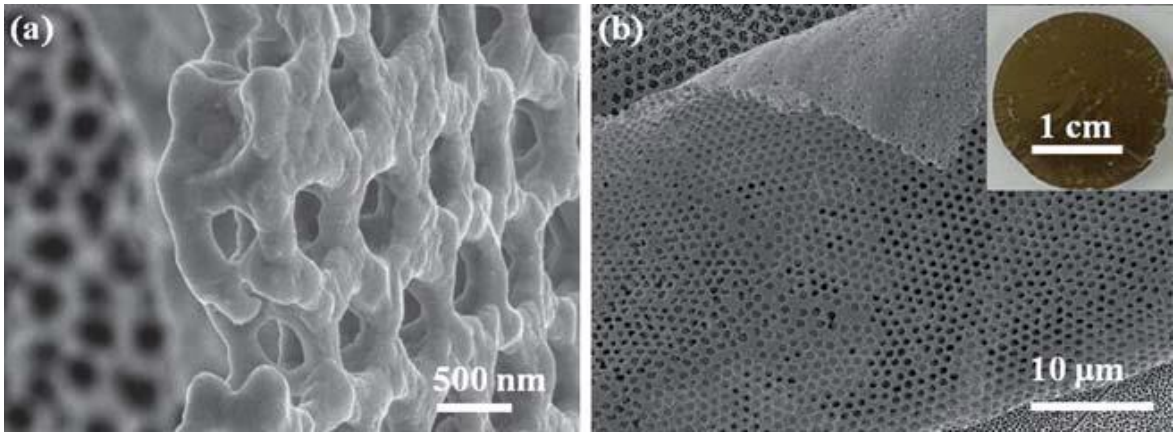

(c) Porous gold nanoparticle films after removing the polystyrene spheres

Figure 2. 26 Nanostrucures fabricated by nanosphere lithography

(*Figure copied from Ref. [161-163]*)

2.2.6 Porous alumina mask deposition

Porous alumina mask deposition (PAMD) employs the alumina mask fabricated by anodization for deposition of material. During anodization, aluminum is oxidized electrochemically. In the anodization process, the aluminum workpiece is the anode in an electrolyte bath, and the cathode is any electrical conductor which is inert in the electrolyte. When the electrical power supply is connected to the anode and cathode, aluminum atoms are ionized to form aluminum anions. Under the electrolyte, the aluminum anions at the

metal surface react with oxygen cations of water molecules to form an oxide layer on the metal. The electrolyte is usually selected so that the oxide layer is insoluble in it; hence, an oxide layer is form on the metal surface. The oxide layer acts as a protection coating from corrosion or an electrical insulation layer. When the electrolyte is a diluted acid, the oxide layer is partially dissolved and becomes porous. As a result, porous alumina layer is produced. A typical experimental set up for anodization is shown in figure 2.27 (a).

Figure 2.27 (b) shows the evolution of porous alumina layer through anodization process. It consists of four steps. In step I, an oxide layer form on the aluminum surface when the aluminum electrode is connected to a DC electric current. Normally, anodization of aluminum is taken placed in an acidic electrolyte, and two competing processes occur at the same time: one is the formation of the oxide layer (alumina layer) through the anodization and the other is the dissolution of the oxide layer in the acidic electrolyte. If the dissolution of oxide layer does not occur, the oxide layer will be thicker and becomes insulating layer which prevent the oxidation process. Consequently, the oxidation process will eventually stop. When the thickness of oxide layer increases, the resistance of this layer increases. This results in an increase in the temperature on the oxide layer and electrical field across the oxide layer. The increase in temperature and high electrical field causes small cracks or fractures on the top surface of oxide layer as seen in step II. In step III, the nanopores are initially formed from these fractures and further develope into large pores when the acidic electrolyte penetrates into the fracture and dissolves the exposed surface of the fracture. In step IV, when the oxidation and dissolution of the oxide layer reach the balance, an ordered hexagonal nanopore structure is formed on the oxide layer.

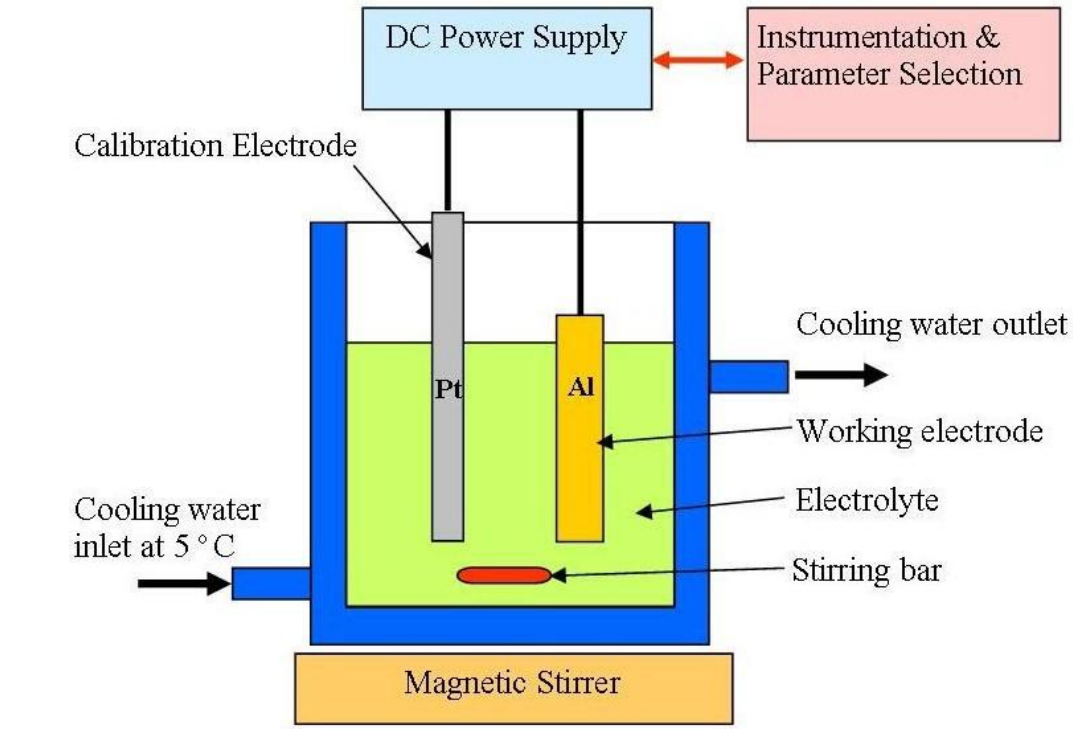

(a) Schematic experimental set up for anodization of aluminum

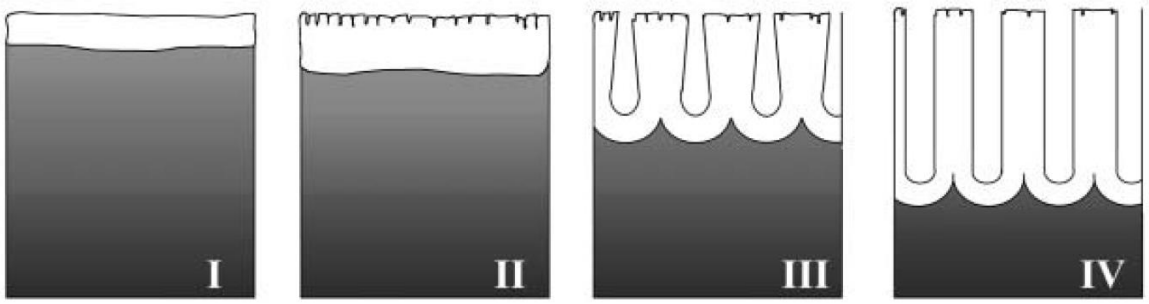

(b) Evolution of prorous alumina layer through anodization process

Figure 2. 27 Experimental setup and evolution of porous alumina layer through anodization process
(*Figure copied from Ref. [164, 165]*)

PAMD has advantages for fabrication of high-density and high aspect-ratio nanostructures which are the challenges for the conventional nanofabrication techniques. Figure 2.28 illustrates some nanostructures fabricated by PAMD. However, PAMD also has several limitations. Firstly, it is very difficult to fabricate and handle the mask in large size. This is because the mask is too thin. Secondly, the arrangement of nanostructure is depends on the order-ness of the pore on the mask which is unchangeable. Finally, the

mask can be used only one time for deposition materials to fabricate nanostructures. Therefore, it is not suitable for high throughput manufacturing.

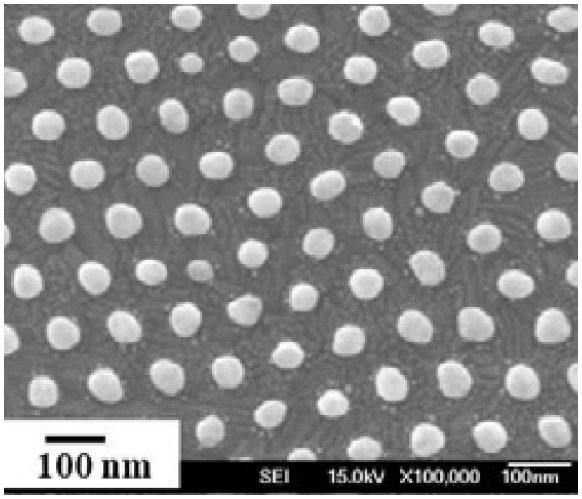

(a) Ordered gold nano dot array

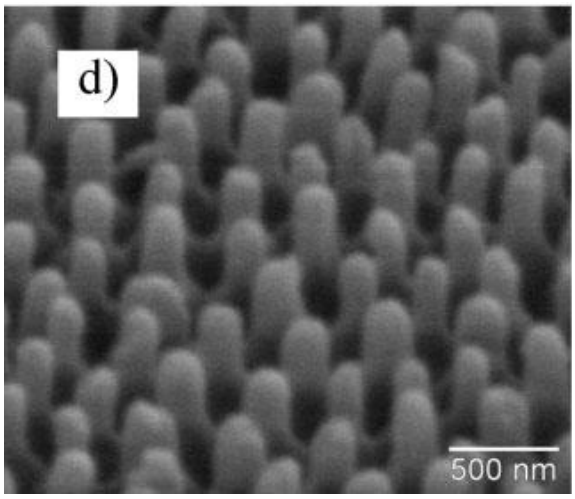

(b) Nanopillar array

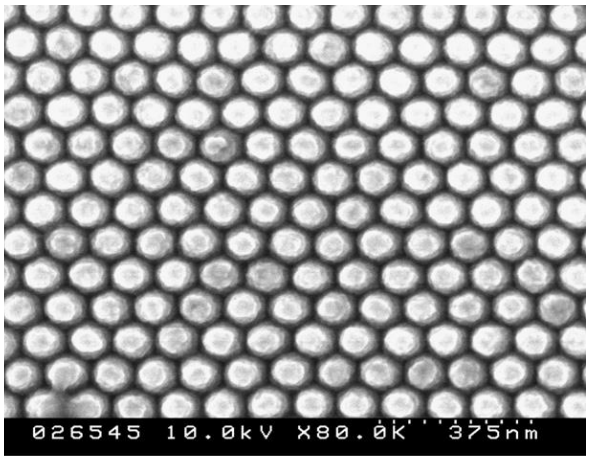

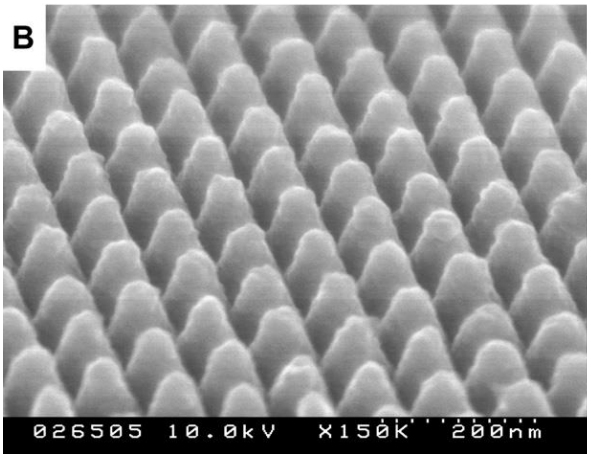

c) Hexagonally ordered conical Ni film

Figure 2. 28 Nanostrucures fabricated by porous anodic alumina deposition

(*Figure copied from Ref. [93, 166, 167]*)

2.2.7 Scanning probe lithography

Scanning probe lithography (SPL) is a simple nanofabrication technique which has capability for drawing of sub-100 nm patterns on various substrate materials by employing a simple, low cost scanning probe microscope (SPM). SPL utilizes the sharp tip of the probe in SPM to transport material to a sample surface to form deposition patterns, or to

pattern on the sample surface by simply scratching, or exposure a thin polymer resist film-coated on the substrate by electron emitted from the probe. SPL can be easily conducted with a scanning tunnel microscope (STM) [168] or an atomic force microscope (AFM) [169] which are two microscopes widely used in laboratories.

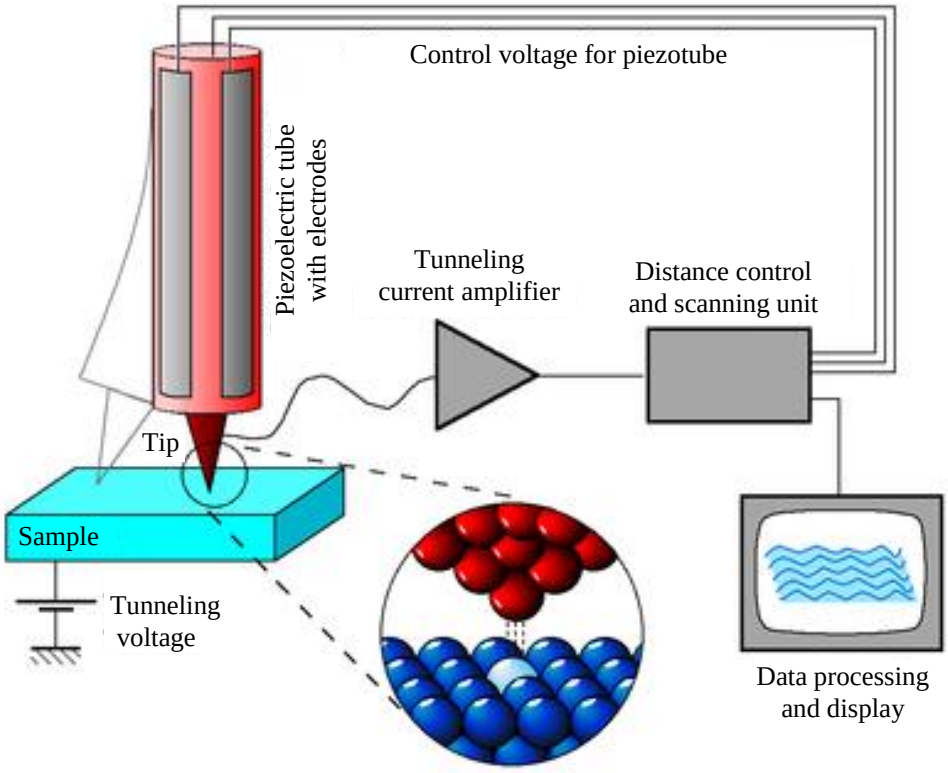

Figure 2. 29 Schematic of scanning tunnelling microscopy

(*Figure copied from Ref. [35]*)

SPL has demonstrated capability of sub-100 nm nanopatterning with accurate alignment and positioning. It can be utilized for either by direct exposure of resists or modification of surface by deposition of mechanically scratching. SPL can be conducted by employing simple, low cost facilities: STM or AFM, which are almost available in laboratories. Figure 2.31 shows some nanopatterns fabricated by SPL. However, SPL also has several limitations. Firstly, SPL employs the tip of the probe to exposure or to modify the sample surface by point-to-point scanning (serial process), the throughput of SPL is very low. Secondly, the energy of the probe tip is very low, so it can be used to exposure only very thin layer of the sample surface or to deposit of pattern with very thin thickness. Thirdly, SPL can fabricate nanopatterns with very small area. Finally, SPL operates based on STM or AFM which are very small in working areas. Therefore, it is unsuitable for large scale nanofabrication.

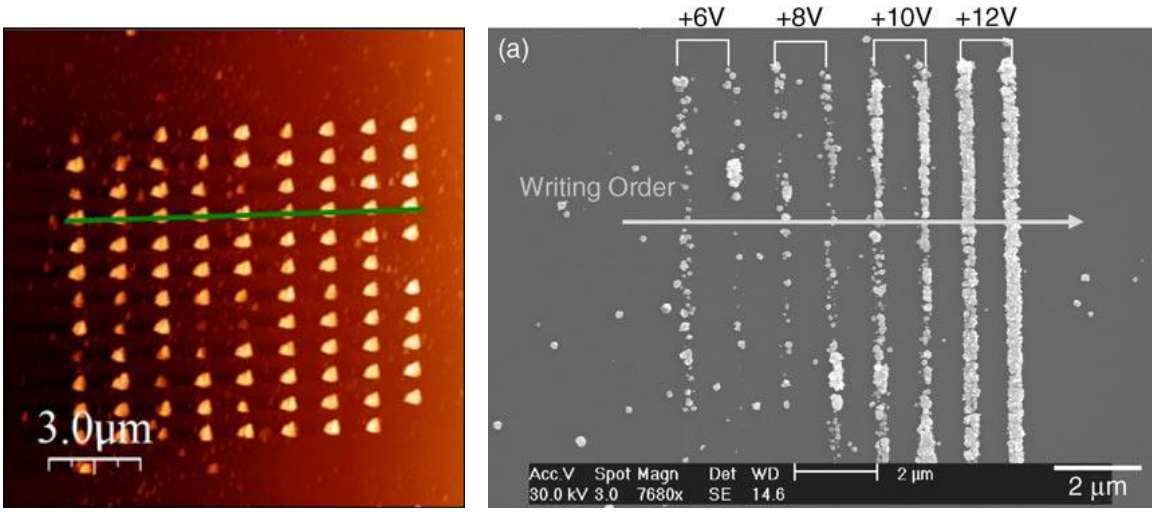

(a) Ti metal nano dot arrays (b) Gold nanowire arrays

Figure 2. 30 Nano dot array and nanowire array fabricated by scanning probe lithography
(*Figure copied from Ref. [170, 171]*)

The major advantages and disadvantages of the aforementioned top-down and bottom-up nanofabrication methods are briefly summarized and shown in figure 2.31.

Methods	Minimum feature size*	Advantages	Disadvantage
UVL	2~1 μm	Very highthroughput Less stringent control Not so expensive facility	Low resolution
DUVL	350~180 nm for 248nm DUV 180~32 nm for 193 nm DUV	High throughput	Expensive facility Stringent control
EUVL	32 nm and below for 13 nm EUV	High throughput	Very expensive facility Very stringent control
XRL	32 nm and below for 13 nm	High throughput	Extreme expensive facility Extreme stringent control
FIB	~20 nm	High resolution	Very low throughput Extreme expensive facility Extreme stringent control
EBL	< 10 nm	Very high resolution	Very low throughput Extreme expensive facility Extreme stringent control
NIL	6 ~ 40 nm	High throughput	Difficult to fabricate the master mold Very expensive master mold
SPL	Few tens nanometers	Low facility cost	Extreme low throughput Very small pattern area
NSL	Few tens nanometers	High througput Low production cost	Limitation in arrangement of structure Limitation in fabrication shape of nanostructure
PAMD	Few tens nanometers	High througput Low production cost	Mask can be used only one time Limitation in area of the mask

** Minimum feature size data is referred from Ref. [13, 152]*

Figure 2. 31 Summary of advantages and disadvantages of nanofabrication processes

2.3 Scope of this research

Recently, with great advances and developments achieved in material science, more and more new materials with outstanding properties have been utilized to replace the conventional materials in semiconductor industry. Among them, plastic semiconductors or polymer semiconductors show great potentials for the future applications such as in organics semiconductor or organics electronic devices [38-42]. This is because plastic materials possess many advanced properties: Light weight, flexible, durable, can produce large area and large quantity, very cheap to produce, and some of them are transparent. These properties make it greatly attractive for the future devices and applications such as bendable display panel, flexible solar cell, etc.

As mentioned previously, metallic nanoparticle/nano dot arrays have great applications to many fields: bio-sensing, bio imaging, and electrical/electronic devices due to their unique properties. In addition, the uniformity and regular arrangement of sub-100 nm in diameter metallic nanoparticle/nano dot arrays shows more improvements and enhancements in the applications than the randomly distributed ones. Therefore, it is expected that the unique properties of ordered metallic nanoparticle/nano dot arrays also can exploited to improve performances of organic semiconductor-based devices, for instant, organic solar cells [139, 140]. In order to employ the unique properties of ordered metallic nanoparticle/nano dot arrays to organic electronics, fabrication techniques to create metallic nanoparticle/nano dot arrays on plastic films or plastic substrates play an important role. However, there is a critical issue that lacking of a cost effective, high throughput, less stringent in operation and environment friendly manufacturing process to fabricate ordered sub-100 nm in diameter metallic nanoparticle/nano dot arrays on plastic films or plastic substrates.

There are many limitations and disadvantages when employing the aforementioned methods to fabricate ordered nanoparticle/nano dot arrays on plastic films (or thin plastic substrate). In the top-down methods like photolithography, EBL or FIB, it is difficult to fix or clamp the plastic film (or thin plastic substrate) accurately on the stage during exposure step since plastic film is very soft as compared with a silicon wafer. The plastic film or plastic substrate is easily bended or form curved surface when it is fixed on the stage since it is soft or flexible. This results in defects in the exposed pattern, hence results in defects in fabricated pattern on plastic film. In addition, the plastic film may be damaged by the

organic solutions used in the development steps of photolithography or EBL. Furthermore, resolution of photolithography is suffered to the diffraction limit; resolution of EBL and FIB are suffered to the scattering of electron in the resist material or ion in the work materials. Also, these methods require very stringent control, and the facility cost is very expensive. NIL lithography provides high throughput in fabrication of nanopatterns on plastic substrate [45-50]. However, the master mold for replicating the elastomer stamp or the hard stamp used in nano-transfer printing is usually fabricated by EBL or FIB or other lithography techniques. Therefore, the disadvantages of conventional lithography techniques still exist in NIL. In addition, the resolution of fabricated master mold is limited by the resolution of those processes.

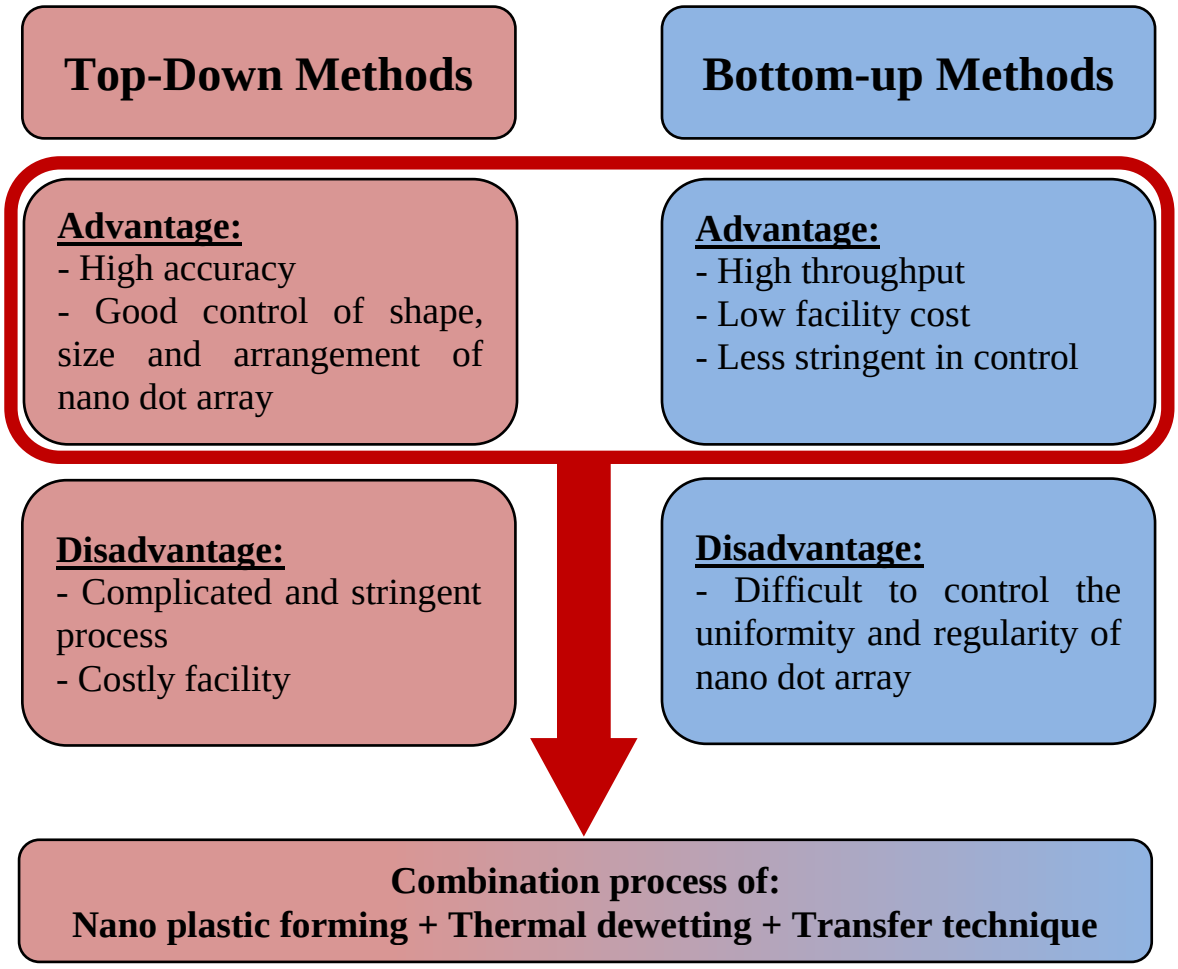

Figure 2. 32 The proposed process for fabrication of a nano dot array on a plastic film

On the other hand, in the bottom-up methods such as NSL, PAMD, and self-assembly methods like thermal annealing have capability of fabrication of nano dot arrays on plastic

film at high throughput and lower production cost. However, it is very difficult to control the regularity and the arrangement of nano dot arrays fabricated by these methods.

In order to overcome the limitations of both top-down methods and bottom-up methods, in this research work, a new fabrication method is developed to fabricate ordered sub-100 nm in diameter metallic nano dot array on plastic film as illustrated in figure 2.32. The process combines the nano-plastic forming assisted thermal dewetting on a patterned substrate and transfer technique. The patterned substrate is fabricated by nano-plastic forming which is high accuracy, simple in operation. NPF simply employs a knife-edge single crystal diamond tool to mechanically indent on the substrate surface to create nanopatterns. NPF does not require expensive facility but provides high resolution, high accuracy, and does not suffer to the diffraction limit as conventional lithography techniques. In addition, it is environmental friendly because no toxic gas or chemical was used. Nano dot array formed on the patterned substrate by thermal dewtting which is also a high throughput process using a simple and low cost electric furnace. Then, the ordered nano dot array is transferred to a plastic film. Therefore, the proposed process is expected to achieve high throughput, high accuracy, simple in operation, and low facility.

2.4 Summary

Nanoparticle/nano dot arrays have broad applications to various fields such as bio-sensing, bio-imaging, and electrical/electronic devices. The future trend of application of nanoparticle shows great demands of ordered nanoparticles/nano dots with good uniformity in shape, size and well aligned in desired arrangements. In addition, fabrication of these nanoparticles/nano dots arrays in large area is also very important to realize their application to commercial devices. Furthermore, fabrication of nanoparticles/nano dot arrays on polymer or plastic film or substrate is highly desired for the development of organic electronic devices.

Various nanofabrication techniques have been developed for fabrication of nanostructures in general and nanoparticle/nano dot array in particular. Especially, in fabrication of an ordered nano dot array on a plastic film, these methods suffer many limitations and disadvantages. With the aim to overcome these limitations and disadvantage, in this research work, a new fabrication process is developed for fabrication of sub-100 nm in diameter nano dot array on a plastic film.

CHAPTER 3

Fabrication of a random nano dot array on a plastic film

In this chapter, firstly, the concept of the process to fabricate a random nano dot array on a plastic film by thermal dewetting and transfer technique is presented. The experimental details including experimental procedure and conditions to investigate the effect of process conditions on the morphology, on the optical property of nano dot array, and on the transfer ratio are presented. Then, the experimental results are presented and discussed. In addition, the mechanism to transfer nano dots from a substrate to a plastic film will be presented. Finally, the main investigations and results are summarized.

3.1 Concept of process to fabricate a random nano dot array on a plastic film by thermal dewetting and transfer technique

Figure 3.1 illustrates the concept of the proposed process to fabricate a random nano dot array on a plastic film [53]. The process consists of three steps; firstly, substrate is deposited with a thin layer of metal. Then, metal coated substrate is subjected to thermal dewetting to cause the aggregation of metal film into nano dot array. Finally, the nano dot array is transferred to a plastic film. It is expected that the substrate can be re-used after transferring the nano dot array to a plastic film. After the nano dot array is transferred to the plastic film, the substrate is cleaned and reused to fabricate another nano dot array on another plastic film by repeating same process. Therefore, it is expected that this process can achieve high throughput.

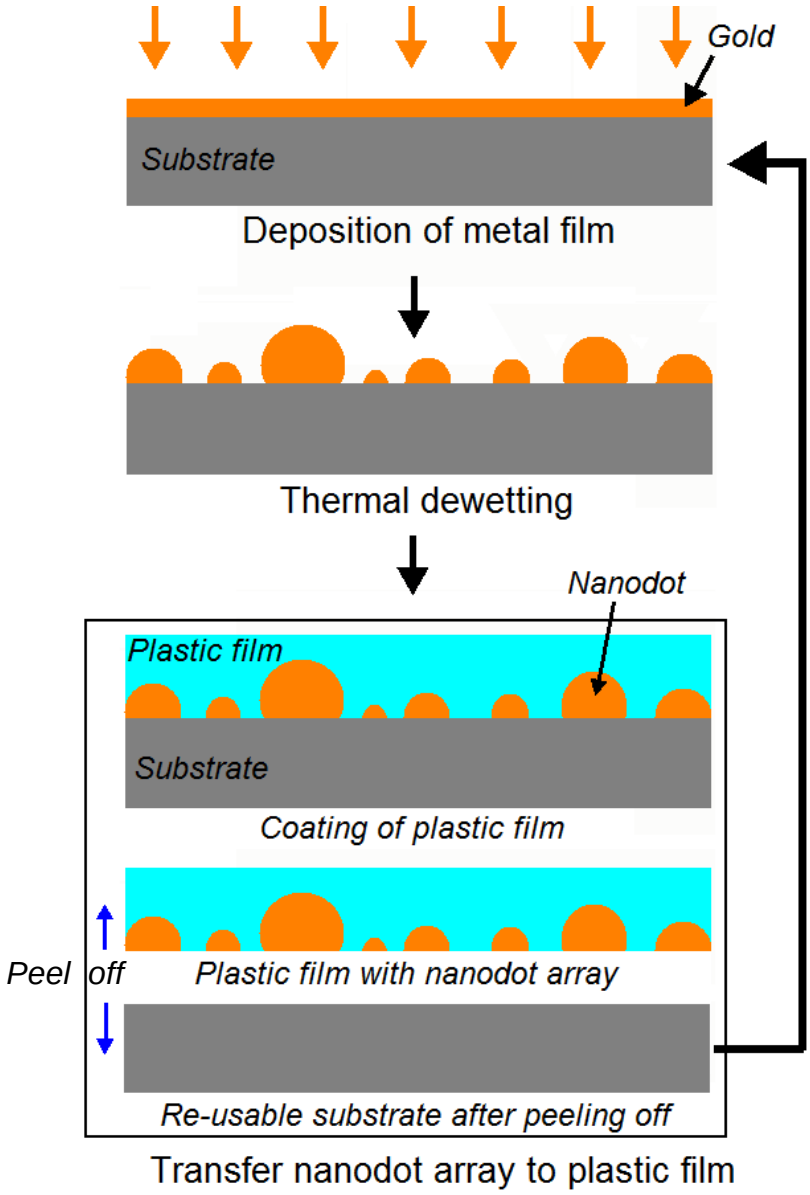

Figure 3. 1 Schematic of process to fabricate a random nano dot array on a plastic film

3.2 Experimental method

3.2.1 Specimen preparation

In the experiments, two kinds of substrate materials were used; one is quartz glass slide (Saito Optics Co., Ltd.) and the other is silicon <110> wafer (Sumco Corp.). Quartz glass slide and silicon wafer were cut in sizes of 10 mm in width and 10 mm in length. The thickness of the quartz glass slide was 1 mm and thickness of the silicon wafer was 0.6 mm. Gold was used as dot material. Three kinds of plastic materials were used. The first

one is polydimethylsiloxane (PDMS); the second one is Araldite rapid epoxy and the last one is SpeciFix-20 epoxy. These plastic materials are selected because they have different adhesion property. It is known that PDMS have poor adhesion property while other two epoxies have good adhesion property. Choosing different adhesion plastic materials is meaningful to investigate the effects of process conditions on the transfer ratio of nano dot array. In addition, PDMS and SpeciFix-20 epoxy are clear and transparent which is useful for investigating the optical property of nano dot array fabricated on plastic film. Moreover, these plastic materials are non-toxic, cheap, and widely used in laboratories.

3.2.2 Experimental procedure, apparatus and conditions

The quartz glass substrate and silicon substrate were cleaned in acetone by using ultrasonic bath for 10 minutes. Then, they were dried by a rubber air blower. Gold was deposited on the surface of the substrates by a DC sputter coater. Figure 3.2 shows the apparatus used for DC sputter coating processes. The sputter gas was Argon (Ar), and its pressure was 15 Pa. The distance between the substrate and a gold target was 35 mm. The sputtering current was kept to 5 mA during sputter deposition. The thickness of the deposited gold film was controlled from 6 nm to 14 nm, by controlling the sputtering time. It was confirmed that when the gold film thickness is thicker than 5 nm, whole substrate surface is covered by gold film, and the gold film appears as a continuous and smooth surface. In order to control the thickness of gold film accurately, the sputter rate was measured beforehand. The sputter rate was determined as follows: Gold was deposited on a substrate for a determined period of time. Then, some part of the gold film on substrate was peeled off by using the Scotch tape. The height of the step between gold surface and peeled off surface was measured by AFM (i.e., the height is the thickness of gold film). The sputter rate was calculated based on AFM data.

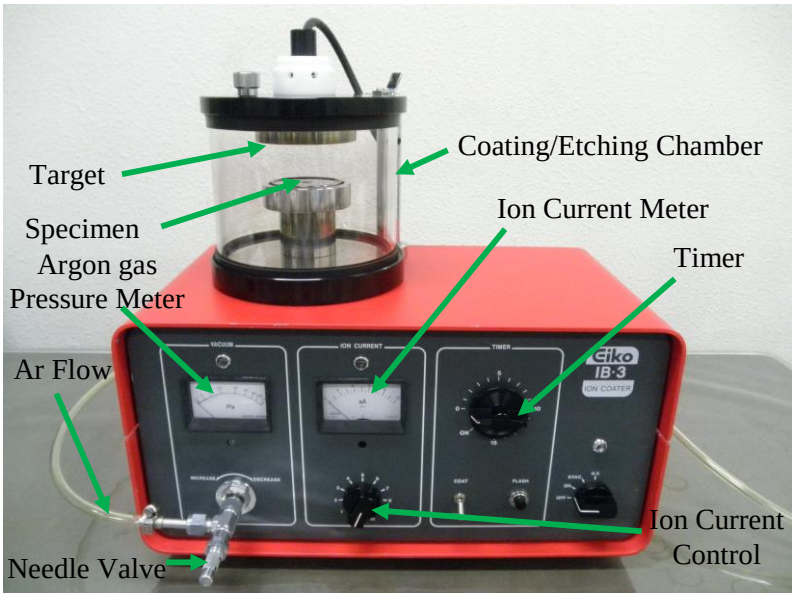

Figure 3. 2 DC sputter coating apparatus

The gold coated substrates were then subjected to thermal annealing in air by using an electric furnace (F-120-SP, TKG Tokyo Japan). Figure 3.3 shows the electric furnace used for the annealing process. The temperature is accurately controlled by a program controller. The furnace chamber is pre-heated to a defined temperature that is maintained throughout the annealing process. The specimen is then inserted into the furnace chamber. In this experiment, five levels of annealing temperatures were examined: 600°C, 700°C, 800°C, 900°C, and 1000°C. Eight annealing time durations were examined: 5, 10, 15, 20, 30, 60, 90, and 120 min. The specimens were then taken out from the furnace and cooled down in the air atmosphere. By this annealing operation, the aggregation of the gold film deposited on the substrates into random gold nano dots was realized. The deposition and thermal annealing conditions are summarized in the Table 3.1.

Table 3. 1 Deposition and annealing conditions

Substrate	Au coating (nm)	Annealing	
		Temp. (^{o}C)	Time (min)
Si <110>, Quartz glass	6, 8, 10, 12, 14	600, 700, 800, 900, 1000	5, 10, 15, 20, 30, 60, 90, 120

Figure 3. 3 Electric furnace used for annealing process

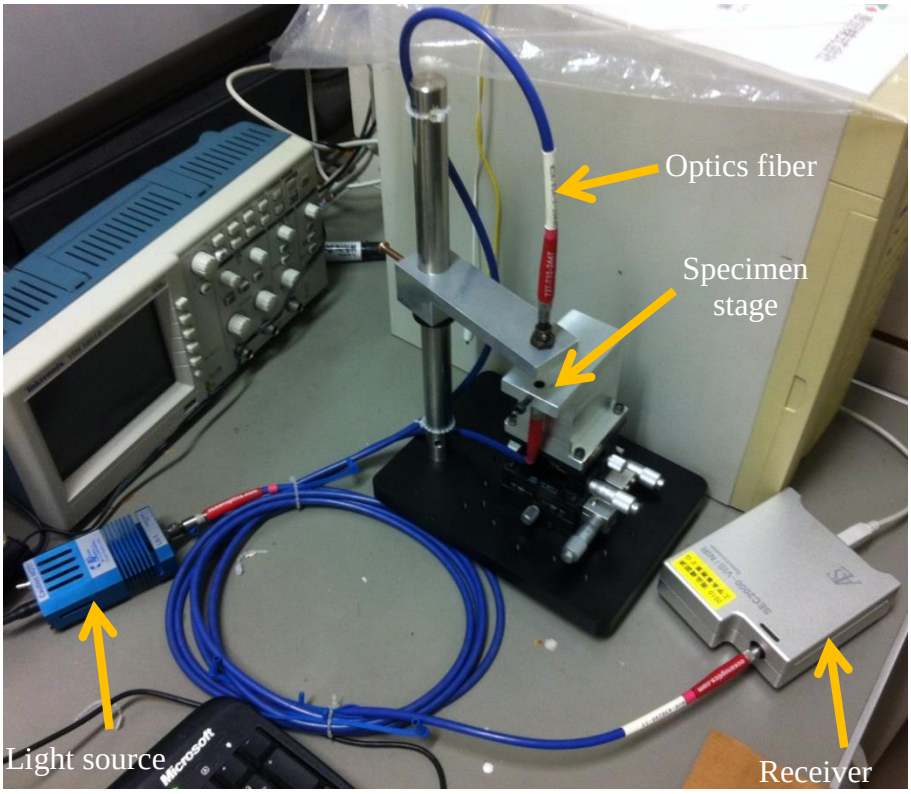

Figure 3. 4 Ultraviolet-visible spectrometer

The LSPR absorption spectrum of the nano dots on the quartz glass substrates was examined by using a transmission ultraviolet-visible (UV-VIS) spectrometer (SEC2000-VIS/NIR spectrometer). Figure 3.4 shows the UV-VIS spectrometer used for absorption spectrum measurement. That is an optical fiber measurement system. The measured spot size is about 0.5 mm in diameter. The absorption spectrum was measured in the visible range (400 nm to 800 nm).

The experiment for transferring of a nano dot array from a substrate to a plastic film is conducted as follows: after annealing, the nano dots on the quartz glass substrates and the silicon substrates were characterized by using a field-emission scanning electron microscope (FE-SEM, JSM-6301F JEOL). After drying the substrates by blowing with hot air for 2 min, the substrates were coated with a thin layer of plastic mixtures. The thickness of the plastic layer is estimated from 0.5 to 1 mm. Three kinds of plastic mixture were examined in the experiment; one is Araldite rapid epoxy (a high viscosity epoxy) and the other is SpeciFix-20 epoxy (a low viscosity epoxy) and the last one is polydimethylsiloxane (PDMS). The processing conditions for each plastic material are as follows:

Araldite rapid epoxy mixture (mass ratio of epoxy:curing agent is 1:1) was coated on the nano dots surface. Then, the epoxy coated substrate was cured at room temperature for 48 hours to completely harden the epoxy film. Finally, the epoxy film was peeled off from the substrate by using tweezers after slightly heat up the substrate at 80°C for 50 s on a hot plate. After peeling off from the substrate, the plastic film was pressed on a flat plate to return to its original form (flat surface of the epoxy film which is in contact with the substrate surface).

SpeciFix-20 epoxy mixture (mass ratio of epoxy:curing agent is 7:1) was coated on the nano dots surface. The epoxy coated substrate was put in vacuum chamber for 15 minutes to remove the bubbles and gas at the interface between the nano dots and the epoxy. Then, the epoxy was cured at room temperature for 48 hours. Finally, the epoxy film was peeled off from the substrate with the same procedures for Araldite rapid epoxy film.

PDMS mixture (SILPOT 184 and SILPOT 184 CAT with mass ratio is 10:1) was coated on the nano dots surfaces. The PDMS coated substrate was put in vacuum chamber for 15 minutes to remove the bubbles and gas at the interface between the nano dots and the PDMS. Then, the PDMS were cured at 120 °C for 2 hours. Finally, the PDMS films were peeled off from the substrate under ambient condition by using tweezers.

It was confirmed that there is almost no damage occurred on the surface of both epoxy films and PDMS film after peeling off from substrates. The processing conditions for these three plastic materials are summarized in Table 3.2.

Table 3. 2 Processing conditions for three plastic materials

	Araldite rapid Epoxy	**SpeciFix-20 epoxy**	**PDMS**
Mass ratio with curing agent	1:1	7:1	10:1
Put in vacuum	No	15 min	15 min
Curing	Room temperate, 48 hours	Room temperate, 48 hours	120^{o}C 2 hours

The morphology of the nano dots on the substrates was then observed by using a field-emission scanning electron microscope (FE-SEM, JSM-6301F JEOL). Five positions were observed for each specimen. The mean diameter, contact angle and circularity of nano dots were evaluated from FE-SEM micrographs by using a graphic analysis system (ImageJ software). In calculation of dot diameter, the area of each dot was determined from FE-SEM micrograph by the graphic analysis system and we assumed that an equivalent circle whose area equals to area of a dot. Then, the equivalent diameter was calculated. The contact angle was evaluated based on the assumption that the metal volume was conserved through annealing process.

3.3 Results and discussions

3.3.1 Effect of process conditions of nano dot morphology

Figure 3.5 shows the FE-SEM micrographs of gold nano dots aggregated on (a) quartz glass substrates and (b) silicon substrates by thermal annealing. The annealing condition was 600 °C for 10 min. The thickness of gold film was varied from 6 to 14 nm. It is found

that the dots become larger when the gold film becomes thicker, and it appears that the morphology of the dots becomes more circular when the gold film is thinner.

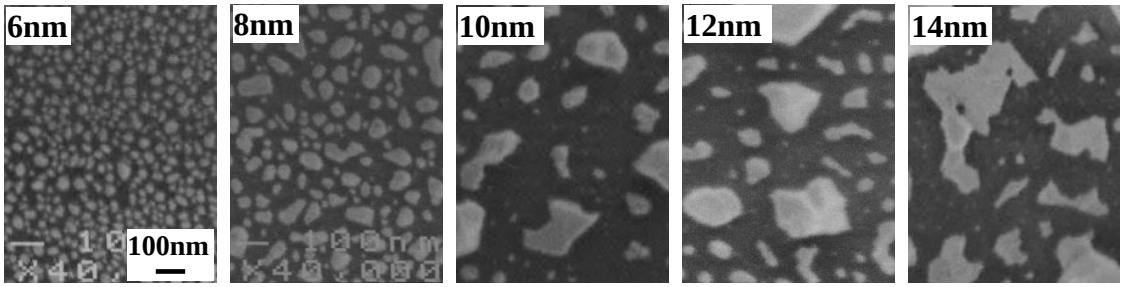

(a) Nano dots on quartz glass substrates

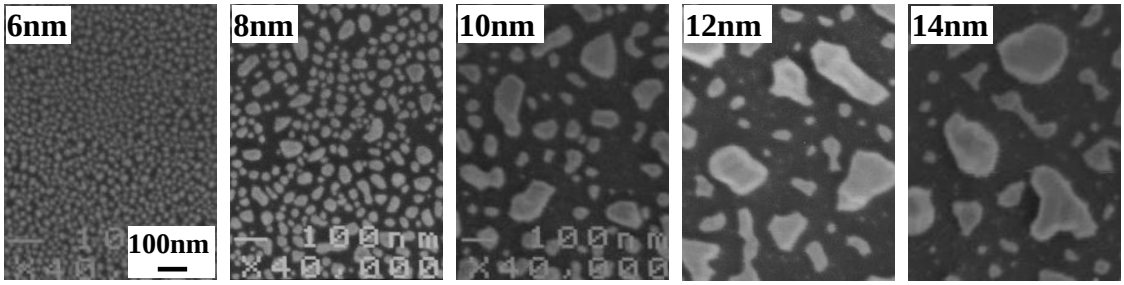

(b) Nano dots on silicon substrates

Figure 3. 5 FE-SEM micrographs of gold nano dots formed on (a) quartz glass substrates and (b) silicon substrates coated with different gold film thicknesses.

Figure 3.6 shows the variation of the mean equivalent diameter of the nano dots and its standard deviation against the thickness of gold film. To calculate the dot diameter, the area of each dot was firstly determined from FE-SEM micrographs using ImageJ analysis software; the diameter of an equivalent circle, whose area equals to area of a dot, was then calculated. Hereafter, for brevity, the word "dot diameter" is used instead of "equivalent diameter of the nano dot." From Figure 3.6, it is found that both the mean diameter of the nano dots and the standard deviation increase with the increase in the thickness of the gold film on both substrates. The mean diameter of the nano dots on the silicon substrate is slightly smaller than that of the nano dots on the quartz glass substrate, when the thickness of gold film is less than 10 nm. It is known that the voids exist on the gold film after deposition on a substrate [172]. During the annealing process, these voids progressively widen and separate the gold film into isolated islands. With an increase in the annealing time, these distorted islands are aggregated into circular dots to minimize the total energy of the system [173].

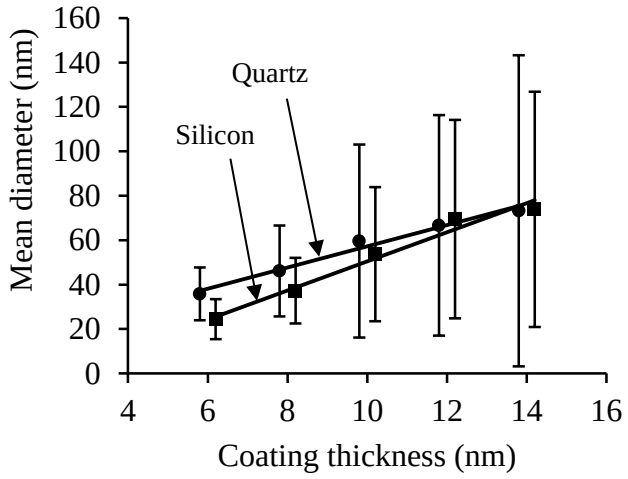

Figure 3. 6 Mean diameter and standard deviation of gold nano dots versus gold film thickness. The annealing condition is at 600°C for 10 min.

When the gold film is thinner (6 to 8 nm), the density of the voids is high. As a result, the mean diameter of the nano dots becomes small. In addition, the aggregation is completed in a shorter time when the dot diameter is small. Thus, most dots are circular, and the standard deviation of the dot diameters is small. On the other hand, when the gold film is thicker (10 to 14 nm), the density of the voids is low. As a result, the dot diameter is large. Since, the aggregation takes a longer time when the dot diameter is larger; most of the large dots remain distorted. Therefore, the standard deviation of dot diameters is larger than that of the small dots.

When the gold film is thicker (10 to 14 nm), the dot aggregation process is not completed. The dot shapes are distorted with a broad dispersion in dot diameters. The dot diameter distributions are almost overlapping and the difference between the morphology of the dots on both substrates is not apparent. However, when the gold film is thinner (6 to 8 nm), dots are aggregated to a greater extent and the dot shape is more circular and uniform. The difference in the dot aggregation characteristics between a silicon substrate and a quartz glass substrate becomes more apparent when the gold film thickness is less than 8 nm, as seen in Figure 3.5 and Figure 3.6; dots on a quartz glass substrate are larger than dots on a silicon substrate. Thus, thickness of gold film is adjusted to 8 nm hereafter for the experiment to investigate the effects of substrate material on the morphology of nano dots.

Figure 3.7 shows the FE-SEM micrographs of gold nano dots aggregated on (a) quartz glass substrates and (b) silicon substrates after annealing. The annealing temperature was varied from 600°C to 1000°C at a step of 100°C, and annealing time was fixed at 10 min for all cases. The thickness of gold film was 8 nm for all specimens. For all cases, it is observed that many gold dots smaller than 100 nm were formed on both substrates. It is found that the dots shape becomes more circular when the annealing temperature is higher. Also, it seems that the dots are smaller when the annealing temperature is higher. Silicon substrates and quartz glass substrates provide different morphologies of nano dots. The dots aggregated on a quartz glass substrate are large and sparse, while the dots aggregated on a silicon substrate are small and dense.

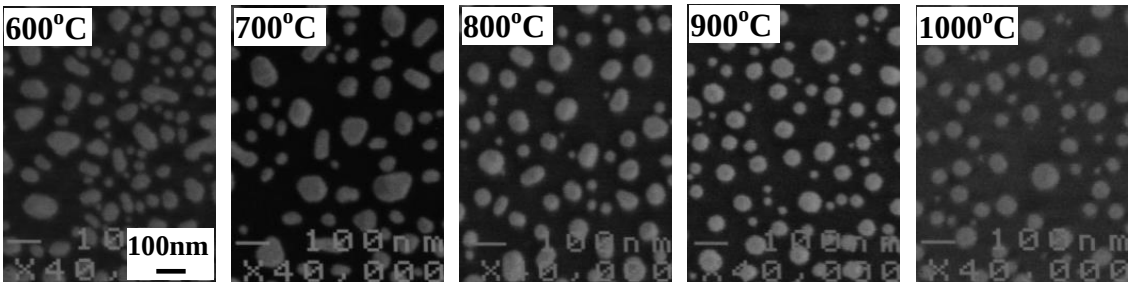

(a) Nano dot array on quartz glass substrate

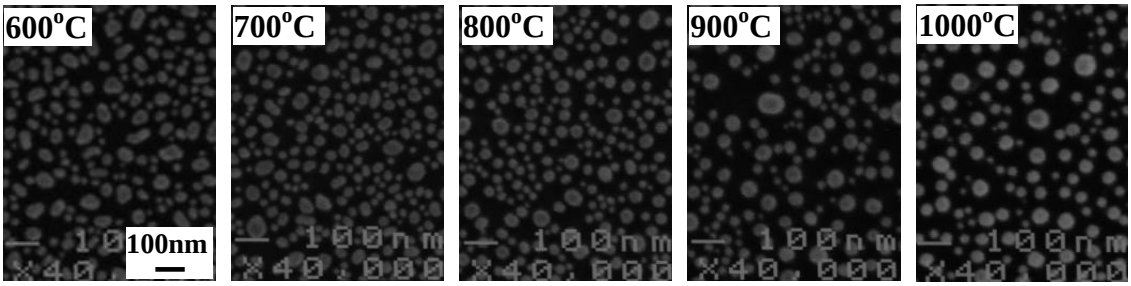

(b) Nano dot array on silicon substrate

Figure 3. 7 FE-SEM micrographs of gold nano dot array formed on (a) quartz glass substrate and (b) silicon substrates after annealing at different temperatures

It is known that the eutectic reaction between gold and silicon occurs at temperature higher than 363°C [174, 175]. However, in this study, it is not considered that this mechanism affected so much to the aggregation of gold film. This is because a thin layer (on the order of tens of nanometers) of silicon dioxide, SiO_2, exists on the surface of the silicon wafer under the ambient condition [176, 177]. Since the silicon dioxide layer was

not removed in our experiment, it may prevent a eutectic reaction between the gold layer and the silicon substrate. In addition, the annealing time in this research was so short that the eutectic reaction occurred.

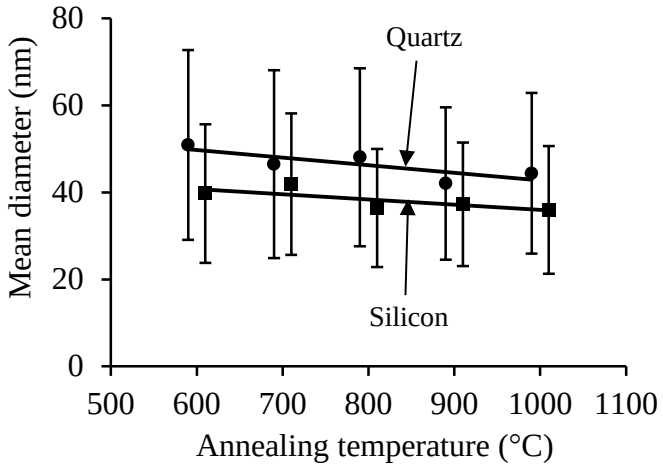

Figure 3. 8 Mean diameter and its standard deviation of gold nano dots versus annealing temperature. Annealing time is 10 minutes. Thickness of gold film is 8 nm.

Figure 3.8 shows the variation in the mean diameter, with the standard deviation of the nano dots against annealing temperature. It is found that the mean diameter of the nano dots slightly decreases with the increase in the annealing temperature both on the quartz glass substrate and the silicon substrate. The standard deviation also slightly decreases when the annealing temperature becomes higher. This is because aggregation depends on surface diffusion, which is governed by the Arrhenius equation:

$$D = D_0 exp(\frac{-Q}{RT}) \tag{3.1}$$

where D is the diffusion coefficient, D_0 is diffusion constant, Q is the activation energy of diffusion, R is gas constant, and T is absolute temperature. D becomes larger under higher annealing temperature. Upon thermal annealing, the voids that exist in the gold film will progressively widen, elongate, and separate the gold film into isolated islands with various shapes. With the increase in the annealing time, these distorted islands aggregate into spherical-cap-shaped dots with a lower surface-to-volume ratio in order to minimize the total energy of the system [173].

When the annealing temperature is low, atomic diffusivity is low and thus, the aggregation process is slow. The aggregation of the distorted islands into dots is not completed. As a result, the dots remain distorted. On the other hand, the atomic diffusivity is higher when the annealing temperature is higher. Thus, the aggregation process is faster. The aggregation of the distorted islands into dots is more complete. As a result, the dots are more circular (as seen in Figure 3.7) with a lower surface-to-volume ratio compared to the dots aggregated at a lower temperature. Therefore, the dot diameters are smaller and more uniform at a higher annealing temperature. Even though the dispersion of the dot diameter is large, a trend of decreasing dot diameter and standard deviation with the increase in the annealing temperature still occurs.

Figure 3.9 shows the variation of surface coverage of the nano dot array against annealing temperature. It was found that the surface coverage decreases as the annealing temperature increases for both the silicon substrate and the quartz glass substrate. The silicon substrates result slightly higher surface coverage of the nano dot array than the quartz glass substrates.

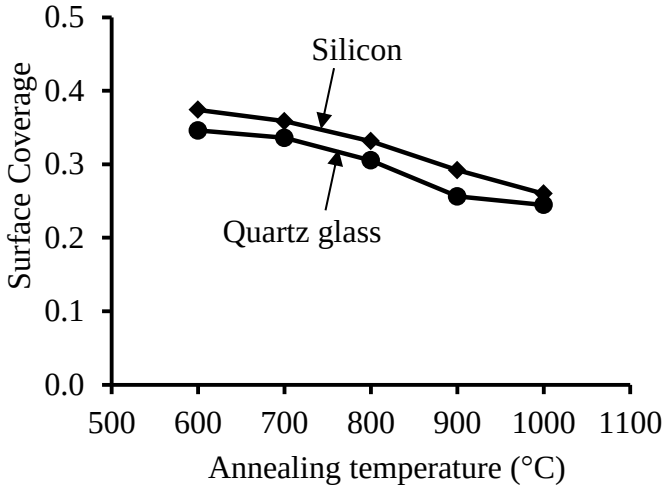

Figure 3. 9 Surface coverage of gold nano dot array versus annealing temperature

The differences in the dots diameters in Figure 3.8 and surface coverage in Figure 3.9 are attributed to the differences in the contact angles between the dots and substrates. Figure 3.10 shows the variation in the contact angle of the nano dots against annealing temperatures. The contact angle is evaluated by the method in Ref. [53]. It is found that the contact angle increases when the annealing temperature becomes higher. This is because the dots were not aggregated completely when the annealing temperature is low (from

600 °C to 800 °C). As seen in Figure 3.7, many distorted dots were generated at annealing temperatures lower than 800 °C. Thus, the dots were still flat, and average contact angle was low. On the other hand, the complete aggregation was achieved and circular dots were formed when the contact angle was high at higher annealing temperatures (900 °C and 1000 °C). The contact angle of the nano dots on a silicon substrate is slightly higher than that of the nano dots on a quartz glass substrate. This is because the surface energy of silicon <110> substrate is lower than that of quartz glass substrate (the surface energy of the silicon <110> substrate is 1510 erg/cm2 [178] and the quartz glass substrate is 1825 erg/cm2 [179]). According to Young's equation, the contact angle of the dot is higher when the surface energy of the substrate is lower.

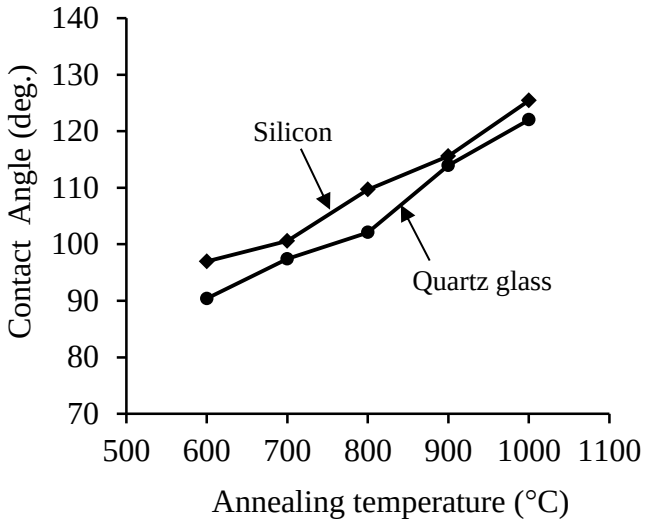

Figure 3. 10 Contact angle of nano dots versus annealing temperature.

Figure 3.11 shows the variation in the average circularity of the nano dots against the annealing time. The solid line is data of the quartz glass substrate, and dashed line is data of the silicon wafer. The circularity is defined as follows:

$$C = \frac{L_{min}}{L_{max}} \tag{3.2}$$

where L_{max} and L_{min} are the length of the major and minor axis of a dot, respectively. When C is equal to 1, the dot shape is a perfect circle. A slight difference is observed between the circularities of the dots on the quartz glass substrate and the silicon substrate. It is found that the circularity of the nano dots increases with the increase in either annealing temperature or annealing time. When the annealing time is long enough, the circularity is

saturated to a certain value that depends on the temperature. It is regarded that the dot aggregation is completed in this stage. This phenomenon is attributed to the surface diffusion of atoms. The annealing time necessary to complete aggregation depends on the annealing temperature.

In this experiment, the aggregation completed in 20 min at 900°C, but 10 min at 1000°C. The saturated circularity increases with the increase in the annealing temperature. Maximum circularity obtained in this experiment is almost 0.9 when the annealing temperature is 1000°C.

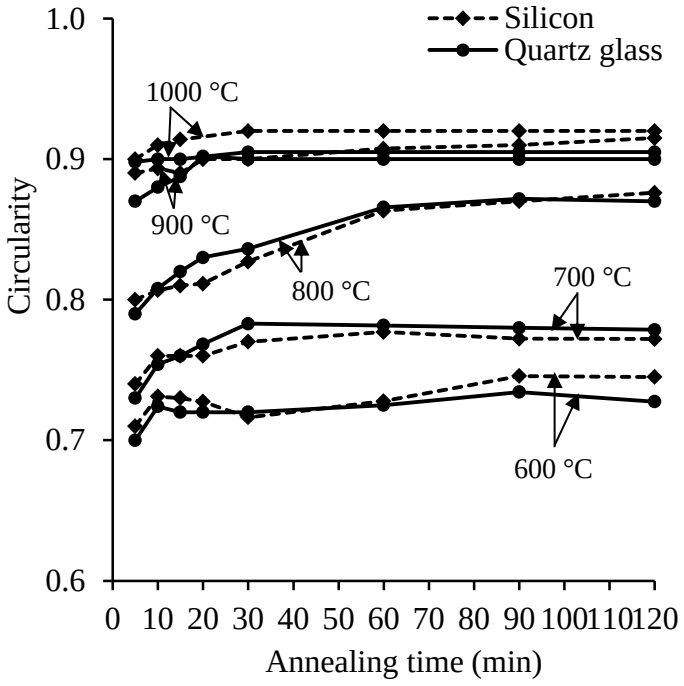

Figure 3. 11 Circularity of nano dots versus annealing time.

3.3.2 Effects of process condition on the LSPR property of nano dot array

The quartz glass substrate is utilized to investigate the LSPR property of the nano dots. Figure 3.12 shows absorbance spectra of the nano dots generated on the quartz glass substrates against thickness of the gold film. In this experiment, five thicknesses of gold film were examined: 6, 8, 10, 12, and 14 nm. The annealing temperature was 600 °C, and the annealing time was 10 min. The peak of absorbance spectra is found in the range of 550 to 750 nm. It is found that the wavelength and intensity of the absorbance peak are dependent on the gold film thickness. With the increase in the gold film thickness, the peak

wavelength and the peak intensity both increase and the peak also becomes broader. The absorbance peak is clearly seen when the gold film thickness is in between 6 and 8 nm, whereas the peak becomes unclear when the gold film thickness is more than 10 nm. This is attributed to the difference in the dot circularity. As shown in Figure 3.5, circular dots are generated when the gold film is thin (6 nm in thickness) but distorted dots are generated when the gold film is thick. It was reported that nano dots with lower aspect ratio and uniform shape have a narrower absorbance spectra peak [173, 180].

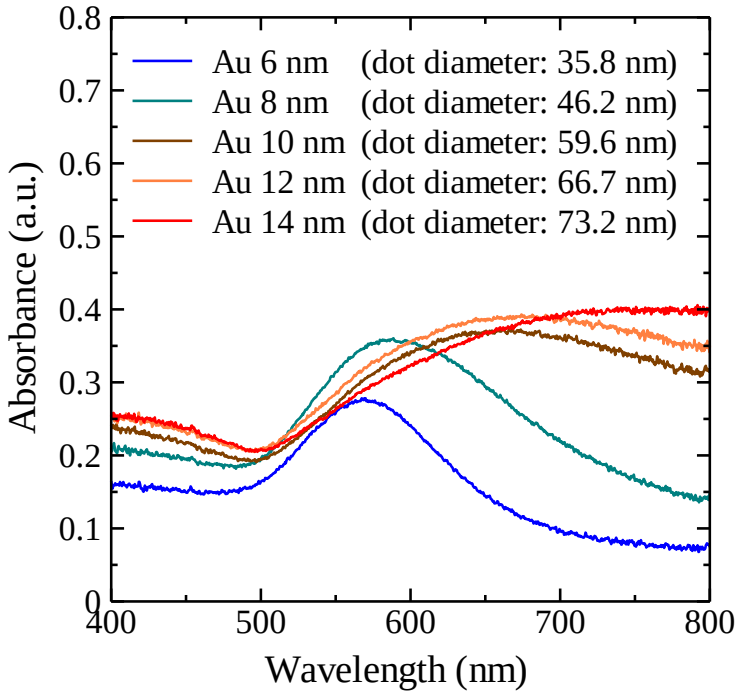

Figure 3. 12 Absorbance spectra of gold nano dots for different gold film thicknesses. Annealing condition is at 600°C for 10 min.

Figure 3.13 shows the effects of annealing temperature and annealing time on the absorbance spectra of the nano dots on the quartz glass substrate. The thickness of gold film was 8 nm. Five annealing temperatures were examined from 600°C to 1000°C at intervals of 100°C. The annealing time was varied from 5 to 120 min. The data of the nano dot diameter and its standard deviation are presented in the Appendix A. It is found that the peak wavelength is shifted to the blue side (short wavelength) when the annealing temperature is increased. It is also found that the peak wavelength is shifted to blue side with an increase in the annealing time. Simultaneously, the peak intensity decreases with the increase in either annealing temperature or annealing time. With the increase in either

annealing temperature or annealing time, the nano dots become smaller, more circular, and more uniform. This results in the absorbance peak shift to the short wavelengths side and the peak becomes sharper [173, 180]. At the same time, the interparticle distance between dots increases. The increase in the interparticle distance between the nano dots weakens the coupling effect of the electromagnetic field between the dots [181, 182]. As a result, the absorbance band shifts to shorter wavelengths with a decrease in the absorbance peak intensity and peak sharpening. In this experiment, the annealing temperature shows more significant effects on the shift of the absorbance peak and the peak intensity than the annealing time.

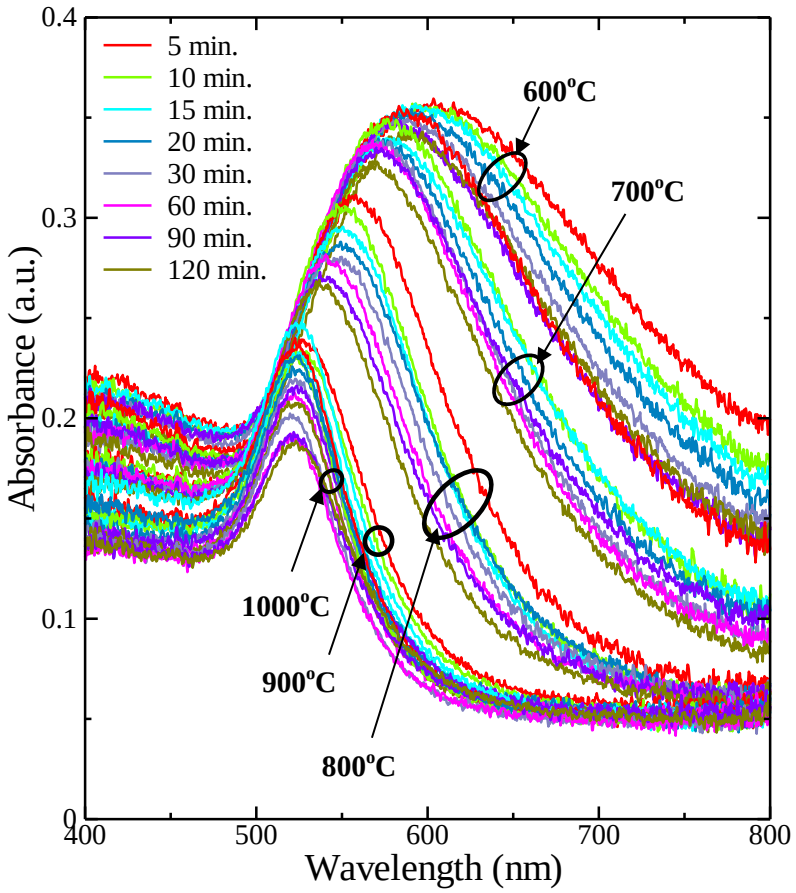

Figure 3. 13 Absorbance spectra of gold nano dots on the quartz glass substrate for different annealing temperature and annealing time

Figure 3.14 shows the variation in the absorbance peak wavelength against the annealing time. It is found that the absorbance peak wavelength decreases with the increase in either the annealing time or annealing temperature. The variation in the absorbance peak wavelength with annealing time can be divided into two regions. The decrease in the peak wavelength is steep when the annealing time is shorter than 30 min, while the peak

wavelength slightly decreases when the annealing time is longer than 30 min. It is found that the variation in the peak wavelength is similar to the variation in the dots circularity seen in Figure 3. 11 and Figure 3.14

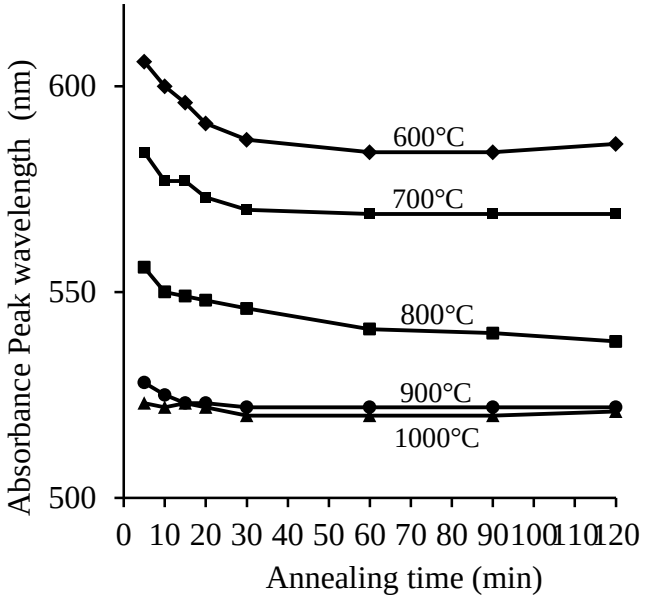

Figure 3. 14 Variation in absorbance peak wavelength against annealing time.

Figure 3.15 shows the variation in the absorbance peak intensity against the annealing time. It is found that the absorbance peak intensity decreases with the increase in either the annealing time or annealing temperature. It is also found that the variation in the peak intensity is similar to the variation in the dots circularity. These results indicate close correlation between the circularity and LSPR property.

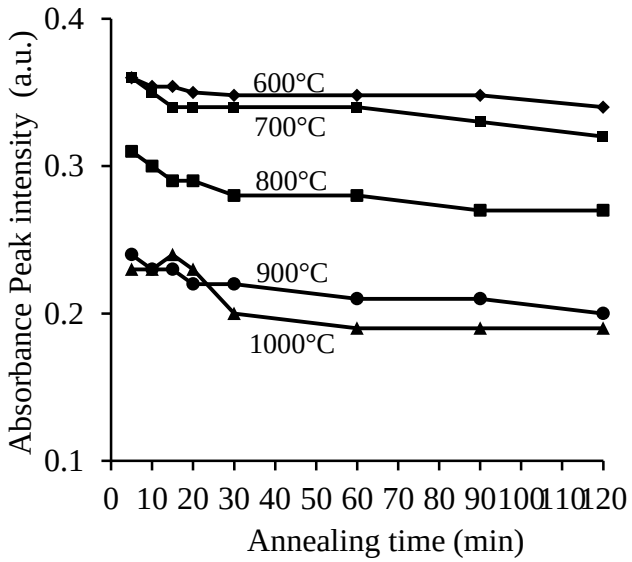

Figure 3. 15 Variation in absorbance peak intensity with annealing time

This result demonstrates that the absorbance spectra of the gold nano dots can be tuned by controlling the gold film thickness, annealing time, or annealing temperature. The tunability of LSPR property plays an important role in bio-sensing devices [60-62] and plasmonic solar cells [56, 65-68].

3.3.3 Effects of process condition on the dots transfer ratio

Figure 3.16 shows the FE-SEM micrographs of the gold nano dot transferred to Araldite rapid epoxy films from (a) quartz glass substrate and (b) silicon substrate. It is found that the gold nano dots were partly transferred to the epoxy films for all annealing temperatures from 600 °C to 1000 °C. Also, it seems that more dots were transferred to the epoxy films when the annealing temperature is lower.

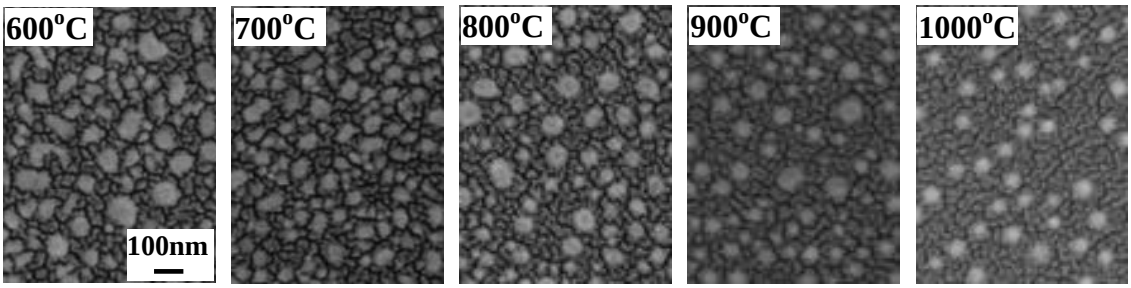

(a) Nano dots from quartz glass substrate transferred to Araldite rapid epoxy film

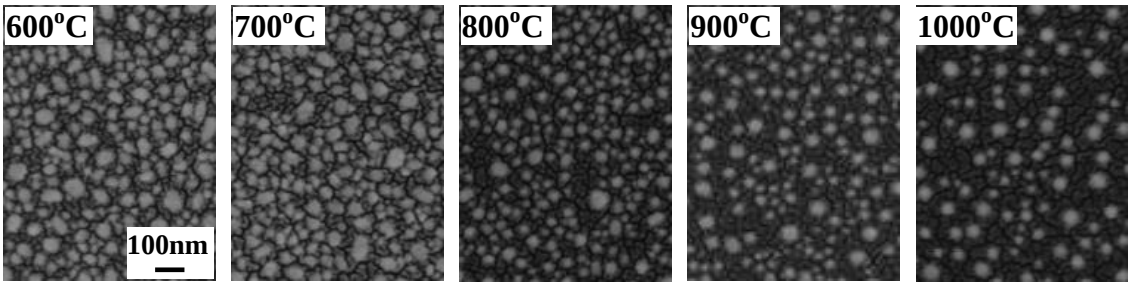

(b) Nano dots from silicon substrate transferred to Araldite rapid epoxy film

Figure 3. 16 FE-SEM micrographs of gold nano dots on Araldite rapid epoxy film transferred from (a) quartz glass substrate; (b) silicon substrate

Figure 3.17 shows the variation of the transfer ratio against annealing temperature. It is found that the transfer ratio decreases with the increase of annealing temperature for both the quartz glass substrate and the silicon substrate. The silicon substrate shows slightly higher transfer ratio than the quartz glass substrate. Highest transfer ratios of 95% and 87% were achieved for the silicon substrate and the quartz glass substrate, respectively, when annealing temperature is 600^{o}C.

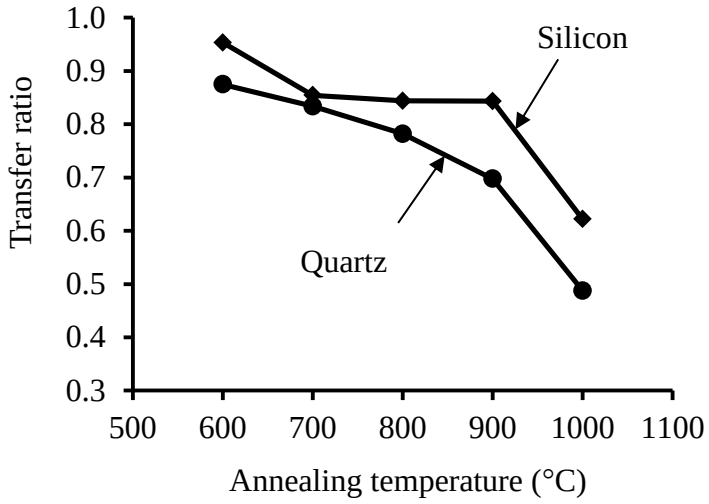

Figure 3. 17 Variation of transfer ratio of gold nano dots versus annealing temperature

Figure 3.18 shows the FE-SEM micrographs of the gold nano dot transferred from quartz glass substrate to (a) Araldite rapid epoxy films, (b) SpeciFix-20 epoxy and (c) PDMS. The thickness of gold film is 8 nm for all specimens. It is found that the gold nano dots were partly transferred to the Araldite rapid epoxy films and SpeciFix-20 epoxy for all annealing temperatures. However, no dot was transferred to PDMS films. It seems that at higher annealing temperatures, more dots were transferred to SpeciFix-20 epoxy than Araldite rapid epoxy.

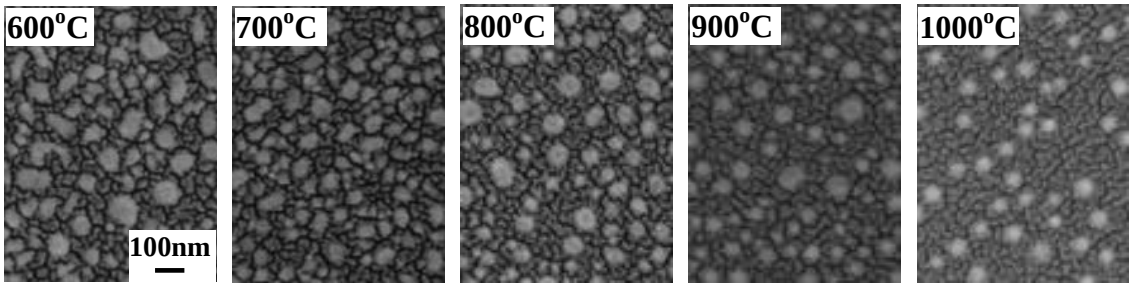

(a) Nano dots from quartz glass substrate transferred to Araldite rapid epoxy film

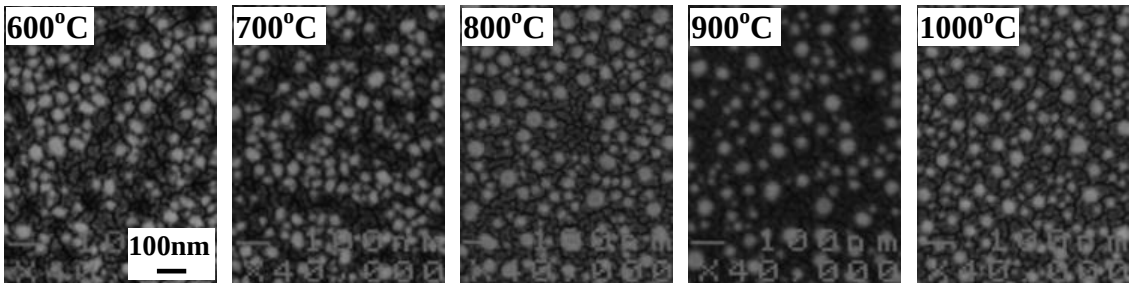

(b) Nano dots from quartz glass substrate transferred to SpeciFix-20 epoxy

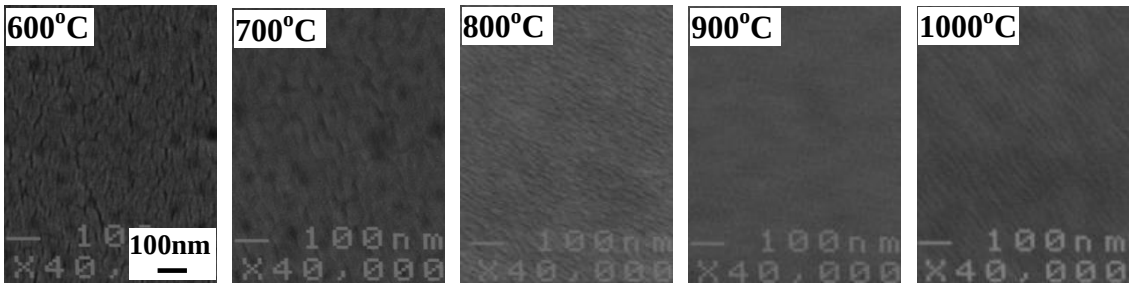

(c) Nano dots from quartz glass substrate transferred to PDMS

Figure 3. 18 FE-SEM micrographs of gold nano dots on transferred from quartz glass substrate to (a) Araldite rapid epoxy films, (b) SpeciFix-20 epoxy and (c) PDMS

Figure 3.19 compares the variation of the transfer ratio of three plastic materials against annealing temperature. It is found that no dot was transferred to PDMS. For the other plastic materials, it is found that they show contrary trends in transfer ratio. The transfer ratio of the Araldite rapid epoxy decreases with the increase of annealing temperature while the SpeciFix-20 epoxy increases. Highest transfer ratios of 87% and 91% were achieved when transferring nano dot array from quartz glass substrate to Araldite rapid epoxy and SpeciFix-20 epoxy, respectively. The reason for the difference of variation of transfer ratio of three plastic materials will be discussed in the next section.

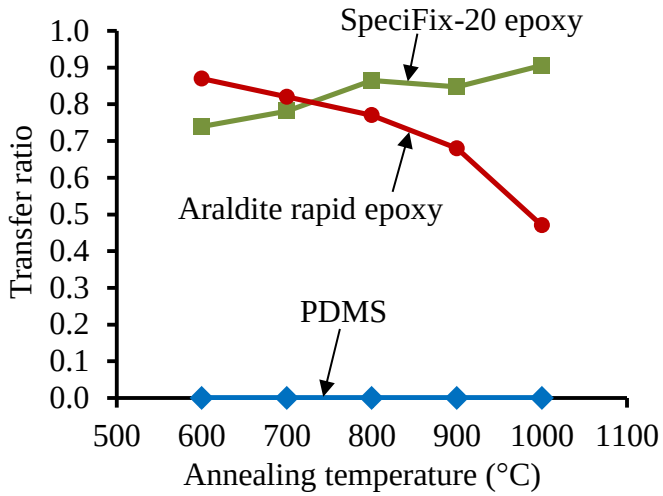

Figure 3. 19 Variation in transfer ratio of gold nano dots to various plastic materials versus annealing temperature

3.3.4 Nano dot transfer mechanism

Consider a model of transferring a dot from a substrate to a plastic film. One of two cases will occur: case I, the dot is not transferred to the plastic film and remained on the substrate; and case II, the dot is transferred to the plastic film as shown in the figure 3.20. Assuming that the dot shape is semi-sphere and the shape of a dot does not change through transferring process. Also, it is assumed that Young's equation is valid in this model. The total free energy of the system in each case is determined by following equations:

$$W_I = S_s\gamma_s + S_d\gamma_d + S_i\gamma_i + S_s\gamma_p + S_d\gamma_p \tag{3.3}$$

$$W_{II} = S_s\gamma_s + S_i\gamma_s + S_s\gamma_p + S_i\gamma_d + S_d\gamma_{p'} \tag{3.4}$$

The difference of total free energy between case I and case II, ΔW is calculated as follows:

$$\Delta W = W_I - W_{II} = (S_s\gamma_s + S_d\gamma_d + S_i\gamma_i + S_s\gamma_p + S_d\gamma_p) - (S_s\gamma_s + S_i\gamma_s + S_s\gamma_p + S_i\gamma_d + S_d\gamma_{p'})$$

$$= S_d(\gamma_d + \gamma_p - \gamma_{p'}) + S_i(\gamma_i - \gamma_s - \gamma_d) \tag{3.5}$$

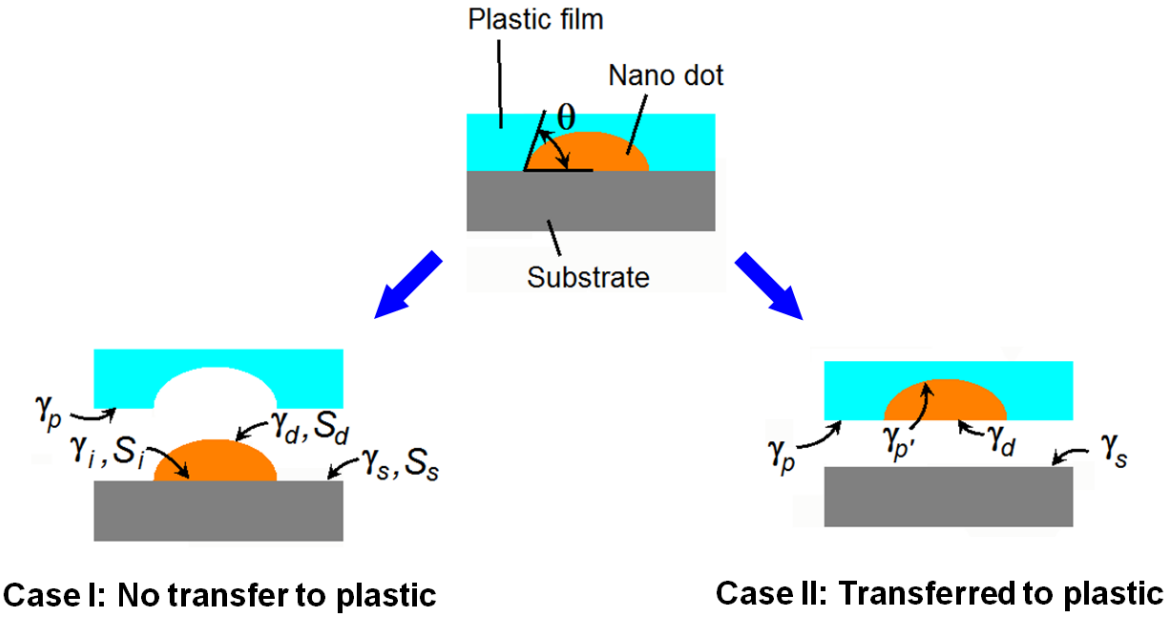

Figure 3. 20 Model of transferring nano dot from a substrate to a plastic film

In the calculation in this session, the notations were used as follows:

W_I : Total free energy of the system in case I

W_{II} : Total free energy of the system in case II

S_s : Area of substrate surface

S_d : Area of the surface of the dot

S_i : Interfacial area between the dot and the substrate

γ_s : Surface energy of the substrate

γ_d : Surface energy of the dot

γ_i : Interfacial energy between the dot and the substrate

γ_p : Surface energy of the plastic

$\gamma_{p'}$: Interfacial energy between the dot and the plastic

θ : Contact angle between the dot and substrate

D : Diameter of the dot

From Young's equation, we have the relation as follows:

$$\gamma_s - \gamma_i = \gamma_d \cos\theta \tag{3.6}$$

By substitute equation (3.6) into equation (3.5), we obtain:

$$\Delta W = S_d(\gamma_d + \gamma_p - \gamma_{p'}) - S_i\gamma_d(1+\cos\theta) \tag{3.7}$$

The surface area S_d of the dot is determined as follows:

$$S_d = \frac{\pi D^2}{2}\frac{1}{1+\cos\theta} \qquad \text{for } \theta < 90^o \tag{3.8}$$

$$S_d = \frac{\pi D^2}{2}(1-\cos\theta) \qquad \text{for } \theta \geq 90^o \tag{3.9}$$

The interfacial area S_i of the dot is determined as follows:

$$S_i = \frac{\pi D^2}{4} \qquad \text{for } \theta < 90^o \tag{3.10}$$

$$S_i = \frac{\pi D^2}{4}\sin^2\theta \qquad \text{for } \theta \geq 90^o \tag{3.11}$$

By substitute equations (3.8) to (3.11) into equation (3.7) we obtain:

$$\Delta W = W_I - W_{II} = \begin{cases} \dfrac{\pi D^2}{4}\dfrac{\gamma_d}{1+\cos\theta}\left\{2\left(1+\dfrac{\gamma_p-\gamma_{p'}}{\gamma_d}\right)-(\cos\theta+1)^2\right\} & \theta < 90° \\ \dfrac{\pi D^2}{4}\gamma_d(1-\cos\theta)\left\{2\left(1+\dfrac{\gamma_p-\gamma_{p'}}{\gamma_d}\right)-(\cos\theta+1)^2\right\} & \theta \geq 90° \end{cases} \tag{3.12}$$

When $\Delta W > 0$, case II occurs, thus, the dot is transferred to the plastic film.

In the equation (3.12), the term $\pi D^2\gamma_d/4$ is constant which can be considered as the unit for ΔW in the relation with contact angle θ between the dot and the substrate.

Consider three cases that: $\dfrac{\Delta\gamma_p}{\gamma_d} = \dfrac{\gamma_p-\gamma_{p'}}{\gamma_d} = -1,0,1$, we obtain the variation of the difference of total free energy between case I and case II, ΔW against the contact angle θ as shown in the figure 3.21.

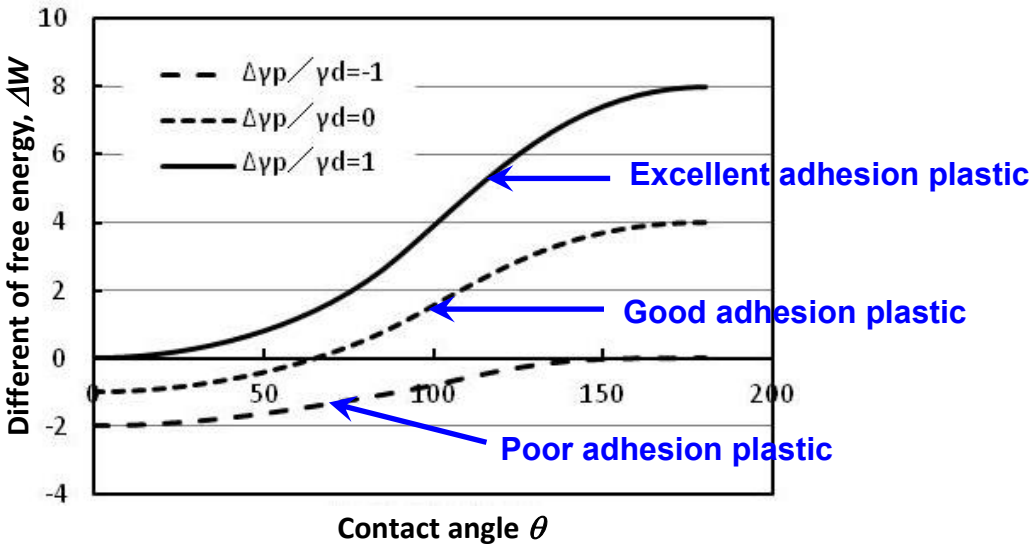

Figure 3. 21 Variation of ΔW against θ

It is found from figure 3.21 that ΔW increases with the increase of θ. This indicates that dot transfer becomes easier when θ becomes higher. In the graph, the three curves represent three adhesive levels of plastic. The continuous curve represents the plastic having excellent adhesion property. The dot is transferred to this plastic regardless of its contact angle. The long-dashed curve represents the plastic having very poor adhesion property. The dot is not transferred to this plastic regardless of its contact angle. The short-dashed curve (the center curve) represents the plastic having good adhesion property (the adhesion property level is in between the poor and excellent adhesion property). The dot is transferred to this plastic if its contact angle is higher than a critical value, and the dot is transferred to this plastic easier when its contact angle increases. As calculated from equation (3.12), the critical contact angle is about 67^{o}.

Compare the experimental data and the transfer mechanism theory based on total free energy; it is found that the PDMS and SpeciFix-20 epoxy show good agreement with the theory. It is known that PDMS has very poor adhesion property. Therefore, no dot was transferred to PDMS regardless of the contact angle of the dot. The SpeciFix-20 epoxy agrees with the theoretical variation of transfer ratio which increases with the increase of contact angle. However, the Araldite rapid epoxy shows contrary variation of transfer ratio against contact angle. Therefore, the difference of transfer ratio between SpeciFix-20 epoxy and Araldite rapid epoxy cannot be explained by the theory of total free energy.

Another possibility is attributed to the difference between viscosities of the epoxies which results in different of contact between the dot and the plastic.

The Araldite rapid epoxy is high viscosity resin (as reported in the product information from manufacturer, the viscosity of the Araldite rapid epoxy mixture after mixing is about 25 ~ 50 Pa.s) and its flowability is poor. When the contact angle of the dot on the substrate is low, this resin is easier to be filled to the whole surface of the nano dot as shown in the Figure 3.22(a). However, when the contact angle of the dot on the substrate is higher, it is very difficult to fill the undercut at the bottom of the dot. Voids or air will exist at the undercut between the dot and the substrate as shown in the Figure 3.22(b). These voids reduce the contact area between the dot and the Araldite rapid epoxy film. It reduces the adhesion of the nano dots to the epoxy film. Therefore, even though the contact angle is higher at higher annealing temperature, the Araldite rapid epoxy results lower transfer ratios.

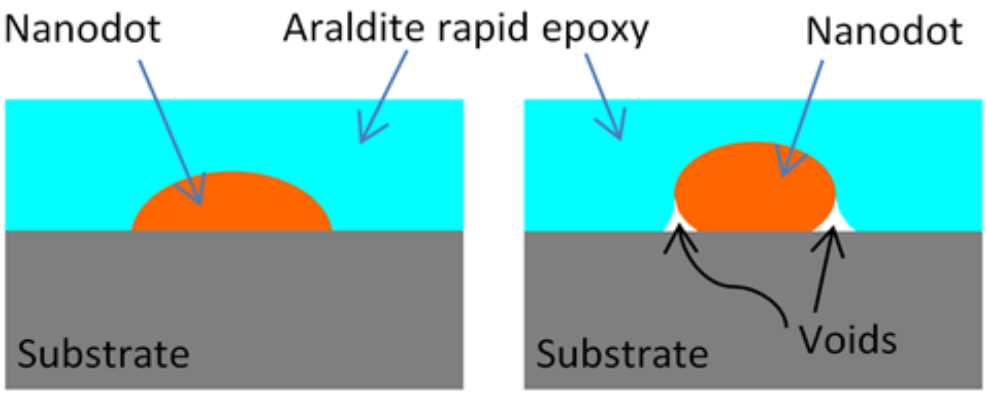

(a) Low contact angle (b) High contact angle

Figure 3. 22 Contact of high viscosity epoxy with the nano dot; (a) low contact angle; (b) high contact angle

In contrast, the SpeciFix-20 epoxy is low viscosity resin (as measurement test, the viscosity of the SpeciFix-20 epoxy mixture after mixing is 0.362 Pa.s) and its flowability is good. It is believed that under vacuum atmosphere, low viscosity resin can be easily filled to the nano dot surface and obtained good contact with the nano dot and substrate as shown in the Figure 3.23. The appearance of small bubbles on the surface of SpecFix-20 epoxy film inside the vacuum chamber may be attributed to the voids or air at the undercut between the nano dot and the quartz glass substrate. Under the vacuum atmosphere, these

voids are filled with SpeciFix-20 epoxy and the air from the undercuts will float to the top of the epoxy film. As a result, higher contact angle increases contact area between nano dot and the epoxy film. Therefore, the transfer ratio increases with the increase of contact angle. This agrees with the theoretical variation as shown in the Figure 3.21.

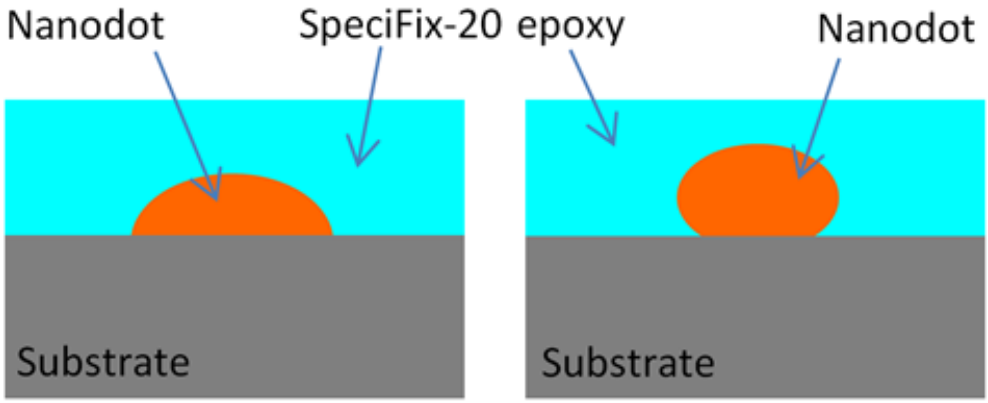

(a) Low contact angle (b) High contact angle

Figure 3. 23 Contact of low viscosity epoxy with a nano dot; (a) low contact angle; (b) high contact angle

3.3.5 Fabrication of a large area nano dot array on a plastic film

As a demonstration for large scale fabrication of nano dot array on plastic film, experiment to fabricate large area of nano dot array on plastic film was conducted. The experimental condition was as follows: Substrate is the quartz glass; Thicnkness of gold coating is 8 nm; annealing temperature is 600 °C; annealing time is 10minutes; Araldite rapid epoxy was used as plastic material. From figure 3.24, it is found that a 20 cm^2 in area of nano dot array was successfully fabricated on Araldite rapid epoxy film. It demonstrated that fabrication of nano dot array on plastic film in large area by the process in this study is feasible.

As mentioned in previous chapter, noble metal nano dot array have broad applications in electrical/electronic devices [136-140, 145] due to their unique LSPR property [55, 56]. Especially, applications of noble metal nano dot array to solar cells, so called plasmonic solar cell, to increase the light absorption in the semiconductor layer. Hence, increase the efficiency of the solar cell. Usually, the solar cell panels are produced in large area in order to provide a sufficient amount of electric power. To realize the applications of nano dot

array to plasmonic solar cells, fabrication of nano dot array in large area is essentially necessary.

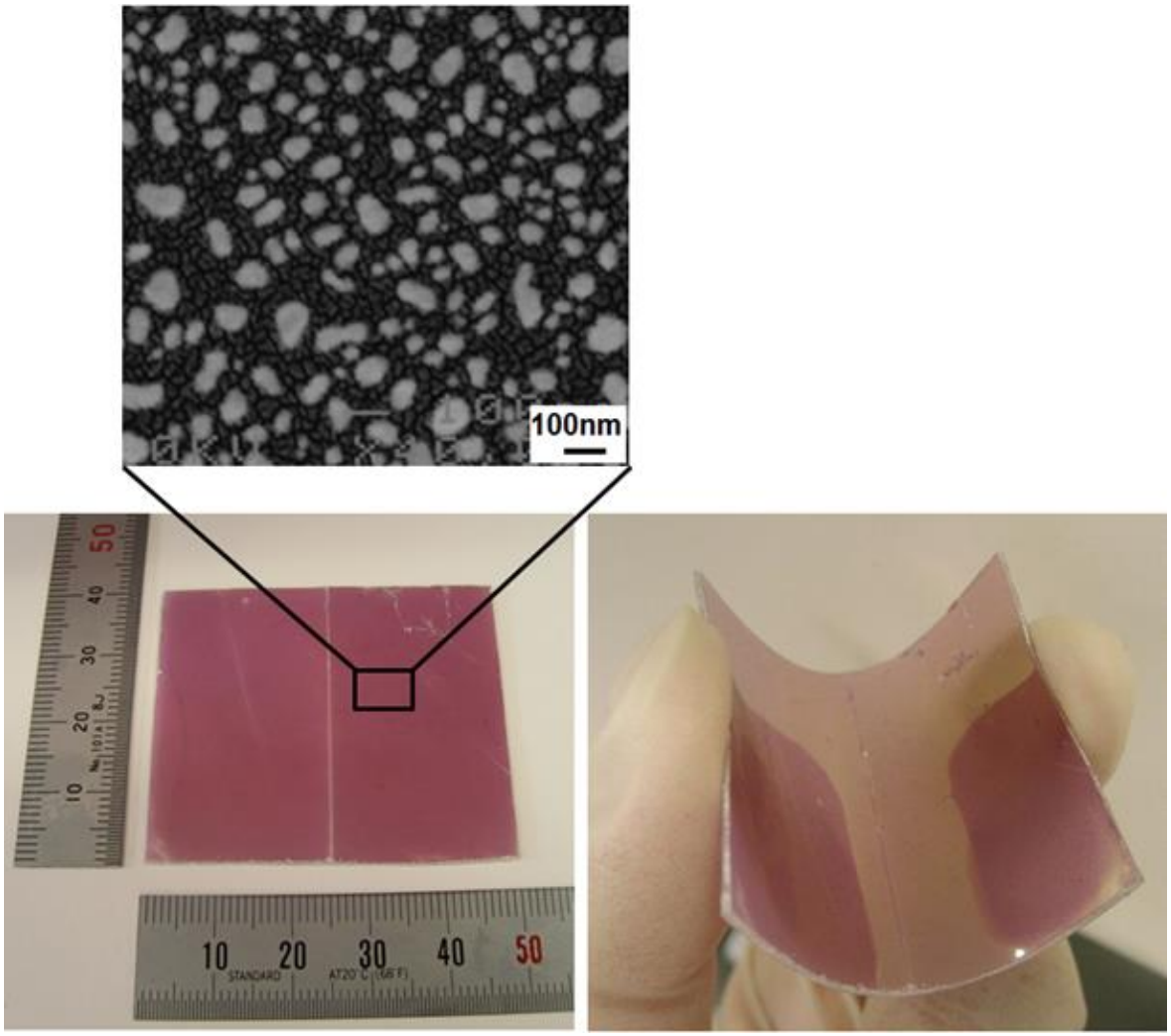

Figure 3. 24 Fabrication of a 20 cm^2 in area of nano dot array on Araldite rapid epoxy film

3.4 Summary

Investigations and results of this chapter are summarized as follows:

1. Effects of process conditions on the morphology of nano dot array

(i) Mean diameter and corresponding standard deviation of the nano dots increases with the increase in the gold film thickness, but decreases with the increase in the annealing temperature. This is attributed to the surface diffusion of gold atoms which affects the aggregation of gold film into nano dots.

(ii) Substrate material affects morphology of the aggregated nano dots. The nano dots aggregated on a quartz glass substrate are large and sparse, while the nano dots aggregated on a silicon substrate are small and dense. The difference of morphologies of nano dot on a quartz glass substrate and a silicon substrate are attributed to the difference in the surface energy of the two substrate materials.

(iii) The contact angle of the nano dots both on a quartz glass substrate and a silicon substrate increases with the increase in the annealing temperature. The silicon substrate results in slightly higher contact angle of nano dots than the quartz glass substrate. The reason is attributed to the difference in the surface energy of the two substrate materials.

(iv) The circularity of nano dots increases with the increase in the annealing time, but becomes saturated to a certain value that depends on the temperature. Maximum circularity of around 0.9 was achieved in this study.

2. Effects of process conditions on the LSPR property of nano dot array

(i) The absorbance spectra of the nano dots on the quartz glass substrate display a unique peak in the visible range. This absorbance peak shifts to longer wavelengths side and becomes broader with the increase in the gold film thickness. This is attributed to the difference in the morphology of nano dot arrays produced by different thicknesses.

(ii) The absorbance peak shifts to shorter wavelengths side, the absorbance peak intensity decreases, and absorbance peak becomes sharper when either the annealing time or the annealing temperature is increased. The annealing temperature shows stronger effects on the variation in LSPR wavelength, peak and intensity than the annealing time in this study. This is attributed to the more uniform, more circular nano dots morphology that weakens the coupling effects of the LSPR of the nano dots.

(iii) It is found that the variation in the LSPR property is closely correlated to the variation in the nano dots circularity.

3. Effects of process conditions on the transfer ratio of nano dot array to a plastic film

(i) The substrate materials affect the transfer ratio of a nano dot array to a plastic film. The silicon substrate shows slightly higher transfer ratio than the quartz glass substrate. This is attributed to the difference between the surface energy of the two substrate materials.

(ii) The plastic materials show contrary trends of variation of transfer ratio against annealing temperature. Araldite rapid epoxy decreases the transfer ratio while the SpeciFix-20 epoxy increases transfer ratio when the annealing temperature becomes higher. This is attributed to the difference between the viscosities of the epoxies.

(iii) Dot transfer mechanism is discussed theoretically based on the different of total free energy and compared with the experimental results. PDMS and SpeciFix-20 epoxy show good agreement with the dot transfer mechanism theory.

(iv) A 20 cm^2 in area of random nano dot array was successfully fabricated on an Araldite rapid epoxy film. It demonstrated the feasibility of the proposed process for large area fabrication of a nano dot array on a plastic film.

CHAPTER 4

Fabrication of an ordered nano dot array on a plastic film

In previous chapter, the process to fabricate a random nano dot array to a plastic film and the experiments to demonstrate the feasibility of the proposed process was presented. The objective of this chapter is to extend the concept of process presented in chapter 3 for fabrication of an ordered nano dot array on a plastic film. In this chapter, first the concept of the proposed process to fabricate an ordered nano dot array on a plastic film by nano-plastic forming assisted thermal dewetting and transfer technique is presented. Then, the equipment and working principle of nano-plastic forming are presented. The effects of nano-plastic forming conditions, coating thickness and annealing condition on the morphology of nano dot array aggregated on a patterned substrate are presented and discussed. Finally, the transfer of an ordered nano dot array from a patterned substrate to a plastic film is presented.

4.1 Concept of process to fabricate an ordered nano dot array on a plastic film

Figure 4.1 illustrates the concept of process to fabricate an ordered nano dot array on a plastic film [51, 52, 54]. The process comprises four steps; (1) fabrication of a square nano-grooves grid on a hard substrate by NPF, (2) deposition of a thin metal layer on the patterned substrate by sputter coating, (3) annealing the metal coated substrate in an electric furnace to form an ordered nano dot array and (4) transfer the ordered nano dot array to a plastic film. It is expected that the patterned substrate can be re-used after transferring, by repeating three steps metal deposition, annealing and transferring (step 2 to 4 in the figure 4.1), ordered nano dot arrays can be fabricated on plastic films at a very high throughput.

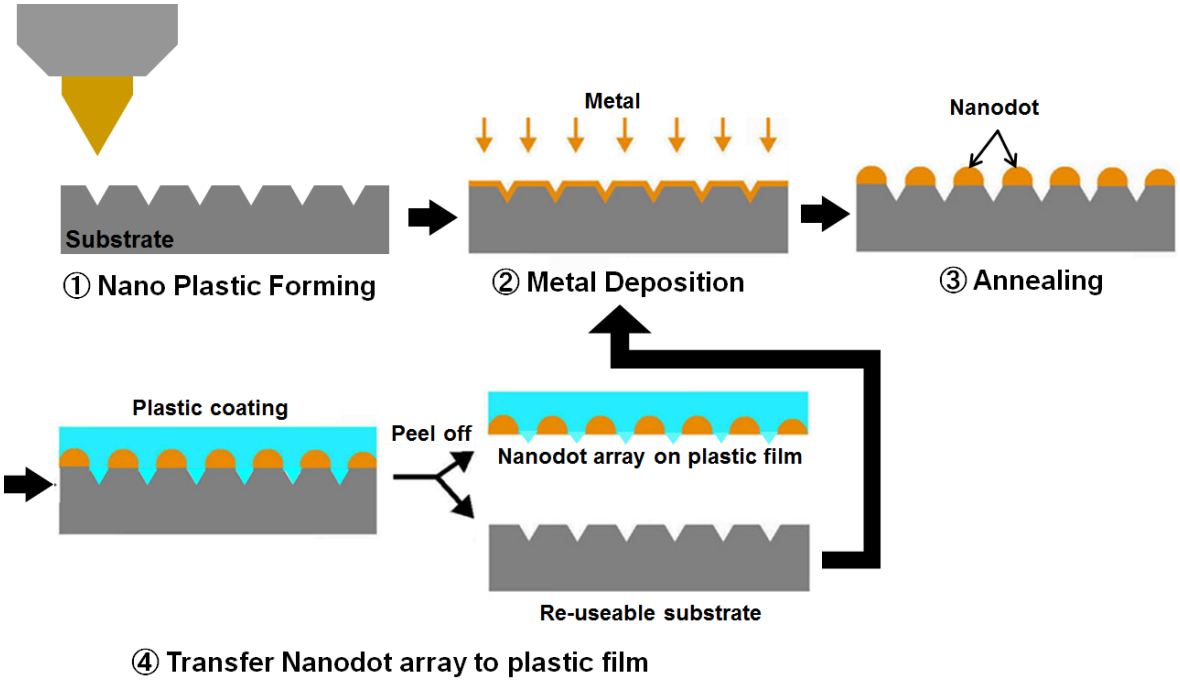

Figure 4. 1 Schematic schedule of process to fabricate an ordered metal nano dot array on a plastic film

4.2 Experimental method

4.2.1 Nano-plastic forming (NPF)

Nano-plastic forming equipment: Figure 4.2 shows the equipment used for the NPF experiments. It consists of precision stages, a load cell, a motion controller, a data acquisition system and a diamond knife-edge tool. The strokes of the *XY*-stage and the *Z*-stage are 20 and 40 mm, respectively. Their feed resolution is 1 nm. The *XY*-stage is mounted on a tilt stage whose resolution is 0.015°. The specimen is mounted on the *XY*-stage. The load cell is mounted the tool holder which is set on the *Z*-stage. The motion of the *XY*-stage and the Z stage (i.e., the motion of specimen and diamond tool) is controlled by a computer. The indentation load is measured by the load cell, and the data are recorded by the acquisition system. The NPF process is monitored with a CCD camera. The process was taken out inside a clean chamber to prevent the effect of dust. Figure 4.3 shows the knife-edge tool used for the experiments. It was made of single crystal diamond. The width of the diamond tool is 0.6 mm, and the edge angle is 60°. The tool was ground very sharp, and its edge radius was around 40 nm.

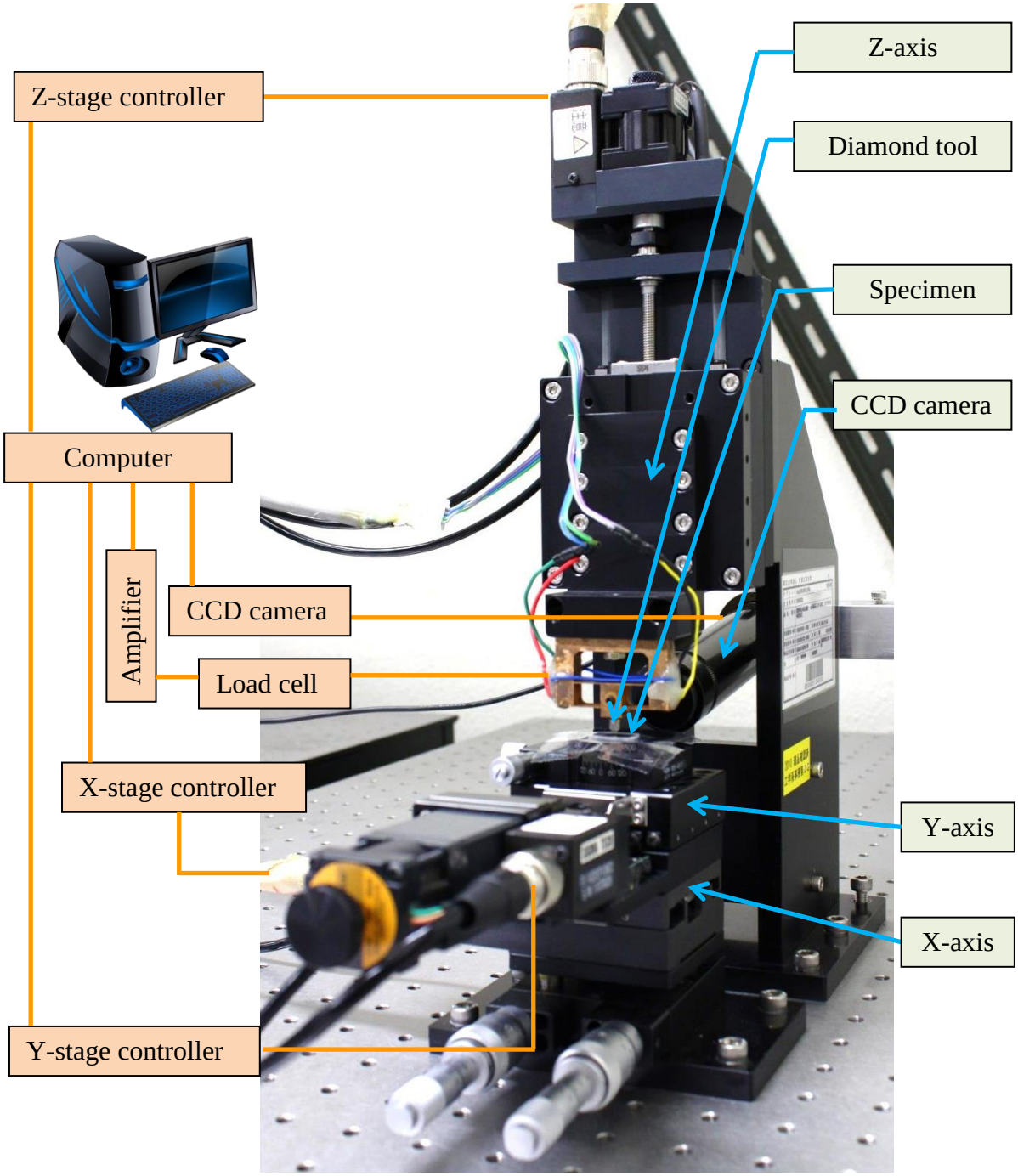

Figure 4. 2 Nano plastic forming equipment

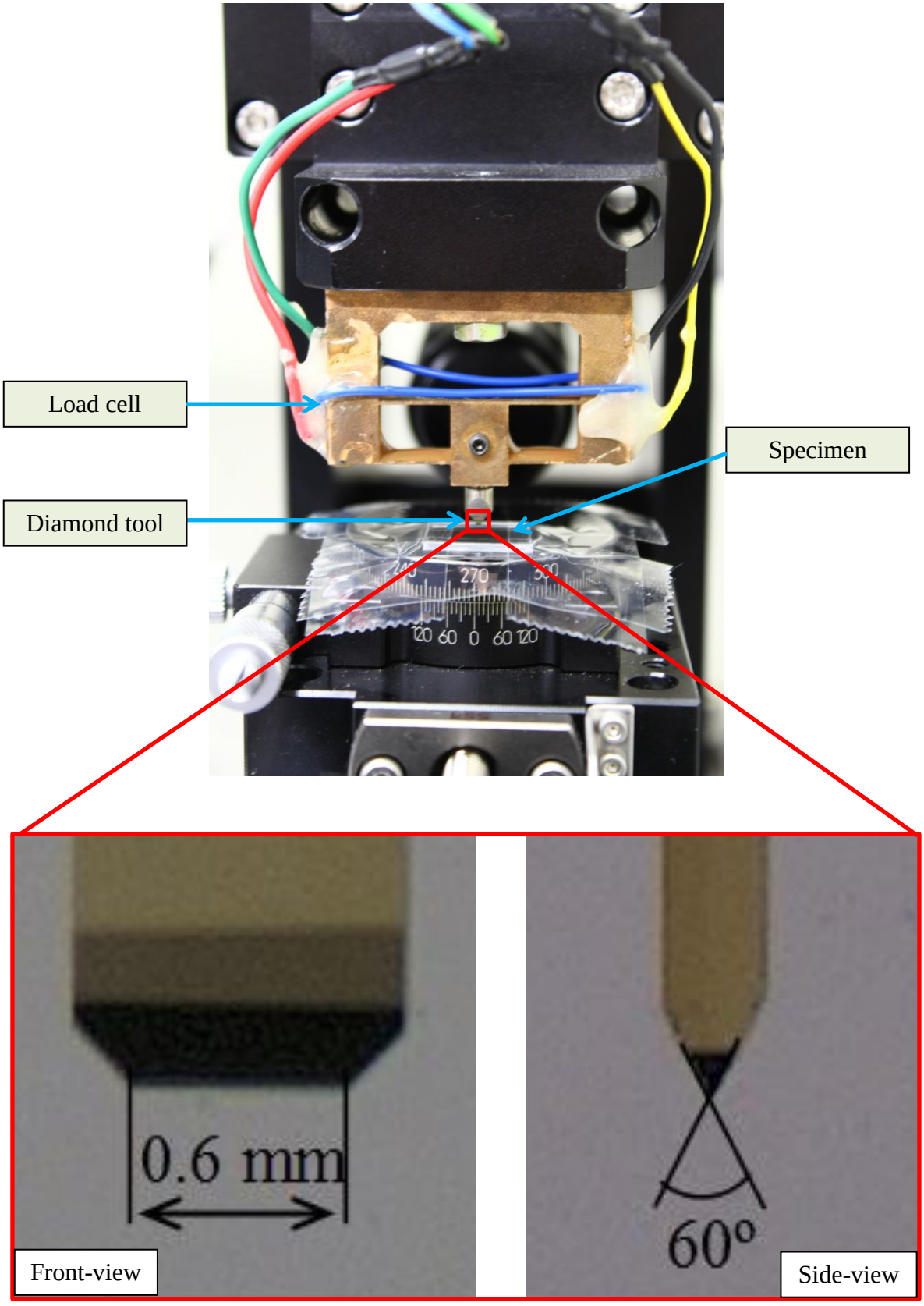

Figure 4. 3 Knife-edge diamond tools

Working principle of nano-plastic forming (NPF): NPF is a nano/microscopic metal forming process. It can fabricate nano/micro structures only by imprinting a specially designed tool directly on the work material. Figure 4.4 illustrates the working principle of NPF. The specimen is mounted on the top of the XY-stage. The diamond knife edge tool is mounted on the tool holder set on the Z stage. Whole NPF process is controlled by a computer program. Firstly, the diamond tool is progressively translated downward and indented onto the specimen surface. When the tool touches the specimen surface, the indentation load increases, the diamond tool is kept indenting to specimen surface until the indentation load reaches a predefined load. Then the diamond tool is retracted, and the first indentation is finished. After that, the specimen mounted on the XY stage is translated in Y direction for a predefined distance called pitch or distance between grooves. Then, the second indentation is conducted by the same manner. This process is repeated until the number of indentations reaches a predefined number of times. Then the indentation process is finished. In order to make grid pattern on the specimen surface, after the indentation in the first direction finishes, the specimen is laterally rotated by a desired angle and the indentation process is repeated by the same manner as the indentation process for the first direction.

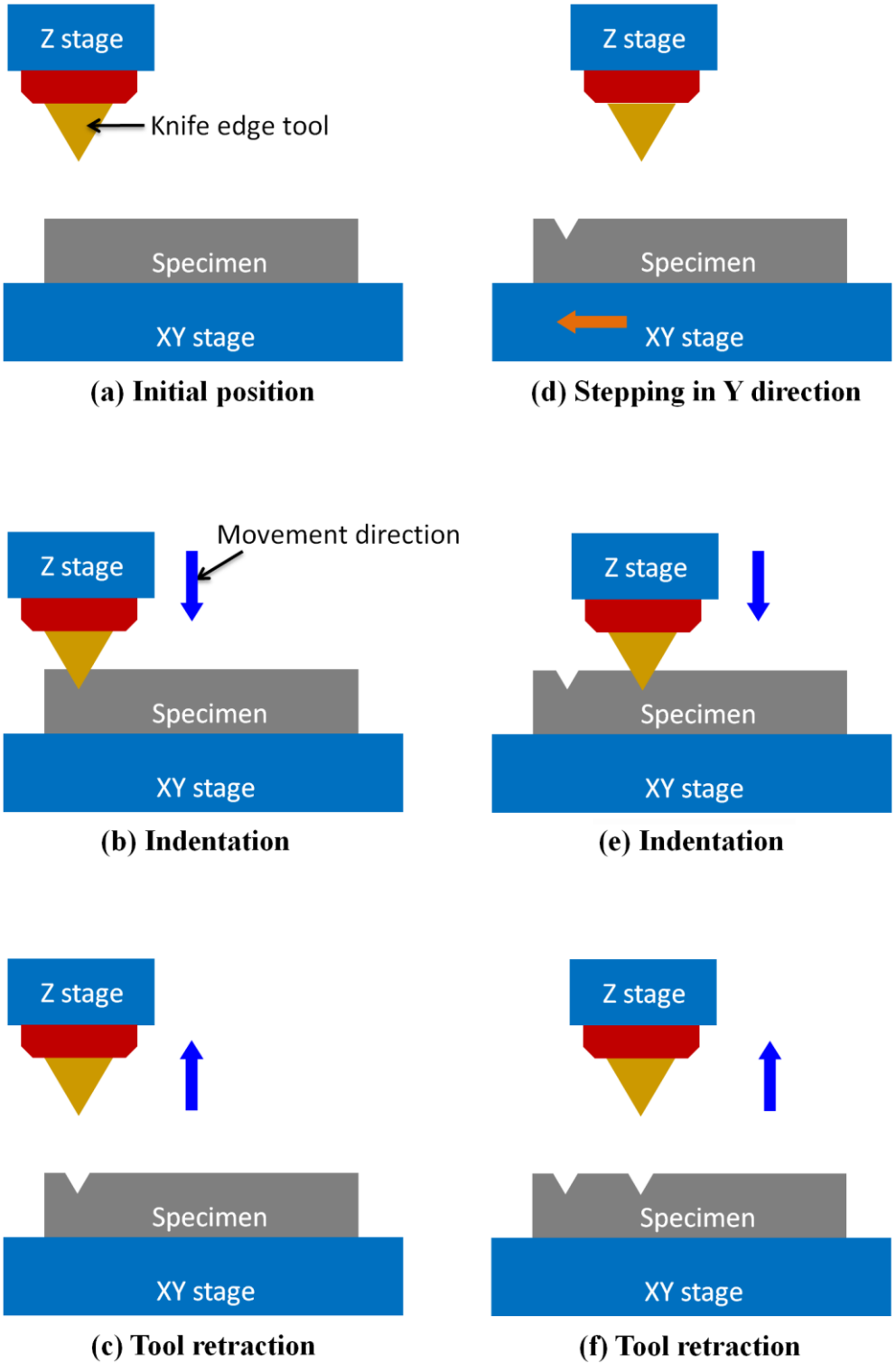

Figure 4. 4 Schematic of nano plastic forming (NPF) working principle

4.2.2 Experimental procedures and conditions

In this experiment, quartz glass slide (Saito Optics Co., Ltd.) was used as substrate material. It was cut in sizes of 10 mm in width and 10 mm in length. The thickness of the quartz glass slide was 1 mm. It was cleaned by ultrasonic vibration in an acetone bath for 10 min. Then, the substrates were dried.

Patterning by NPF: A square grid pattern was fabricated on the cleaned quartz substrate by NPF. Firstly, a series of parallel nano-grooves was fabricated on a substrate by indenting the diamond knife-edge tool. The distance between grooves was 100 nm in this experiment. The indentation load was controlled at a pre-defined load and kept constant for all grooves. Six levels of indentation load were examined: 0.4, 0.6, 0.8, 1.0, 1.2, and 1.5 N. The indentation load was determined so that indentation depth becomes smaller than the critical depth of quartz glass [183, 184], under which depth ductile manner deformation is maintained and no fracture or crack occurs on the quartz substrate. After the first series of grooves was fabricated, the substrate was laterally rotated for 90°, and another series of parallel grooves was fabricated on the pre-formed grooves by the same manner. As a result, a square grid pattern was fabricated on the surface of the substrate. Figure 4.5 illustrates the fabrication of nano-grooves grid pattern on a substrate. The length of the grooves patterned is 1.2 mm in both X and Y direction. The centered region of the pattern is a square grid pattern with an area of 0.6 mm × 0.6 mm, and the grid size is 100 nm.

Metal deposition: The patterned substrate was again ultrasonically cleaned in an acetone bath for 10 min, and it was dried. Then, gold was deposited on the surface of the substrate by a DC sputter coater. The DC sputter coater is the same as the one use for sputter coating in chapter 3. The thickness of gold coating layer was controlled by adjust the sputter time. In the experiments, six levels of gold thickness were investigated in the experiment: 6, 8, 10, 12, 14, and 16 nm.

Thermal dewetting: The gold-coated patterned substrates were subjected to thermal dewetting in an electric furnace. The furnace is the same as the one used for thermal dewetting process in chapter 3. Three levels of annealing temperature were examined: 600°C, 800°C, and 1000°C. Two annealing time durations were examined: 10 and 30 min. Then the specimens were taken out of the furnace and cooled down in the air atmosphere. The experimental parameters are summarized in Table 4.1.

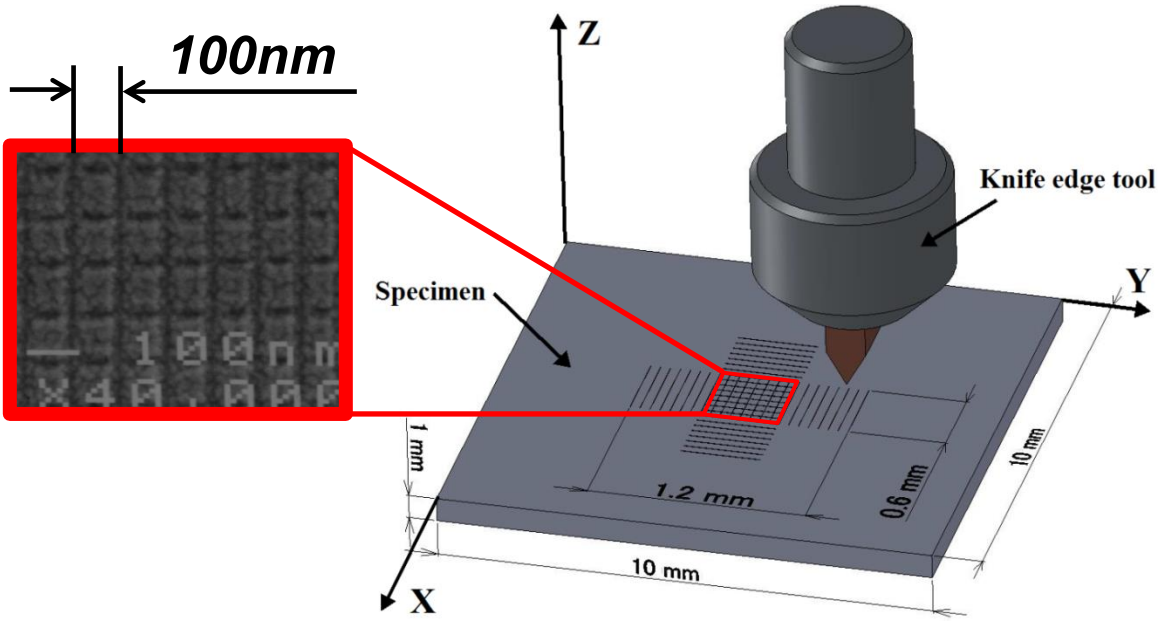

Figure 4. 5 Illustration of fabrication of a grid pattern on a substrate

Table 4. 3 Experimental conditions

Parameter / Study effects of	NPF patterning parameters		Coating	Annealing	
	Grid size (nm)	Indentation Load (N)	Au thickness (nm)	Temp. (^{o}C)	Time (min)
Gold film thickness	100	1.0	6, 8, 10, 12, 14, 16	600	10
				1000	30
Indentation load	100	0.4, 0.6, 0.8, 1.0, 1.2, 1.5	12	1000	30
Annealing temperature	100	1.0	12	600, 800, 1000	30

Transfer the ordered nano dot array to a plastic film: The ordered nano dot array on the patterned substrate were dried by blowing hot air for 2 minutes to improve the adhesion between nano dots and a plastic film. Then, the substrate was coated with a thin layer of plastic. The thickness of the plastic film coating is about 0.5 to 1 mm. Two plastic materials were examined: Araldite rapid epoxy and SpeciFix-20 epoxy. The processing conditions for these two plastic materials are the same as in Table 3.2 in chapter 3.

The nano-grooves grid pattern and the morphology of the nano dot arrays formed on the patterned quartz glass substrate were characterized by a FE-SEM and a graphic analysis system (ImageJ software).

4.3 Results and discussion

4.3.1 Effect of gold film thickness on the morphology of nano dot array aggregated on patterned substrate.

Figure 4.6 shows the FE-SEM micrographs of nano dot arrays aggregated on the patterned quartz glass substrates after annealing at (a) 600°C for 10 min and (b) 1000°C for 30 min. Thicknesses of gold films were: 6, 8, 10, 12, 14, and 16 nm. It is found that patterning on a substrate improves the uniformity and regularity of the nano dot array when the substrate is deposited with an adequate thickness of gold film. It is also found that the morphology evolution of the nano dot array with different gold film thicknesses is similar for both annealing conditions.

In figure 4.6 (a), the annealing condition is at 600°C for 10 min. When the gold coating layer is 6 nm, the gold layer was aggregated into random small dots both on the grid square units and on the grooves; the regularity of the nano dot array is very poor. When the thickness is increased to 8 nm, the uniformity and regularity of the nano dot array is improved. Some dots are almost aligned on a grid pattern, while others randomly aggregate on both grid square units and on the grooves. When the gold film thickness is further increased to 10 nm, the uniformity and regularity of the nano dot array is further improved. The dots are almost aligned on a grid patterns, and the regularity is more apparent. However, few small dots aggregate on a same grid square unit. Also, many tiny dots aggregate on the grooves. When the thickness is increased to12 nm, a good uniformity and regularity in alignment of nano dot array is achieved. The dots are aligned on a grid pattern whose pitch coincides with the pitch of the grid pattern pre-formed on the substrate. But very few tiny dots aggregate on the grooves. When the gold thickness is further increased to 14 nm, the uniformity and regularity of the nano dot array become worse because some dots are connected with the adjacent dots. When the gold film thickness is too thick (16 nm), the dots are randomly aggregated on the substrate.

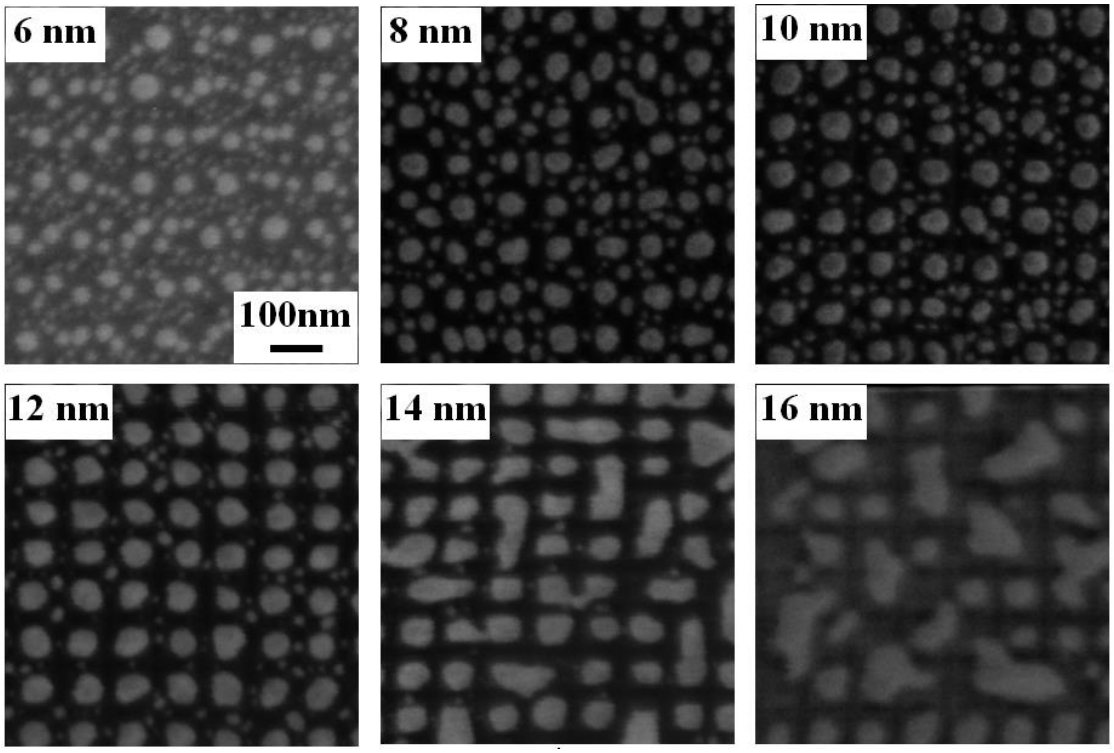

(a) Annealing at 600°C for 10 min

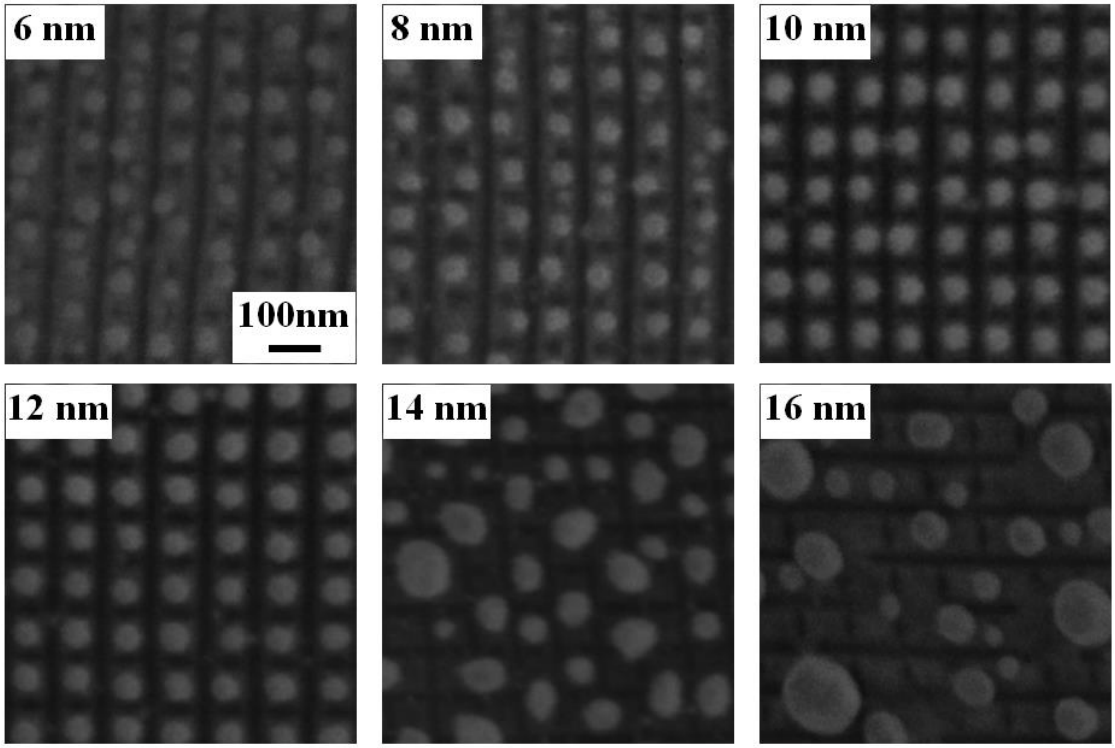

(b) Annealing at 1000°C for 30 min

Figure 4. 6 FE-SEM micrographs of nano dot array aggregated on patterned quartz glass substrates after annealing: (a) at 600°C for 10 min and (b) at 1000°C for 10 min

Gold film thickness of 12 nm shows the best uniformity and regularity of the nano dot array. However, few tiny dots aggregate on the grooves, and deteriorate the uniformity and regularity of the nano dot array.

In figure 4.6 (b), the annealing condition is at 1000°C for 30 min. It is found that the evolution of morphology of the nano dot arrays with the increase in the gold film thickness is similar to those ones at 600°C for 10 min shown in figure 4.6 (a). It is found that, few dots aggregate on the grooves when the gold film thickness is between 6 and 8 nm, while almost no tiny dots aggregate on the grooves when the gold film thickness is more than 10 nm. When the gold film thickness is 10 nm and 12 nm, the best uniformity and regularity of nano dot arrays are achieved. Furthermore, it is also found that the nano dots become more circular when the annealing temperature is higher as seen in figure 4.6 (a) and (b). The difference of morphology of nano dot annealed at different annealing temperatures will be discussed more detail in the next section for investigating effect of annealing temperature on morphology of nano dot array.

Figure 4.7 shows the variation in the mean diameter of the nano dot array and the relative alignment error (RAE) against the thickness of gold film. The mean diameter of the nano dots is evaluated from FE-SEM micrographs by using a graphic analysis software (ImageJ software). The vertical bars on the graph indicate the standard deviation of the diameter of the nano dots. The RAE represents the degree of irregularity of a nano dot array. It is defined as the mean square root of deviation from the ideal position, i.e. the square grid pattern [183]. For both annealing conditions, it is found that the mean diameter increases with the increase in gold film thickness. Meanwhile, the standard deviation of the dot diameter decreases with the increase in the gold film thickness when the thickness is less than 12 nm. The standard deviation becomes minimum at 12 nm, and it increases with the increase in the film thickness when the film is thicker than 12 nm. The variation of RAE is similar to that of standard deviation of dot diameter. RAE becomes minimum when gold film thickness is 12 nm. This implies that uniformity and regularity of the nano dot array become the best when the gold film thickness is 12 nm.

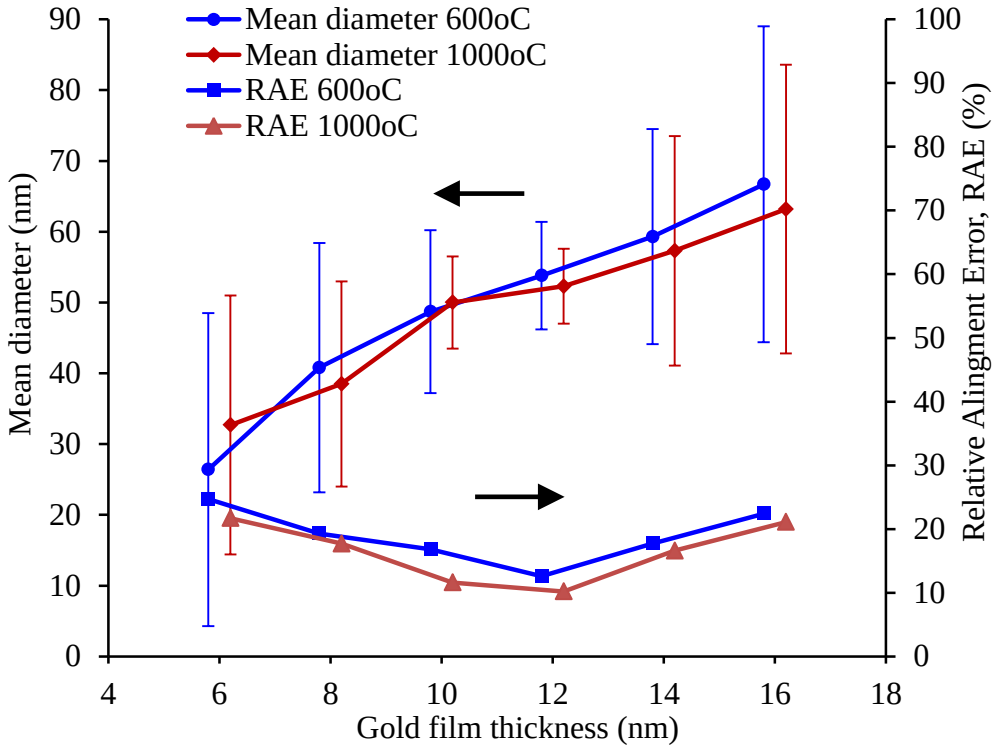

Figure 4. 7 Mean diameter of the nano dot array and its standard deviation and RAE versus gold film thickness

Figure 4.8 illustrates three types of dot aggregation patterns observed in the experiments. As shown in figure 4.8 (a), when the gold film is very thin, the metal film is aggregated into many small dots. It is known that many tiny voids exist randomly in a deposited thin film [172]. Due to the annealing, the voids progressively are widened, and are connected to adjacent voids. Since the density of the voids is fairly high, the gold film of a grid square is separated into many islands. These islands aggregate into many small dots, and as a result, many dots are formed on a grid square randomly. When the gold film is of proper thickness as shown in figure 4.8 (b), the metal film is separated only at the groove grid because the voids density is low. The metal film on a grid square aggregates into one dot. As a result, dots of uniform size are aligned as a grid pattern. When the metal film is too thick as shown in figure 4.8 (c), the depth of the debossed grooves grid pattern on the gold film surface is very narrow. As a result, the metal film is not separated at the groove grid perfectly. Thus, some dots are connected with the adjacent dots, and they form larger dots. As a result, uniformity and regularity of the nano dot array become poor.

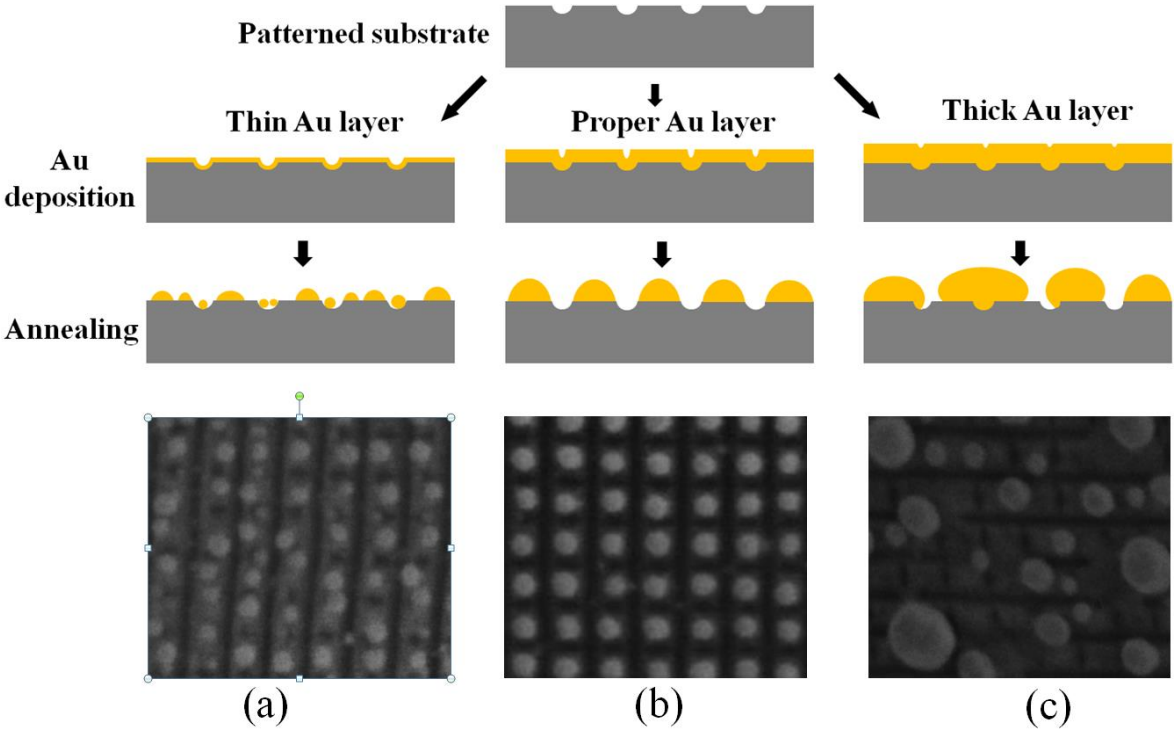

Figure 4. 8 Schematic illustration of dot formation on patterned substrate; (a) Thin Au layer, (b) proper Au layer thickness and (c) thick Au layer

4.3.2 Effect of annealing temperature on the morphology of the nano dot array

Figure 4.9 shows the FE-SEM micrographs of the nano dot arrays aggregated on patterned substrates after annealed at (a) 600°C, (b) 800°C and (c) 1000°C. The annealing time is 30 min for all specimens. In the experiment, the grid size is 100 nm and indentation load are 1.0 N. The thickness of Au film is 12 nm. It is found that the annealing temperature strongly influences on the morphology of nano dot array. When the annealing temperature is low (600°C), the gold film aggregates both on the grid square units and on the grooves. The gold film on the grid square unit aggregates into one large dot which positioned almost at the center of each grid square unit. While the gold film on the grooves aggregates into multiple small dots which randomly distributed on the grooves. As a result, the besides the ordered nano dot array aligned in a grid pattern, tiny dots are generated and randomly distributed on the grooves as seen in the figure 4.9 (a). In addition, it is found that the shape of the large dots on each grid square unit is not so circular. When the annealing is increase to 800°C, it is also found that the gold film aggregates both on the

grid square units and on the grooves. The circularity of the nano dots aggregated on each grid square unit is improved. The large dots are aligned on a grid pattern with good uniformity and regularity. However, tiny dots still exist and randomly distributed on the grooves as seen in the figure 4.9 (b). When the annealing temperature is further increase to 1000°C, the gold film aggregates only on grid size unit and does not aggregate on the grooves. As a result, an ordered nano dot array with good uniformity and well aligned are generated on the patterned substrate as seen in the figure 4.9 (c). It is also found that the shapes of the large dots on each grid square unit are more circular.

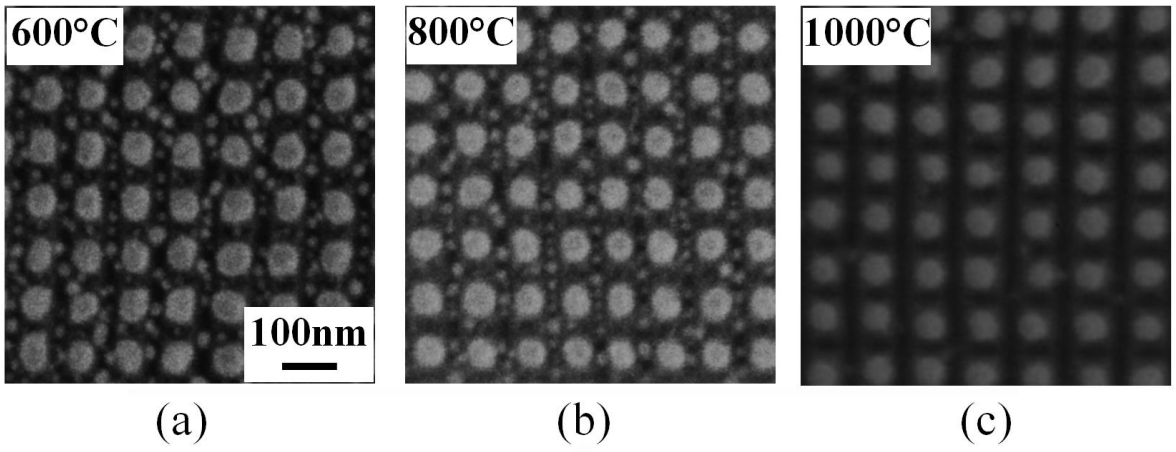

Figure 4. 9 SEM micrographs of nano dot array for annealed at different temperature: (a) 600°C, (b) 800°C and (c) 1000°C. Annealing time is 30 min

Figure 4.10 shows the variation in the mean diameter of the nano dot array and the relative alignment error (RAE) against the annealing temperature. The grid size is 100 nm and indentation load are 1.0 N. The thickness of Au film is 12 nm. The annealing time is 30 min for all specimens. It is found that both mean diameter of the nano dot array and standard deviation slightly decrease with the increase in annealing temperature. Also, the RAE slightly decreases with the increase in annealing temperature. Among these three annealing conditions, the standard deviation of diameter of nano dots and REA become smallest at 1000°C. This implies that uniformity and regularity of the nano dot array annealed at 1000°C are better than those of nano dot array annealed at 600°C and 800°C.

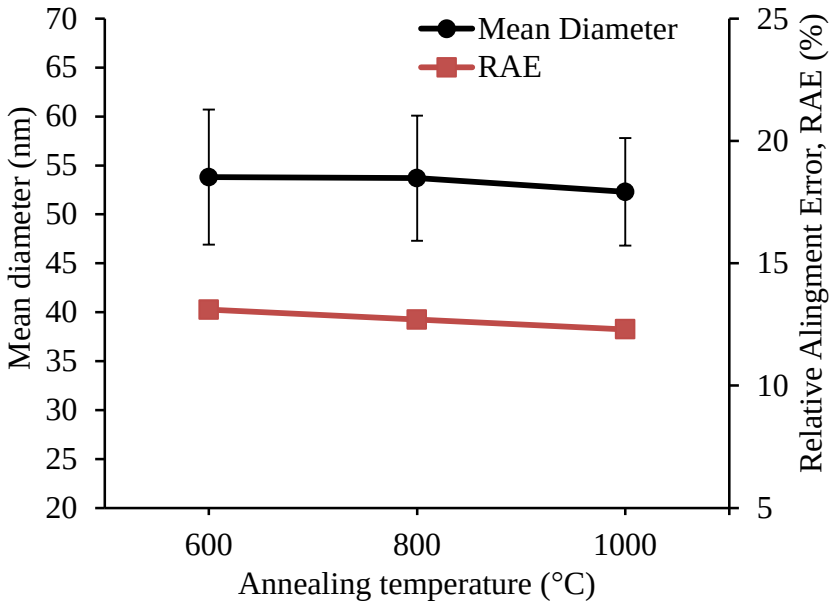

Figure 4. 10 Mean diameter of the nano dot array and its standard deviation and RAE versus against annealing temperature

Figure 4.11 illustrates two types of dot aggregation patterns observed in the experiments. As shown in figure 4.11 (a), when the annealing temperature is low, the gold film aggregates both on the grid square units and on the grooves. While, the gold film only aggregates on the grid square unit and does not aggregate on the grooves when the annealing temperature is high. This phenomenon can be explained by the model of nano dot aggregation on curved surfaces which were previously reported by Li et al. (2012) [185]. It was reported that the gold film tends to aggregate on a flat surface other than on a curved surface [185]. This is because the total free energy of the dot/substrate system after annealing decreases more on a flat surface than on a curved surface [185]. In addition, the nano dots also tend to aggregate on flat surface when the contact angle is higher [185]. It was reported that the contact angle of the nano dots on a quartz glass substrate increases with the increase in the annealing temperature [53, 186]. Therefore, when the annealing temperature is low (from 600°C to 800°C), the contact angle of the dot is low. As a result, the nano dots aggregate on both the flat surface (i.e. the grid square units) and curved surface (i.e. the grooves) as seen in figure 4.11 (a). On the other hand, the contact angle of the nano dots is high at high annealing temperature (at 1000°C). As a result, the nano dots tend to aggregate on flat surfaces (grid square units) and does not aggregate on the grooves as seen in figure 4.11 (b).

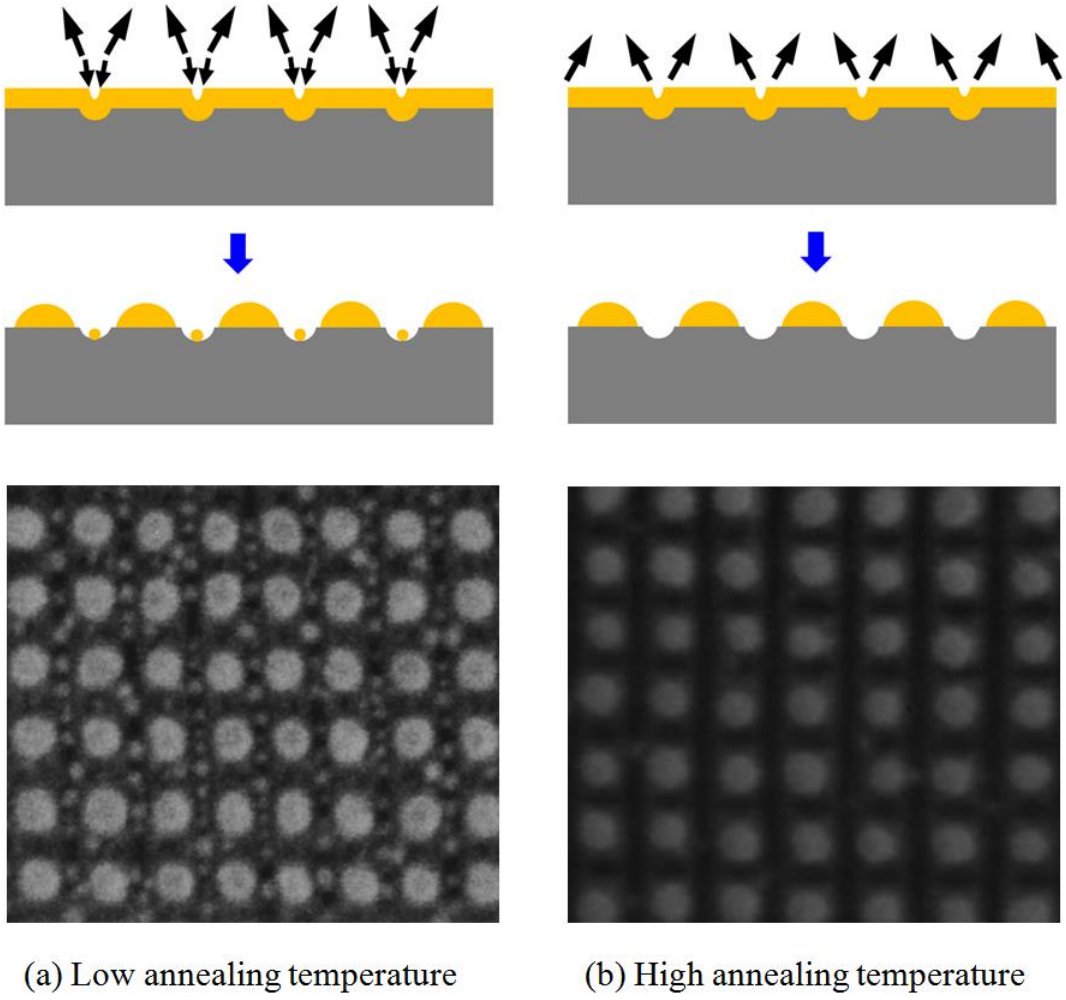

Figure 4. 11 Schematic illustration of dot formation on patterned substrate for different annealing temperatures; (a) Low annealing temperatures and (b) High annealing temperatures

4.3.3 Effect of NPF indentation load on the morphology of nano dot array aggregated on patterned substrate.

Figure 4.12 (a) shows the FE-SEM micrographs of the grid patterns fabricated by NPF. The grid size is 100 nm for all specimens and the indentation load is varied from 0.4 N to 1.5 N. It is found that the width of the grooves increases with the increase in indentation load. This implies that the depth of the grooves also increases with the increase in indentation load. When the load is 1.5 N, the chipping occurs and the grid pattern was not fabricated. It is noted that only line pattern was fabricated when the load is 1.5 N due to the chipping.

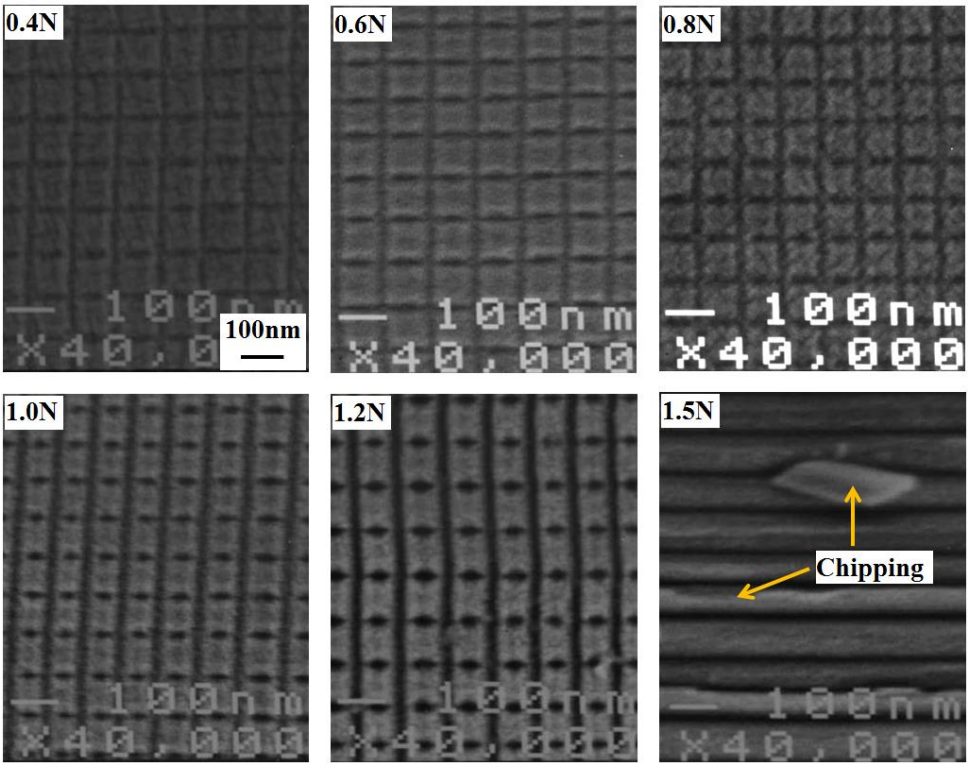

(a) Grid pattern with different indentation load

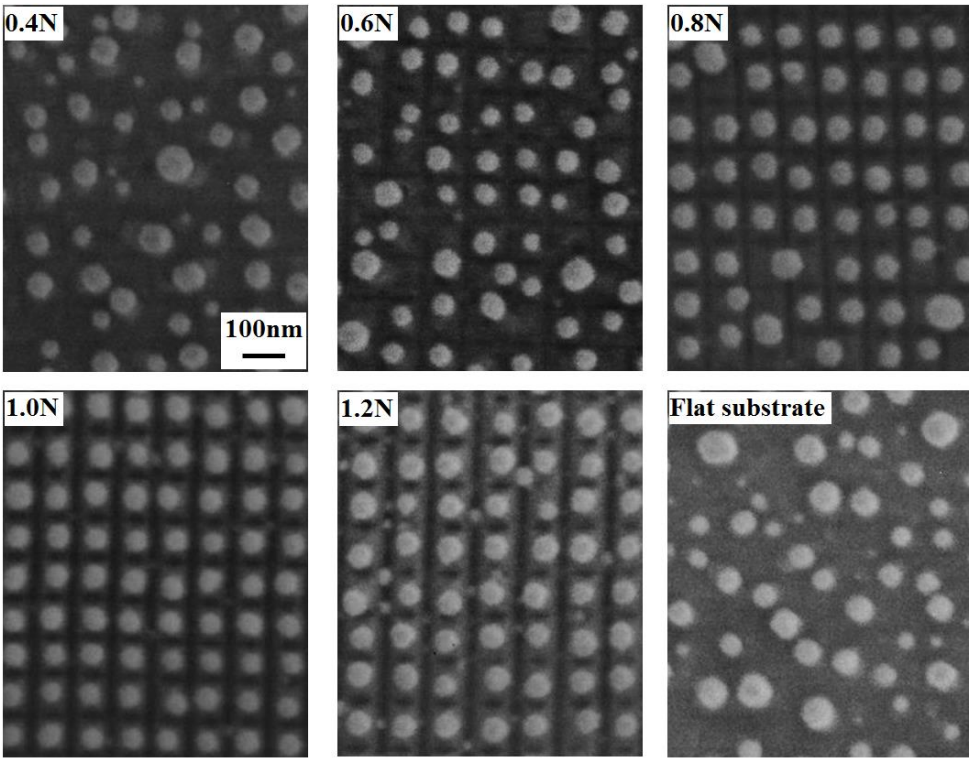

(b) Nano dot arrays aggregated on patterned substrate by thermal annealing

Figure 4. 12 SEM micrographs of: (a) Grid pattern with different indentation load and (b) Nano dot array aggregated on patterned substrate by thermal annealing

Figure 4.12 (b) shows the FE-SEM micrographs of the nano dot arrays aggregated on the patterned substrates after annealing at 1000^{o}C for 30 minutes. It is found that the indentation load strongly affects the morphology of the nano dot arrays. When the indentation load is small (0.4 N), the dots are aligned randomly with different sizes. When the indentation load is increased (0.6 N), the regularity and uniformity of nano dot array is improved. However, the regularity of the nano dot array is not so clear. Some dots are aligned in a grid pattern while others are randomly distributed. When the indentation load is further increased to 0.8 N, the dots are almost aligned in a grid whose pitch coincides with the pitch of the grooves grid pattern fabricated by NPF. However, some dots are connected with the adjacent dots, and formed larger dots which randomly aggregate on both the grid square units and the grooves. When the indentation load is increased to 1.0 N, each dot is aggregated on one grid square unit. The nano dot array is well aligned and good uniformity. When the indentation load is further increased to 1.2 N, the alignment and uniformity of the nano dot array become worse. Most of the dots are aggregated on the grid unit while some others are aggregated on the grooves. The dots aggregate on the grooves degrade the uniformity and regularity of the nano dot array. The lower, right-hand side corner micrograph shows a nano dot array randomly aggregated on a flat substrate coated with 12 nm gold film and subjected to same annealing condition. It is obvious that with proper indentation load, the patterning by NPF improves the uniformity and regularity of the nano dot array.

Figure 4.13 shows the variation in the mean diameter of the nano dot array and the RAE against the indentation load. The vertical bars on the graph denote the standard deviation of the diameter of the nano dots. It is found that the mean diameter of the nano dot array does not fluctuate so much with the increase in indentation load from 0.4 N to 1.2 N. When the indentation load is 0.8 N, the diameter of the nano dot array is slightly larger than the ones aggregated on substrate patterned with other indentation loads. This is because some dots merge with the adjacent dots, and form larger dots. The standard deviation of the diameter of the nano dots decreases with the increase in the indentation load when the load is smaller than 1.0 N. It becomes minimum at 1.0 N, and it increases with the increase in indentation load when the indentation load is larger than 1.0 N. The variation of RAE with the increase in the indentation load is similar to the variation of standard deviation. Also, it is found that RAE becomes minimum when the indentation

load is 1.0 N. This implies that uniformity and regularity of the nano dot array become the best when the indentation load is 1.0 N in this study.

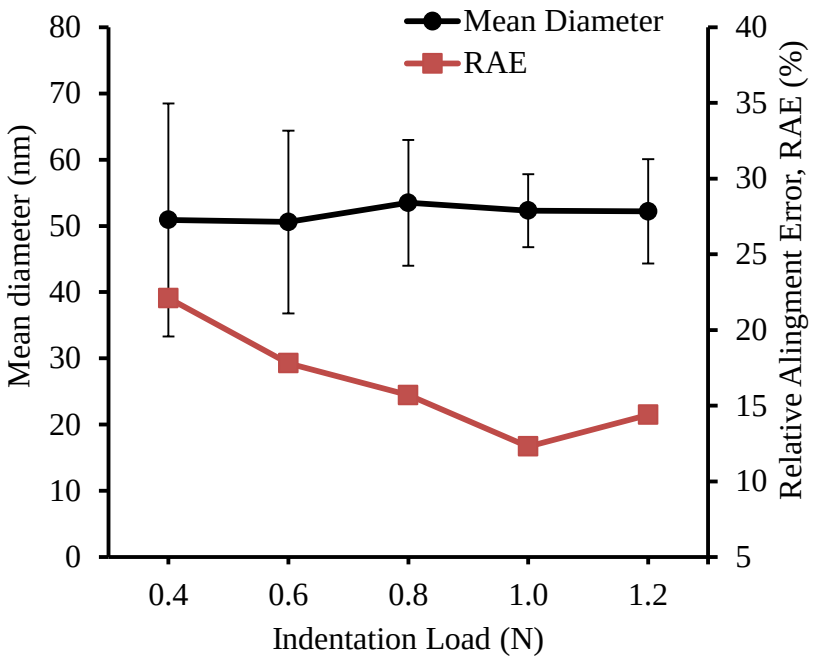

Figure 4. 13 Mean diameter of the nano dot array and its standard deviation and RAE versus indentation load

Figure 4.14 illustrates three types of dot aggregation patterns observed in the experiments with different indentation loads. As shown in figure 4.14 (a), when the indentation load is small, the depth of the grooves is small and the width of the grooves is narrow. As a result, the depth of debossed grooves grid pattern on the gold film surface is very small. Therefore, the metal film is not separated by the groove grid pattern perfectly. The metal film aggregates into many dots randomly distributed on substrate. When the indentation load is in proper range as shown in figure 4.14 (b), the metal film is separated only at the groove grid, and aggregates into one dot on each grid square unit. As a result, the nano dot array is good uniformity and well aligned on a grid pattern. When the indentation load is large as shown in figure 4.14 (c), both the depth and width of the grooves are large. The gold film is separated well at the groove grid. In addition, since the groove is wide and deep, some parts of gold film aggregates onto grooves, and form tiny dots on the groove as seen in figure 4.14 (c). These tiny dots on the grooves deteriorate the uniformity and regularity of the nano dot array.

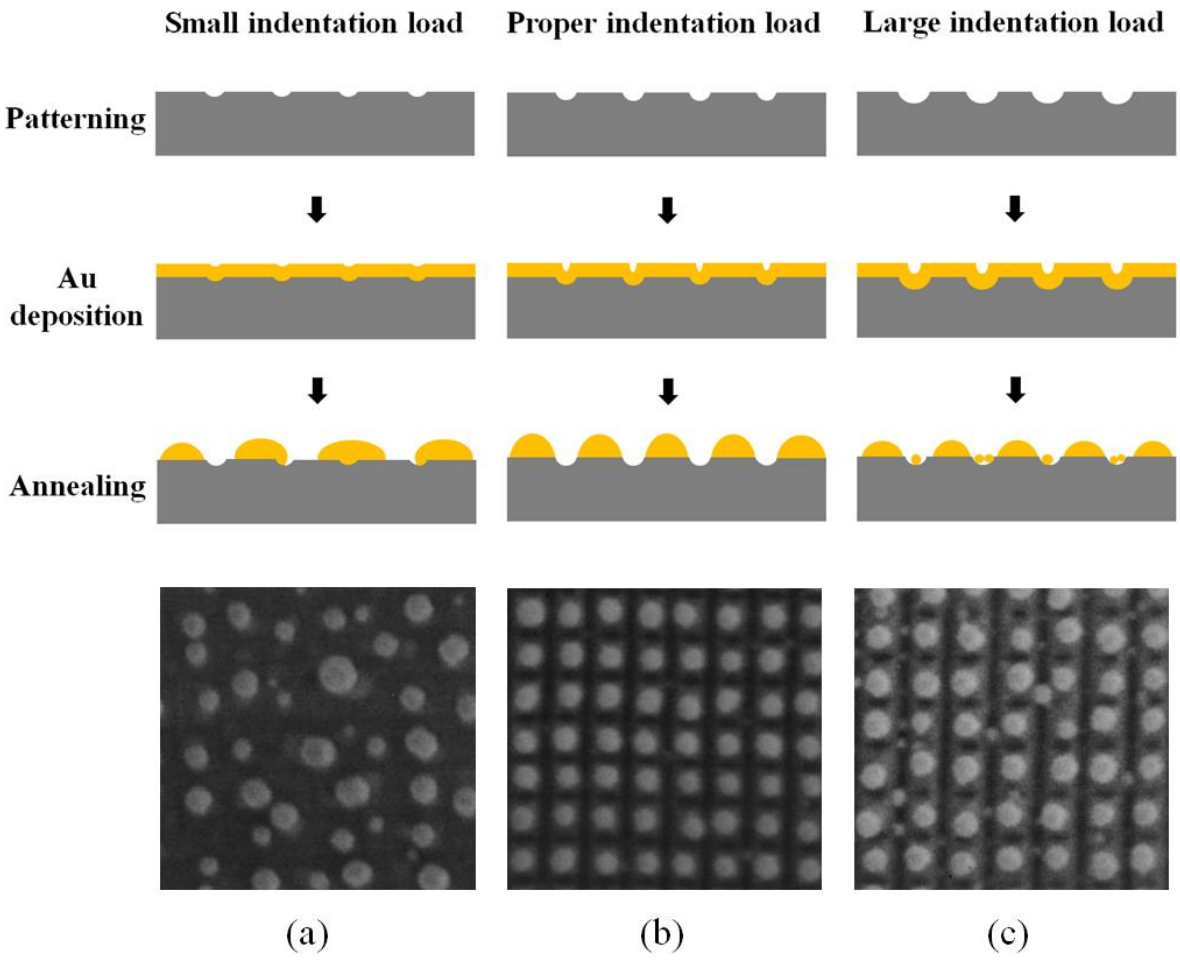

Figure 4. 14 Schematic illustration of dot formation on patterned substrate: (a) Small indentation load, (b) proper indentation load and (c) large indentation load

4.3.4 Transfer of an ordered nano dot array to a platic film

From experimental results in chapter 3, it was found that for Araldite rapid epoxy the nano dot transfer ratio decreases with the increase in annealing temperature, and annealing temperature at 600^{o}C results in highest transfer ratio when transfer of a random nano dot array to an Araldite rapid epoxy film. In contrast, the SpeciFix-20 epoxy shows increase of transfer ratio with the increase in annealing temperature, and annealing temperature at 900^{o}C and 1000^{o}C results in very high transfer ratio when transfer of a random nano dot array to a SpeciFix-20 epoxy film. Therefore, in the experiment for transferring of an ordered nano dot array to an Araldite rapid epoxy film, the annealing temperature at 600^{o}C is investigated. While in the experiment for transferring of an ordered nano dot array to a SpeciFix-20 epoxy film, the annealing temperatures at 900^{o}C and 1000^{o}C are investigated.

Transfer of an ordered nano dot array to Araldite rapid epoxy:

Figure 4.14 shows the FE-SEM micrographs of (a) ordered nano dot arrays on quartz glass substrates and (b) the ordered nano dot arrays transferred to Araldite rapid epoxy films. The grid size is 100 nm, and indentation load is 1.0 N. The gold film thickness is varied from 8 to 14 nm. Annealing condition is at 600^{o}C for 10 min. The experimental procedures and conditions to transfer of an ordered nano dot array to an Araldite rapid epoxy film are the same as those ones to transfer a random nano dot array to an Araldite rapid epoxy film presented in chapter 3. From figure 4.14, it was found that the gold film thickness affects the transfer ratio of nano dot array to Araldite rapid epoxy. When the gold film thickness is 8 nm, the nano dot array was successfully transferred to Araldite rapid epoxy. When the gold film thickness is more than 10 nm, the nano dot arrays are not transferred to Araldite rapid epoxy. Only some tiny dots aggregated on the grooves are transferred to Araldite rapid epoxy. This maybe because the difference in contact angle of the nano dots generated from different gold film thicknesses. It is known that the aggregation of the gold film into nano dots is faster when the gold film is thinner [188]. In addition, the smaller dots generated from thinner gold film also aggregate faster into circular shape than the larger ones [188]. Therefore, when the gold film is thin (8 nm), the aggregation of golf film into nano dots is very fast. This results in higher contact angle between the nano dots and the substrate, and thus smaller contact area between the dot and the substrate. This results in weak adhesion between the dots and the substrate. Therefore the nano dots array is transferred to the Araldite rapid epoxy film.

On the other hand, when the gold film thickness is more than 10 nm, the aggregation of gold film into nano dots is slower. As a result, the nano dots are remained distorted and flat. Thus, the contact angle between the dots and the substrate is low and the contact area between the dots and the substrate is large. This results in stronger adhesion between the dots and the substrate when the gold film is thicker. Therefore, the nano dot arrays are not transferred to Araldite rapid epoxy film when the gold film thickness is more than 10 nm. However, some tiny dots aggregated on the grooves of the pattern are transferred to Araldite rapid epoxy film when the gold film thickness is more than 10 nm. This can be also attributed to the higher contact angle and lower contact area of the tiny dots on the grooves. This is because the dots aggregate on the grooves are much smaller than those ones aggregate on the grid square units. The smaller dots aggregate faster and thus results

in higher contact angle and smaller contact area. Therefore, the tiny dots on the grooves are transferred to Araldite rapid epoxy film, while the larger dots on the grid square units are remained on the quartz glass substrates when the thickness of gold film is thicker than 10 nm.

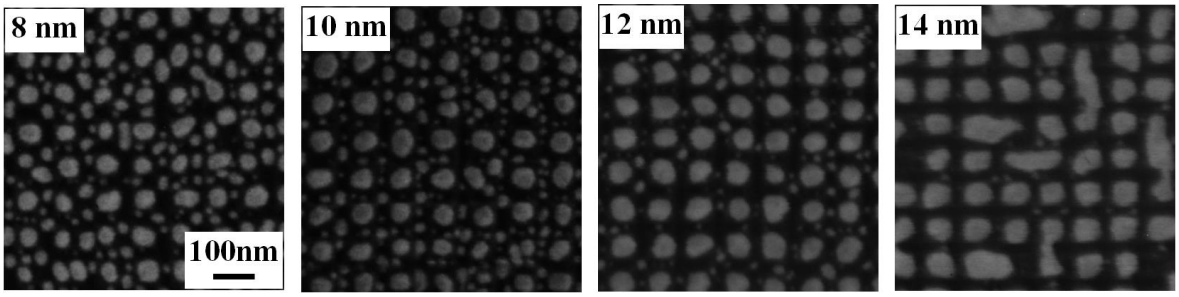

(a) Nano dot array of quartz glass substrate

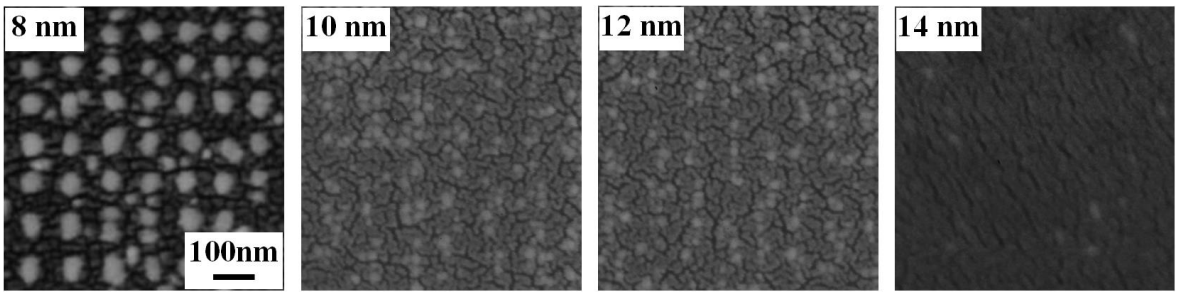

(b) Nano dot array transferred to Araldite rapid epoxy

Figure 4. 15 FE-SEM micrographs of: (a) nano dot array on quartz glass substrate, (b) nano dot array transferred to Araldite rapid epoxy

When the gold film thickness is 8 nm, the nano dot array is successfully transferred to an Araldite rapid epoxy film. After the nano dot array is transferred to the Araldite rapid epoxy film, substrate was re-employed to investigate the re-usability of the patterned substrate. After transferring, the patterned substrate is subjected to cleaning step as follows: the substrate was emerged into the Aurum solution for 30 min to remove the gold dots remained on the patterned substrate after transferring. Then, it is cleaned in acetone by using ultrasonic bath for 10 min for twice. It was dried. After that, cleaned substrate is used for the second time of transferring of another ordered nano dot array to another Araldite rapid epoxy film by repeating three steps: gold deposition for 8 nm in thickness, annealing

at 600^{o}C for 10 min, and transfer of the ordered nano dot array to another Araldite rapid epoxy film.

Figure 4.16 shows the FE-SEM micrographs of the (a) grid patterned fabricated on a quartz glass substrate by NPF, the substrated is deposited with gold film for 8 nm in thickness, (b) gold nano dots array aggregated on the patterned substrate afterannealing at 600oC for 10 minutes, (c) gold nano dot array transferred to an Araldite rapid epoxy film, (d) the patterned substrate after transferring, (e) patterned substrate after cleaning, the cleaned substrate is deposited with gold film for 8 nm in thickness, (f) the nano dot array

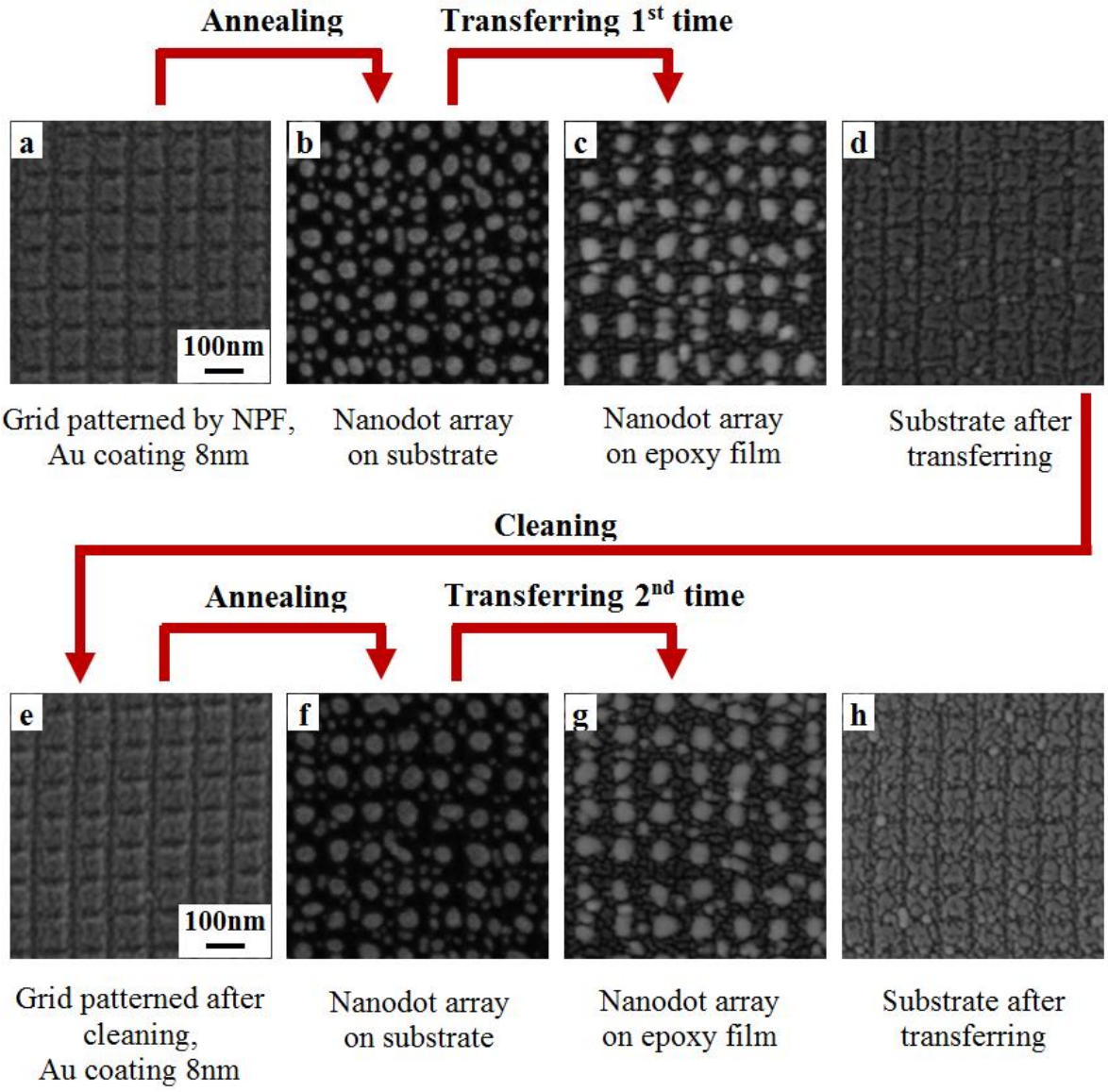

Figure 4. 16 The first time and second time of using the patterned substrate for transferring of ordered nano dot array to Araldite rapid epoxy films

aggregated on the patterned substrate after annealing for 2nd time, (g) gold nano dot array transferred to another Araldite rapid epoxy film, and (h) the patterned substrate after the 2nd time transferring. It is found that another ordered gold nano dot array was successfully fabricated on another Araldite rapid epoxy film as seen in figure 4.16 (g) by re-employing the patterned substrate. It is also found that the morphology of the nano dot array on the quartz substrate and the Araldite rapid epoxy film for the first time transferring is similar to those accordingly ones in the second time of transferring. The dot transfer ratio around 90% was achieved for both two times of transferring. This demonstrates that the patterned substrate can be used repeatedly. Since, the fabrication of nano grooves grid patterns by NPF (step 1 in figure 4.1) is the most time consuming but the three steps: metal deposition, thermal dewetting, and nano dot transferring (from step 2 to 4 in the figure 4.1) require very short time. In addition, it is noted that in the second time of transferring, only three steps: metal deposition, thermal dewetting and nano dot transferring (from step 2 to 4 in the figure 4.1) were implemented, and the NPF step was not used. Therefore, the throughput of the proposed process is expected to be very high.

Transfer of an ordered nano dot array to SpeciFix-20 epoxy:

The annealing temperature at 900^{o}C and 1000^{o}C were examined to fabricate an ordered nano dot array on the patterned substrate and transfer the ordered nano dot array to a SpeciFix-20 epoxy film. Figure 4.17 shows the FE-SEM micrographs of (a) ordered nano dot arrays on quartz glass substrates and (b) the nano dots arrays transferred to SpeciFix-20 epoxy films. The grid size is 100 nm, and indentation load is 1.0 N. The gold film thickness is varied from 10 to 14 nm. Annealing condition is at 900^{o}C for 30 min. The experiment procedures and conditions to transfer ordered nano dot arrays to SpeciFix-20 epoxy films are the same as those ones to transfer random nano dot array to SpeciFix-20 epoxy film presented in chapter 3. It is found that the ordered nano dot arrays were successfully transferred to SpeciFix-20 epoxy films for both three gold film thicknesses. Although several nano dots were not transferred to SpeciFix-20 epoxy films, the nano dot arrays on SpeciFix-20 epoxy films are good uniformity and regularity.

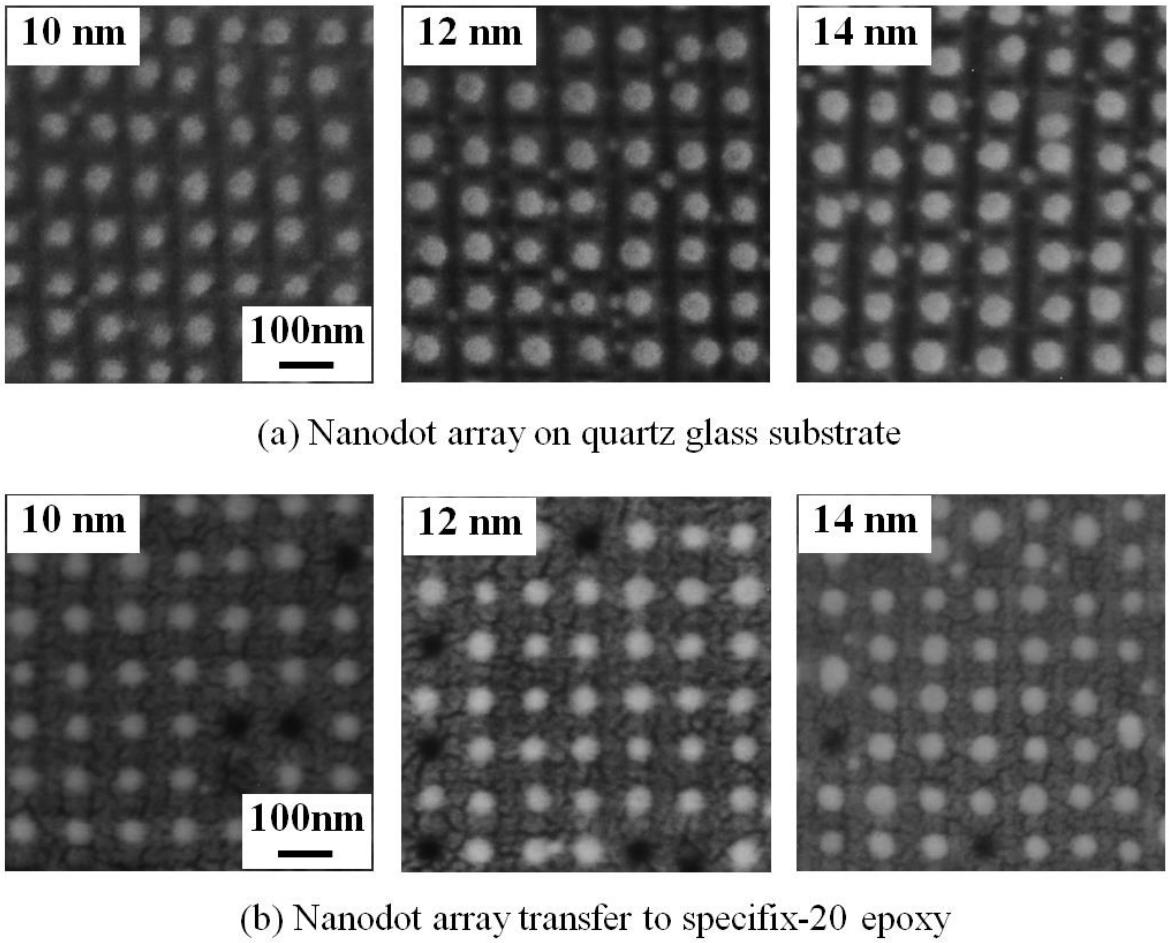

Figure 4. 17 FE-SEM micrographs of: (a) nano dot array on quartz glass substrate, (b) nano dot array transferred to SpeciFix-20 epoxy, the annealing condition is at 900^{o}C for 30 min

Figure 4.18 shows the FE-SEM micrographs of (a) ordered nano dot array on quartz glass substrate and (b) the nano dots array transferred to SpeciFix-20 epoxy. The grid size is 100 nm, and indentation load is 1.0 N. The gold film thickness is varied from 10 to 14 nm. Annealing condition is at 1000^{o}C for 30 min. It is found that the nano dot array were partially transferred to SpeciFix-20 epoxy film when the gold film thickness is in between 10 and 12 nm, but no dots were transferred to SpeciFix-20 epoxy when the gold film thickness is 14 nm.

When transferring a random nano dot array to a sepcifix-20 epoxy film, both annealing temperatures at 900^{o}C and 1000^{o}C result in high transfer ratios. However, when transferring an ordered nano dot array to a SpeciFix-20 epoxy film, two annealing temperatures result in different transfer ratios of nano dot array to SpeciFix-20 epoxy. When annealing temperature is at 900^{o}C, high transfer ratio of nano dot array was obtained and the ordered nano dot arrays were successfully transferred to SpeciFix-20 epoxy films.

However, the ordered nano dot arrays were partially transferred to SpeciFix-20 epoxy films with a low transfer ratio when the annealing temperature is at 1000^{o}C. The reason may be attributed to the surface quality of the substrates, the contamination on the surface of the substrates between the experiments, or the humidity of the environment which strongly affect the transfer ratio of nano dot array to SpeciFix-20 epoxy. Although different transfer ratios obtained at different annealing temperatures, ordered nano dot arrays were successfully transferred to SpeciFix-20 epoxy film when the annealing temperature is at 900^{o}C. This result demonstrates the feasibility of the process proposed in this research work for fabrication of sub-100 nm in diameter of an ordered nano dot array on a plastic film.

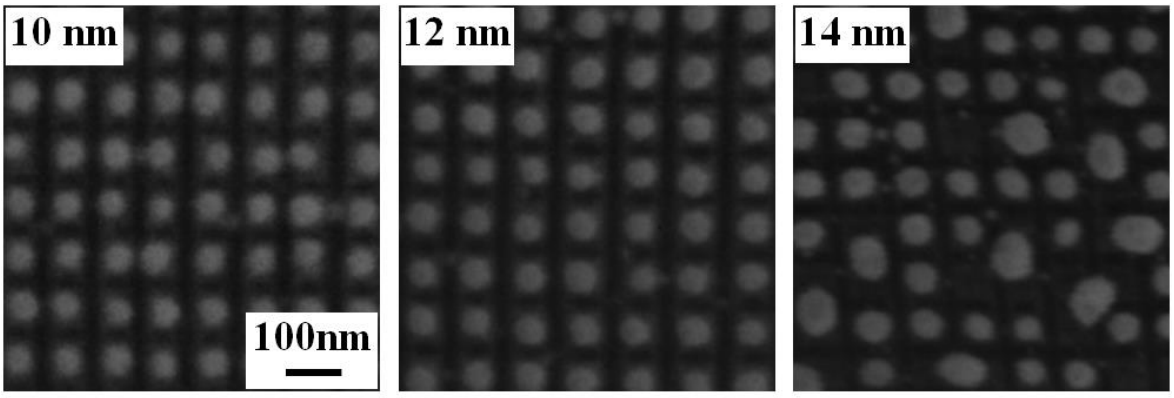

(a) Nanodot array on quartz glass substrate

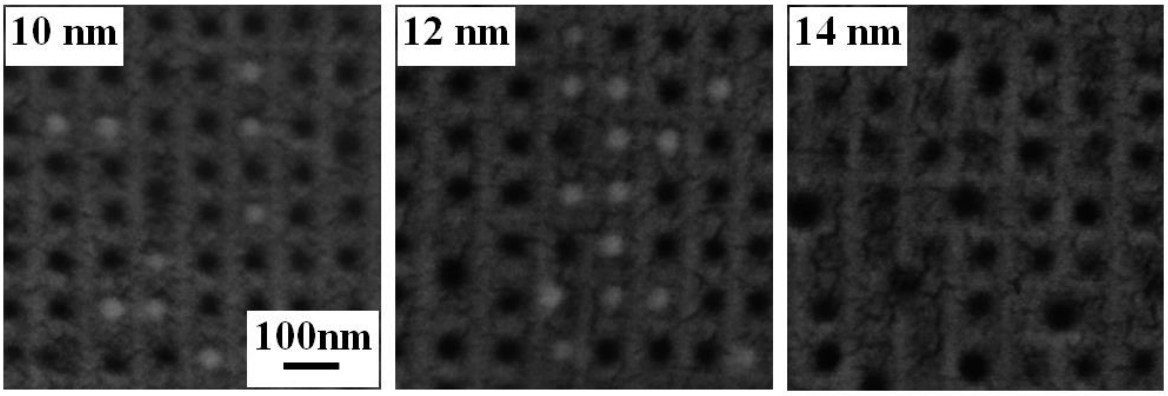

(b) Nanodot array transfer to specifix-20 epoxy

Figure 4. 18 FE-SEM micrographs of: (a) nano dot array on quartz glass substrate, (b) nano dot array transferred to SpeciFix-20 epoxy, the annealing condition is at 1000^{o}C for 30 min

When the proper condition is found, it is expected that an ordered nano dot array can be transferred to a plastic film at a very high transferred ratio. In addition, when more

advanced plastic materials are developed; many plastic films or plastic substrates have good adhesion to metal nano dots, fabrication of ordered nano dot arrays on plastic films or plastic substrates by the process proposed in this research is easily implemented. The experimental results in previous section demonstrated that the patterned substrate can be re-used for second time of transferring nano dot array to a plastic film. When more proper and advanced substrate materials are employed for the patterned substrate, it is expected that the substrate can be re-used many time. Therefore, the throughput of this process is very high.

For future work to develop this study, first of all, the process condition is optimized to obtained high transferred ratio when transfer of an ordered nano dot array from a patterned substrate to a plastic film. In addition, more advanced of substrate materials and plastic materials are also necessary to obtain high throughput of fabrication process by using repeatedly the patterned substrate to transfer of ordered nano dot arrays to a plastic film. Once, the optimum process condition is obtained, it is necessary to fabrication of ordered nano dot arrays on plastic films in large area to realize the applications of ordered nano dot arrays on plastic films to various fields such as bio-sensors, plasmonic organic solar cells. In order to fabricate large area of ordered nano dot arrays on a patterned substrate, the patterned area on the substrate should be large. This can be accomplished by utilizing scratching process which is similar to NPF, but the difference is from the fact that in scratching, a diamond tool is scratch on the surface of a substrate to make the nanopattern instead of indentation the surface with a diamond tool. In NPF indentation, the patterned area is limited by the width of the tool. However, in scratching process, the patterned area is not limited by tool size. Therefore, large area of nanopattern on substrate can be achieved by employing scratching process.

4.4 Summary

Investigations and results of this chapter are summarized as follows:

1. Effects of gold film thickness on the morphology of a nano dot array aggregated on a patterned substrate

(i) The thickness of gold film strongly influences the morphology of nano dot array. When the gold film thickness is thin, the gold film aggregates on both the grid square

units and on the grooves, the uniformity and regularity of nano dot array is poor. When the gold film thickness is in a proper range, the gold film aggregates on the grid square units and forms a good uniformity and regularity of nano dot array. When the gold film is thick, some dots are merged with adjacent ones, and form larger dots randomly distributed on substrate, the uniformity and regularity of nano dot array is poor.

(ii) The mean diameter of the nano dot array increases when the gold film is thicker. Patterning on a substrate improves the uniformity of regularity of the nano dot array after annealing only when gold coating thickness is in a proper range. A good uniformity and regularity nano dot array was achieved when the gold film thickness is 12 nm in this study.

2. Effects of annealing temperature on the morphology of a nano dot array aggregated on a patterned substrate

(i) Annealing temperature also strongly influences the morphology of a nano dot array aggregated on a patterned substrate. When the annealing temperature is low, the gold film aggregates on both the grid square units and on the grooves. When the annealing temperature is high, the gold film aggregates only the grid square units and do not aggregate on the grooves, and results in good uniformity and regularity of nano dot array. The reason is attributed to the fact that gold film tends to aggregate on a flat surface other than on a curved surface due to the total energy of the dot/substrate system reduces more on a flat surface than on a curved surface. A good uniformity and regularity of nano dot array was achieved when the annealing temperature is at 1000^{o}C.

3. Effects of indentation load on the morphology of nano dot array aggregated on parttened substrate

(i) Indentation load also strongly influences the morphology of a nano dot array aggregated on a patterned substrate. When the indentation load is small, the gold film aggregates into random nano dot array. When the indentation load is in proper range, the gold film is separated well by the grid grooves and aggregates into an ordered

nano dot array. When the indentation load is large, the gold film is aggregates on both the grid square units and on the grooves, the uniformity and regularity of nano dot array becomes worse. A good uniformity and regularity nano dot array was achieved when the indentation load is 1.0 N in this study.

(ii) Patterning on substrate by NPF improves the uniformity and regularity of the nano dot array through annealing process under proper conditions of gold film thickness, annealing temperature, and indentation load.

4. Transfer of an ordered nano dot array to a plastic film

(i) An ordered nano dot array was successfully transferred to an Araldite rapid epoxy when the gold film thickness is 8 nm.

(ii) The substrate can be re-used after transferring of an ordered nano dot array to an Araldite rapid epoxy film. The substrate was used for the second time of transferring of an ordered nano dot array to array to another Araldite rapid epoxy film. A transfer ratio around 90% was achieved for both two times of transferring.

(iii) Ordered nano dots arrays were also successfully fabricated on SpeciFix-20 epoxy films when the annealing temperature is at 900^{o}C. The nano dot arrays transferred to SpeciFix-20 epoxy film are good uniformity and regularity. Ordered nano dots arrays were partially transferred to SpeciFix-20 epoxy film at a low transfer ratio when the annealing temperature is at 1000^{o}C.

(iv) The feasibility of process proposed in this research work for fabrication of sub-100 nm in diameter ordered nano dot array on a plastic film is demonstrated. It is also verified that under proper condition, the patterned substrate can be re-used for transferring nano dot array to a plastic film. Once, the optimum condition is obtained, and more advanced substrate materials and plastic materials are employed, the process can achieve high transfer ratio and high throughput.

CHAPTER 5

Conclusions

In this research work, a new fabrication process of a metallic nano dot array on a plastic film by thermal dewetting and dot transfer technique is proposed. Firstly, the process for fabrication of a random metallic nano dot array on a plastic film by thermal dewetting on a flat substrate and dot transfer technique studied. The experiments were conducted to verify the feasibility of the process. Then, the proposed process is extended to fabrication of an ordered metallic nano dot array on a plastic film by nano-plastic forming assisted thermal dewetting on a patterned substrate and dot transfer technique. The experiments were conducted to demonstrate the feasibility of the extended process. The investigations in this study lead to the following conclusions.

For the first process: fabrication of a random metallic nano dot array on a plastic film by thermal dewetting on a flat substrate and dot transfer technique. The experimental results show that the morphology of a random nano dot array strongly depends on the annealing temperature, annealing time, substrate material, and gold film thickness. In addition, it is found that the LSPR property of a nano dot array strongly depends on its morphology, especially, the circularity of the nano dot array. It is also found that the transfer ratio is strongly influenced by the substrate material, plastic material, and annealing temperature. The main results are summarized as follows:

Effects of process conditions on the morphology of nano dot array

(i) Mean diameter and corresponding standard deviation of the nano dots increases with the increase in the gold film thickness, but decreases with the increase in the annealing temperature. This is attributed to the surface diffusion of gold atoms which affects the aggregation of gold film into nano dots.

(ii) Substrate material affects morphology of the aggregated nano dots. The nano dots aggregated on a quartz glass substrate are large and sparse, while the nano dots aggregated on a silicon substrate are small and dense. The difference between morphologies of nano dots on a quartz glass substrate and on a silicon substrate are

attributed to the difference in the surface energy of the two substrate materials.

(iii) The contact angle of the nano dots both on a quartz glass substrate and on a silicon substrate increases with the increase in the annealing temperature. The silicon substrate results in slightly higher contact angle of nano dots than the quartz glass substrate. The reason is attributed to the difference in the surface energy of the two substrate materials.

(iv) The circularity of nano dots increases with the increase in the annealing time, but becomes saturated to a certain value that depends on the annealing temperature. Maximum circularity of around 0.9 was achieved in this study.

Effects of process conditions on the LSPR property of a nano dot array

(i) The absorbance spectra of a nano dot array on a quartz glass substrate display a unique peak in the visible range. This absorbance peak shifts to longer wavelengths side and becomes broader with the increase in the gold film thickness. This is attributed to the difference in the morphology of nano dot array generated by different thicknesses of gold film.

(ii) The absorbance peak shifts to shorter wavelengths side, the absorbance peak intensity decreases, and absorbance peak becomes sharper when either the annealing time or the annealing temperature is increased. The annealing temperature shows more significant effects on the variation in LSPR absorbance peak wavelength and peak intensity than the annealing time in this study. This is attributed to the more uniform, more circular nano dots morphology which weakens the coupling effects of the LSPR of the nano dots.

(iii) It is found that the variation in the LSPR property is closely correlated to the variation in the nano dots circularity.

Effects of process conditions on the transfer ratio of nano dot array to a plastic film

(i) The substrate material affects the transfer ratio of a nano dot array to a plastic film.

The silicon substrate shows slightly higher transfer ratio than the quartz glass substrate. This is attributed to the difference between the surface energy of the two substrate materials.

(ii) The plastic materials show contrary trends of variation of transfer ratio against annealing temperature. Araldite rapid epoxy decreases the transfer ratio while the SpeciFix-20 epoxy increases transfer ratio when the annealing temperature becomes higher. This is attributed to the difference between the viscosities of the two epoxies.

(iii) Dot transfer mechanism is discussed theoretically based on the difference of total free energy and compared with the experimental results. PDMS and SpeciFix-20 epoxy show good agreement with the dot transfer mechanism theory.

(iv) A 20 cm^2 in area of random nano dot array was successfully fabricated on an Araldite rapid epoxy film. It demonstrated feasibility of the proposed process for large area fabrication of a nano dot array on a plastic film.

For the second proposed process: fabrication of an ordered metallic nano dot array on a plastic film by nano-plastic forming assisted thermal dewetting on a patterned substrate and dot transfer technique. The experimental results show that the uniformity and regularity of a nano dot array strongly depends on the gold film thickness, the annealing temperature and the indentation load. The ordered nano dot array is then transferred to a plastic film to evaluate the feasibility of the process. The main results are summarized as follows:

Effects of gold film thickness on the morphology of a nano dot array aggregated on a patterned substrate

(i) The thickness of gold film strongly influences the morphology of nano dot array aggregated on a patterned substrate through thermal annealing process. When the gold film is thin, it aggregates on both the grid square units and on the grooves, the uniformity and regularity of nano dot array are poor. When the gold film thickness is in a proper range, the gold film aggregates on the grid square units and form good uniformity and regularity of nano dot array. When the gold film is thick, some dots are merged with adjacent ones, and form larger dots randomly distributed on substrate,

the uniformity and regularity of nano dot array are poor.

(ii) The mean diameter of the nano dot array increases when the gold film is thicker. Patterning on a substrate improves the uniformity of regularity of the nano dot array after annealing only when gold film thickness is in a proper range. A good uniformity and regularity nano dot array was achieved when the gold film thickness is 12 nm in this study.

Effects of annealing temperature on the morphology of a nano dot array aggregated on a patterned substrate

(i) Annealing temperature also strongly influences the morphology of a nano dot array aggregated on a patterned substrate through thermal annealing process. When the annealing temperature is low, the gold film aggregates on both the grid square unit and on the grooves. When the annealing temperature is high, the gold film aggregates only the grid square units and does not aggregate on the grooves, and results in good uniformity and regularity of nano dot array. The reason is attributed to the fact that gold film tends to aggregate on a flat surface other than on a curved surface due to the total energy of the dot/substrate system reduces more on a flat surface than on a curved surface. A good uniformity and regularity of nano dot array was achieved when the annealing temperature is at 1000^{o}C.

Effects of indentation load on the morphology of a nano dot array aggregated on a patterned substrate

(i) Indentation load also strongly influences the morphology of a nano dot array aggregated on a patterned substrate. When the indentation load is small, the gold film aggregates into a random nano dot array. When the indentation load is in proper range, the gold film is separated well by the grid grooves and aggregates into an ordered nano dot array. When the indentation load is large, the gold film aggregates on both the grid square units and on the grooves, the uniformity and regularity of nano dot array becomes worse. A good uniformity and regularity nano dot array was achieved when the indentaion load is 1.0 N in this study.

(ii) Patterning on substrate by NPF improves the uniformity and regularity of the nano

dot array through annealing process only under proper conditions of gold film thickness, annealing temperature, and indentation load.

Transfer of an ordered nano dot array to a plastic film

(i) An ordered nano dot array was successfully transferred to an Araldite rapid epoxy when the gold film thickness is 8 nm.

(ii) The substrate can be re-used after transferring of an ordered nano dot array to an Araldite rapid epoxy film. The substrate was used for the second time of transferring of an ordered nano dot array to array to another Araldite rapid epoxy film. A transfer ratio around 90% was achieved for both two times of transferring.

(iii) Ordered nano dots arrays were successfully fabricated on SpeciFix-20 epoxy films when the annealing temperature is at 900^{o}C. The nano dot arrays transferred to SpeciFix-20 epoxy films are good uniformity and regularity. Ordered nano dots arrays were partially transferred to SpeciFix-20 epoxy film at a low transfer ratio when the annealing temperature is at 1000^{o}C.

(iv) The feasibility of process proposed in this research work for fabrication of sub-100 nm in diameter ordered nano dot array on a plastic film is demonstrated. One the optimum condition is obtained and more advanced of substrate materials and plastic materials are employed, the process can achieve high transfer ratio and high throughput.

For future work to develop this research work, the process condition is optimized to obtained high transfer ratio when transfer of an ordered nano dot array from a patterned substrate to a plastic film, and to enhance the throughput of this process. In addition, it is desired to fabricate of ordered nano dot arrays on plastic films in large area to realize the applications of order nano dot arrays on plastic films to various fields such as bio-sensors, plasmonic organic solar cells. Furthermore, it is necessary to develop an automatic system to transfer of nano dot arrays from a substrate to a plastic film.

REFERENCES

[1] From National Nanotechnology Initiative (NNI) of US government http://www.nano.gov/sites/default/files/pub_resource/nanotechnology_bigthingsfromatinyworld-print.pdf

[2] Taniguchi N. (1974) "On the Basic Concept of Nanotechnology," Proceedings of the International Conference of Production Engineering, London, Part II. British Society of Precision Engineering

[3] Feynman R. P. (1992) "There's Plenty of Room at the Bottom," *Journal of Microelectromechanical Systems* **1** 60–6

[4] Drexler E. (1987) Engines of Creation: The Coming Era of Nanotechnology, New York: Broadway Books

[5] Hullmann A. (2006) The economic development of nanotechnology-An indicators-based analysis

[6] Roco M. C., Mirkin C. C., Hersam M. C. (2011) Nanotechnology research directions for societal needs in 2020: summary of international study *J. of Nanoparticle Research* **13**, pp.897-919

[7] Pimpin A. and Srituravanich W. (2012) Reviews on Micro- and Nanolithography Techniques and their Applications *Engineering Journal* **16**, issue 1.

[8] Brunner T. A. (2003) Why optical lithography lives forever. *J Vac Sci Technol B* **21** (6), pp. 2632-2637

[9] Mordechai R. et al (2003) Recent trends in optical lithography. *Linc Lab J* **14**:221-236

[10] Pease R. P. and Chou S. Y. (2008) Lithography and Other Patterning Techniques for Future Electronics *Proceedings of the IEEE* **96**, No. 2

[11] Ito T. (2009) Nanolithography: Length–Scale Limitations *Taylor & Francis Group LLC publication*

[12] Wong A. K. K. (2001) Resolution Enhancement Techniques in Optical Lithography *Optical Engineering Press*, Bellingham, WA

[13] Cui Z. (2008) Nanofabrication: Principles, Capabilities and Limits *Springer Science & Business Media, LLC*

[14] Early K., Schattenberg M. L. and Smith H. I. (1990) Absence of resolution degradation in x-ray lithography. *Microelectronic Engineering*, **11**, pp. 317–321.

[15] Vladimirsky Y. *et al.* (1999), Demagnification in proximity X-ray lithography and extensibility to 25 nm by optimizing Fresnel diffraction. *J. Phys. D: Appl. Phys*. **32**: p. L114.

[16] Tseng A. A., Chen K., Chen C. D., Ma K. J. (2003) Electron beam lithography in nanoscale fablication: recent developments. *IEEE Transactions on Electronic Packaging Manufacturing* **62**, pp.141-149

[17] Fischer B. P., Chou S. Y. (1993) 10 nm Electron Beam Lithography and Sub-50 nm Overlay Using a Modified Electron Scanning Microscope. *Appl Phys Lett* **62,** pp. 2989-2991

[18] Huigao D., Donald W, Joel K. W. Y., Bryan M. C., Vitor R. M., Karl K. B. (2010) Sub-10-nm half-pitch electron-beam lithography by using poly (methylmethacrylate) as a negative resist. *J Vac Sci Technol B* **28** (6): pp. C6C58-C6C62

[19] Gierak J., Vieu C., Launois H., Assayag G. B. and Septier A. (1997) Focused ion beam nanolithography on AlF3 at a 10 nm scale *Appl. Phys. Lett.* **70** (15)

[20] Wang D. and Schaaf P. (2011) Two-dimensional nanoparticle arrays formed by dewetting of thin gold films deposited on pre-patterned substrates *J. Mater. Sci., Mater. Electron.* **22**, pp. 1067–1070

[21] Chou S. Y., Krauss P. R. and Renstrom P. J. (1995) Imprint of sub-25 nm vias and trenches in polymers *Appl. Phys. Lett.* **67**, pp. 3114–3116

[22] Chou S. Y., Krauss P. R. and Renstrom P. J. (1996) Imprint lithography with 25-nanometer resolution. *Science* **272**, pp. 85-87

[23] Chou S. Y., Krauss P. R., Zhang W., Guo L. and Zhuang L. (1997) Sub-10 nm imprint lithography and applications *J. Vac. Sci. Technol. B* **15** (6), pp. 2897-2904

[24] Chou S. Y. and Krauss P. R. (1997) Imprint lithography with sub-10 nm feature size and high throughput *Microelectronics Engineering* **35**, pp.237-240

[25] Guo L. J. (2007) Nanoimprint lithography: methods and material requirements. *Adv. Mater.* **19**, pp.495-513

[26] Helmut S. (2008) Nanoimprint lithography: An old story in modern times? A review. *J. Vac. Sci. Technol. B* **26** (2), pp.458-480

[27] Wu W. *et al.* (2008) Sub-10 nm nanoimprint lithography by wafer bowing. *Nano letters* **8** (11), pp.3865-3869

[28] Zankovych S., Hoffmann T., Seekamp J., Bruch J. U. and Torres C. M. S. (2001) Nanoimprint lithography: challenges and prospects. *Nanotechnology* **12**, pp. 91-95

[29] Morecroft D. *et al.* (2009) Sub-15 nm nanoimprint molds and pattern transfer. *J Vac Sci Technol B* **27** (6), pp. 2837-2840

[30] Guo L J. (2004) Recent progress in nanoimprint lithography and its applications. *J Phys D: Appl. Phys.* **37,** pp.123-141

[31] Jung G. Y., Li Z., Wu W., Chen Y., Olynick D. L., Wang S. Y., Tong W. M. and Williams R. S. (2005) Vapor-Phase Self-Assembled Monolayer for Improved Mold Release in Nanoimprint Lithography *Langmuir* **21** 1158.

[32] Choi D. G., Lee D. I., Kim K. D., Jeong J. H., Choi J. H. and Lee E. S. (2009) Measurement of Surface Adhesion Force of Adhesion Promoter and Release Layer for UV-Nanoimprint Lithography *J. Nanosci. Nanotechnol*. **9**, 769.

[33] Kim K. S., Kim J. H., Lee H. J. and Lee S. R. (2010) Tribology issues in nanoimprint lithography *J. Mech Sci Technol* **24**, pp. 2-12

[34] Pierre Colson P., Henrist C. and Cloots R. (2013) Nanosphere Lithography: A Powerful Method for the Controlled Manufacturing of Nanomaterials *Journal of Nanomaterials* **2013** , 948510, 19 pages

[35] Chen C. J. (1993 and 2008) Introduction to scanning tunneling microscopy. *Oxford University Press*

[36] Brutting W. (2005) Physics of Organic Semiconductors *WILEY-VCH Verlag GmbH & Co. KGaA*, Weinheim ISBN 3-527-40550-X

[37] Yoshiro Y. (2009) Organic semiconductors for organic field-effect transistors *Sci. Technol. Adv. Mater.* **10**, 024313

[38] Burroughes J. H., Bradley D. D. C., Brown A. R., Marks R. N., Mackay K., Friend R. H., Burn P. L. and Holmes A. B. (1990) Light-emitting diodes based on conjugated polymers *Nature* **347**, 539

[39] Hee T. Y., Marcia M. P., John E. A. and Vitaly P. (2012) Ultra-flexible solution-processed organic field-effect transistors *Nature Communications* **3**, 1259

[40] Jason D. M. and Jiangeng X. (2012) Organic Semiconductors and their Applications in Photovoltaic Devices *Polymer Reviews*, **52**, pp. 1–37

[41] Kang M. G. and Guo L. J. (2007) Semitransparent Cu electrode on a flexible substrate and its application in organic light emitting diodes *J. Vac. Sci. Technol B* **25**, 2637

[42] Kang M. G., Park H. J., Ahn S. H. and Guo L. J. (2010) Transparent Cu nanowire mesh electrode on flexible substrates fabricated by transfer printing and its application in organic solar cells *Solar Energy Materials & Solar Cells* **94**, pp.1179–1184

[43] Smith P. J., Shin D. Y., Stringer J. E., Derby B. and Reis N. (2006) Direct ink-jet printing and low temperature conversion of conductive silver patterns *J. Mater. Sci.* **41**, pp. 4153-4158

[44] Park B. K., Kim D. J., Jeong S. H., Moon J. H. and Kim J. S. (2007) Direct writing of copper conductive patterns by ink-jet printing *Thin Solid Films* **515**, pp. 7706–771

[45] Unno N. and Tanaguchi J. (2011) Fabrication of the metal nano pattern on plastic substrate using roll nanoimprint *Microelectronic Engineering* **88**, pp. 2149‑2153

[46] Kim J. W., Yang K. Y., Hong S. H. and Lee H. (2008) Formation of Au nano-patterns on various substrates using simplified nano-transfer printing method *Applied Surface Science* **254**, pp. 5607–5611

[47] Lee J. H., Yang K. Y., Hong S. H., Lee H. and Choi K. W. (2008) Fabrication of 70 nm narrow metal nanowire structure on flexible PET film by nanoimprint lithography *Microelectronic Engineering* **85**, pp. 710–713

[48] Ahn S. H. and Guo L. J. (2008) High-speed roll-to-roll nanoimprint lithography on flexible plastic substrates *Adv. Mater.* **20**, pp. 2044-2049

[49] Chen C. H., Yu T. H. and Lee Y. C. (2011) Direct metal transfer lithography for fabricating wire-grid polarizer on flexible plastic substrate *Journal of Microelectromechanical System* **20**, pp. 916-921

[50] Hong S. H., Hwang J. Y., Lee H., Lee H. C. and Choi K. W. (2009) UV nanoimprint using flexible polymer template and substrate *Microelectronic Engineering* **86**, pp. 295-298

[51] T. D. Phuc, A. Yamanaka and M. Yoshino (2012) Study on Nano Dots Formation by Thermal Dewetting and Transfer to Plastic Films *Proceeding of Conference of the Japan Society for Precision Engineering*, (JSPE 2012).

[52] T. D. Phuc, A. Yamanaka and M. Yoshino (2012) High Throughput Method to Fabricate Ordered Nano dot array on Various Plastic Films *Journal of Key Engineering Materials*, **523-524**, pp. 633-638

[53] T. D. Phuc, M. Yoshino, A. Yamanaka and T. Yamamoto (2013) Fabrication of Gold Nano dots on Plastic Films for Bio-sensing, *Procedia CIRP* **5**, pp.47-52

[54] M. Yoshino, T. D. Phuc and T. Yamamoto, (2013) High throughput manufacturing process of a nano dot array on a plastic film, Proceeding of Conference of the Japan Society for Precision Engineering 2013, (JSPE 2013).

[55] Eustis S. and El-Sayed M. A. (2006) Why Gold Nanoparticles Are More Precious than Pretty Gold: Noble Metal Surface Plasmon Resonance and Its Enhancement of the Radiative and Nonradiative Properties of Nanocrystals of Different Shapes. *Chem.Soc. Rev.* **35**, pp. 209–217

[56] Pillai S. and Green M. A. (2010) Plasmonics for photovoltaic applications *Solar Energy Materials & Solar Cells* **94**, pp. 1481–1486

[57] Katherine A. W. and Van Duyne, R. P. (2007) Localized Surface Plasmon Resonance Spectroscopy and Sensing, *Annual Review of Physical Chemistry* **58**, pp. 267-297

[58] Sagle L. B., Ruvuna L. K., Ruemmele J. A. and Van Duyne R. P (2011) Advances in localized surface plasmon resonance spectroscopy biosensing, *Nanomedicine* **6** (8), pp.1447–1462

[59] Jeffrey N. A., Hall W. P., Lyandres O., Shah N. C., Jing Z. and Van Duyne R. P. (2008) Biosensing with plasmonic nanosensors *Nature Materials* **7** (6), pp. 442-453

[60] Hu M., Novo C., Funston A., Wang H. N., Staleva H., Zou S. L., Mulvaney P., Xia Y. N. and Hartland G. V. (2008) Dark-field microscopy studies of single metal nanoparticles: understanding the factors that influence the linewidth of the localized surface plasmon resonance, *J. Mater. Chem.* **18**, pp.1949-1960

[61] Yguerabide J. and Yguerabide E. E. (1998) Light-Scattering Submicroscopic Particles as Highly Fluorescent Analogs and Their Use as Tracer Labels in Clinical and Biological Applications I. and II. *Anal. Biochem.* **262**, pp. 137–176

[62] Huang X., El-Sayed I. H., Qian W. and El-Sayed M. A. (2006) Cancer Cell Imaging and Photothermal Therapy in the Near-Infrared Region by Using Gold Nanorods *J. Am. Chem. Soc.* **128**, pp. 2115–2120

[63] Huang X., Jain P. K, El-Sayed I. H. and El-Sayed M. A. (2007) Gold Nanoparticles: Interesting Optical Properties and Recent Applications in Cancer Diagnostics and Therapy *Nanomedicine* **2**, pp. 681–693

[64] O'Neal D. P., Hirsch L. R., Halas N. J., Payne J. D. and West J. L. (2004) Photo-thermal Tumor Ablation in Mice Using near Infrared-Absorbing Nanoparticles *Cancer Lett.* **209**, pp. 171–176

[65] Maria L., Maria M. G., Giuseppe V. B., Alberto S., Pio C. and Giovanni B., (2009) Enhanced absorption in Au nanoparticles/a-Si:H/c-Si heterojunction solar cells exploiting Au surface plasmon resonance *Solar Energy Materials & Solar Cells* **93**, pp. 1749–1754

[66] Nakayama K., Tanabe K. and Atwater H. A. (2008) Plasmonic nanoparticle enhanced light absorption in GaAs solar cells *Applied Physics Letters* **93**, 121904

[67] Wen L., Xiaodong W., Yueqiang L., Zhaoxin G., Fuhua Y. and Jinmin L. (2011) Surface plasmon enhanced GaAs thin film solar cells *Solar Energy Materials & Solar Cells* **95**, pp.693–698

[68] Moulin E., Sukmanowski J., Schulte M., Gordijn A., Royer F. X. and Stiebig H. (2008) Thin-film silicon solar cells with integrated silver nanoparticles *Thin Solid Films* **516**, pp. 6813–6817

[69] https://www1.hgst.com/hdd/research/storage/pm/index.html

[70] Benjamin S. and Mashford *et al.* (2013) High-efficiency quantum-dot light-emitting devices with enhanced charge injection *Nature Photonics* **7**, pp. 407–412

[71] Singamaneni S., Bliznyuk V. N., Binek C. and Tsymbal E. Y. (2011) Magnetic nanoparticles: recent advances in synthesis, self-assembly and applications. *J. Mater. Chem.* **21**, pp. 16819–16845

[72] Bohren C. F. and Huffman D. R. (1983) Absorption and Scattering of Light by Small Particles *John Wiley and Sons: New York* pp. 530.

[73] Kelly K. L., Coronado E., Zhao L. L. and Schatz G. C. (2003) The Optical Properties of Metal Nanoparticles: The Influence of Size, Shape, and Dielectric Environment. *J. Phys. Chem. B* **107**, pp. 668–677

[74] Jain P. K., Lee K. S., El-Sayed I. H. and El-Sayed M. A. (2006) Calculated Absorption and Scattering Properties of Gold Nanoparticles of Different Size, Shape, and Composition: Applications in Biological Imaging and Biomedicine. *J. Phys. Chem. B* **110**, pp. 7238–7248.

[75] Chen H. J., Kou X. S., Yang Z., Ni W. H., and Wang J. F., (2008) Shape- and Size-Dependent Refractive Index Sensitivity of Gold Nanoparticles *Langmuir* **24**, pp.5233-5237

[76] Chen H. J., Shao L., Woo K. C., Ming T., Lin H. Q. and Wang J. F. (2009) Shape-Dependent Refractive Index Sensitivities of Gold Nanocrystals with the Same Plasmon Resonance Wavelength *J. Phys. Chem. C*, **113** (41), pp. 17691–17697

[77] Zhao J., Zhang X. Y., Yonzon C. R. Haes A. J. and Van Duyne R. P. (2006) Localized surface plasmon resonance biosensors *Nanomedicine* **1** (2), pp.219-228

[78] McFarland A. D. and Van Duyne R.P. (2003) Single silver nanoparicles as real-time optical sensors with zeptomole sensitivity. *Nano Lett.* **3**, pp.1057-1062

[79] Haes A. J. and Van Duyne R. P. (2003) Nanoscale optical biosensors based on localized surface plasmon resonance spectroscopy *Proceedings of SPIE* **5221** Plasmonics: Metallic Nanostructures and Their Optical Properties

[80] Lee S. W., Lee K. S, Ahn J., Lee J. J., Kim M. G. and Shin Y. B. (2011) Highly sensitive biosensing using arrays of plasmonic Au nanodisks realized by nanoimprint lithography *ACS Nano* **5**, pp. 897-904

[81] Larsson E. M., Alegret J., Kall M. and Sutherland D. S. (2007) Sensing characteristics of NIR localized surface plasmon resonances in gold nanorings for application as ultrasensitive biosensors. *Nano Lett.* **5**, pp.1256-1263

[82] Venkataramani A., Yeswanth L. R. and Guigen Z. (2006) Nanopillar array structures for enhancing biosensing performance *International Journal of Nanomedicine* **1**, pp.73–79

[83] Jain P. K. and El-Sayed M. A. (2007) Surface Plasmon Resonance Sensitivity of Metal Nanostructures: Physical Basis and Universal Scaling in Metal Nanoshells *J. Phys. Chem. C* **111**, pp. 17451–17454

[84] Sun Y. and Xia Y. (2002) Increased Sensitivity of Surface Plasmon Resonance of Gold Nanoshells Compared to That of Gold Solid Colloids in Response to Environmental Changes *Anal. Chem.* **74**, pp.5297-5305

[85] William J. G., Sarah A. S., Martin J. M., Andrea T., Peidong Y. and Jay T. G. (2009) A Nanocube Plasmonic Sensor for Molecular Binding on Membrane Surfaces *Nano Lett.* **9** (5), pp. 2077–2082

[86] Tobias K., Rajesh K., Zachary A. C., Mahmoud. A. M., Mostafa A. El-S. and Vladimir V. T. (2013) Silver Nanocube Aggregates in Cylindrical Pores for Higher Refractive Index Plasmonic Sensing *Part. Part. Syst. Charact.* WILEY-VCH Verlag GmbH & Co. KGaA, Weinheim 2013

[87] Lee K. S. and El-Sayed M. A. (2006) Gold and silver nanoparticles in sensing and imaging. *J. Phys. Chem. B* **110**, pp. 19220-19225

[88] Chung P. Y., Lin T. H., Schultz G., Batich C. and Jiang P. (2010) Nanopyramid surface plasmon resonance sensors *Appl. Phys. Lett.* **96**, 261108

[89] Dondapati S. K., Sau T. K., Hrelescu C., Klar T. A., Stefani F. D. and Feldmann J. (2010) Label-free biosensing based on single gold nanostars as plasmonic transducers *ACS Nano* **4**, pp. 6318-6322

[90] Rostislav B. and Jennifer S. S. P. (2007) Highly Tunable Infrared Extinction Properties of Gold Nanocrescents *Nano Lett.***7** (5), pp. 1113–1118

[91] Wang H., Brandl D. W., Le F., Nordlander P. and Halas N. J. (2006) Nanorice: A Hybrid Plasmonic Nanostructure *Nano Lett.* **6**, 827

[92] Yoo H. W., Jung J. M., Lee S. K. and Jung H. T. (2011) The fabrication of highly ordered silver nano dot patterns by platinum assisted nanoimprint lithography *Nanotechnology* **22**, 095304 (7pp)

[93] Jung M., El-Said W.A., Choi J. W. (2011) Fabrication of Gold Nano dot Arrays on a Transparent Substrate as a Nanobioplatform for Label-Free Visualization of Living Cells *Nanotechnology* **22**, pp. 235304

[94] Corrigan T. D., Guo S., Phaneuf R. J. and Szmacinski H. (2005) Enhanced Fluorescence from Periodic Arrays of Silver Nanoparticles *J. Fluoresc.* **15**, 777

[95] Billot L., Lamy L. C., Grimault A. S., Vial A., Barchiesi D., Bijeon J. L., Adam P. M. and Royer P. (2006) Surface enhanced Raman scattering on gold nanowire arrays: Evidence of strong multipolar surface plasmon resonance enhancement *Chemical Physics Letters* **422**, pp. 303–307

[96] Hong S., Nicolas G., Jérémy R., Marc L. C. and Timothée T. (2012) Optimized plasmonic nanostructures for improved sensing activities *Optics Express* **20** (19), pp. 21278-21290

[97] García-Vidal F. J. and Pendry J. B. (1996) Collective Theory for Surface Enhanced Raman Scattering *Phys. Rev. Lett.* **77**, pp. 1163–1166

[98] Tian Z. Q., Ren B. and Wu D. Y. (2002) Surface-Enhanced Raman Scattering: From Noble to Transition Metals and from Rough Surfaces to Ordered Nanostructures *J. Phys. Chem. B* **106** (37), pp. 9463–9483

[99] Stewart M. E., Anderton C. R., Thompson L. B., Maria J., Gray S. K., Rogers J. A. and Nuzzo R. G. (2008) Nanostructured plasmonic sensors *Chem Rev.* **108** (2), pp. 494-521

[100] Otto A., Mrozek I., Grabhorn H. and Akemann W (1992) Surface-enhanced Raman scattering *J. Phys.: Condens, Matter* **4**, pp.1143-1212

[101] Steven R. E., William E. H. and Shuming N. (1998) Direct Observation of Size-Dependent Optical Enhancement in Single Metal Nanoparticles *J. Am. Chem. Soc.* **120** (31), pp. 8009–8010

[102] Xu H. X., Aizpurua J., Kall M. and Apell P. (2000) Electromagnetic contributions to single-molecule sensitivity in surface-enhanced Raman scattering *Phys. Rev. E* **62**, pp. 4318–4324

[103] Shuming N. and Steven R. E. (1997) Probing Single Molecules and Single Nanoparticles by Surface-Enhanced Raman Scattering *Science* **275** (5303), pp. 1102-1106

[104] K. Kneipp *et al.* (1997) Single Molecule Detection Using Surface-Enhanced Raman Scattering (SERS) *Phys. Rev. Lett.* **78**, 1667

[105] Xu H., Bjerneld E. J., Kall M. and Borjesson L. (1999) Spectroscopy of single hemoglobin molecules by surface enhanced Raman scattering *Phys. Rev. Lett.* **83** 4357-4360.

[106] Le Ru E. C., Meyer M. and Etchegoin P. G. (2006) Proof of single-molecule sensitivity in surface enhanced Raman scattering (SERS) by means of a two-analyte technique *J. Phys. Chem. B* **110**, pp. 1944-1948

[107] Dieringer J. A., Lettan II R. B., Scheidt K. A. and Van Duyne R. P. (2007) A frequency domain existence proof of single-molecule surface-enhanced Raman spectroscopy. *J. Am. Chem. Soc.* **129**, pp.16249-16256

[108] Eric L. R. and Pablo G. E. (2009) Principles of Surface-Enhanced Raman Spectroscopy: and related plasmonic effects *ISBN: 978-0-444-52779-0*

[109] Campion A., Ivanecky J. E., Child C. M. and Foster M. (1995) On the mechanism of chemical enhancement in surface-enhanced Raman scattering *J. Am. Chem. Soc.* **117**, pp.11807-11808

[110] Koo T. W. *et al*. (2004) Specific chemical effects on surface enhanced Raman spectroscopy for ultra-sensitive detection of biological molecules *Appl. Spectrosc.* **58**, pp.1401-1407

[111] Le Ru E. C., Blackie E., Meyer M. and Etchegoint P. G. (2007) Surface enhanced raman scattering enhancement factors: a comprehensive study, *Journal of Physical Chemistry C* **111** (37), pp. 13794–13803

[112] Stiles P. L., Dieringer J. A., Shah N. C. and Van Duyne R. P. (2008) Surface-Enhanced Raman Spectroscopy *Annu. Rev. Anal. Chem.* **1**, pp.601‑626

[113] Milton K. (1985) Effect of optical constants on calculated values of surface-enhanced Raman scattering *J. Opt. Soc. Am. B* **2** (8), pp. 1327-1329

[114] Jain P. K., Huang X. H., El-Sayed I. H. and El-Sayed M. A. (2008) Noble Metals on the Nanoscale: Optical and Photothermal Properties and Some Applications in Imaging, Sensing, Biology, and Medicine *Acc. Chem. Res.***41** (12), pp. 1578–1586

[115] Faulds K., Littleford R. E., Graham D., Dent G. and Smith W. E. (2004) Comparison of Surface-Enhanced Resonance Raman Scattering from Unaggregated and Aggregated Nanoparticles *Anal Chem* **76**, pp. 592-598

[116] Aroca R. F., Alvarez-Puebla R. A., Pieczonka N., Sanchez-Cortez S. and Ramos J. V. (2005) Surface-enhanced Raman scattering on colloidal nanostructures *Adv. Colloid Interface Sci.* **116**, pp. 45-61.

[117] Liang H. Y., Li Z. P., Wang W. Z., Wu Y. S. and Xu H. X. (2009) Highly Surface-roughened "Flower-like" Silver Nanoparticles for Extremely Sensitive Substrates of Surface-enhanced Raman Scattering *Adv. Mater.* **21**, pp.4614–4618

[118] Yang J. Y., Cheng H. W., Chen Y., Li Y., Lin C. H. and Lu K. L. (2011) Hydrothermally roughened surface-enhanced Raman scattering-active substrates with low background signals for chemical sensing application *J. Nanosci. Nanotechnol.* **11** (3), 2012-7.

[119] Gunnarsson L., Bjerneld E. J., Xu H., Petronis S., Kasemo B. and Käll M. (2001) Interparticle coupling effects in nanofabricated substrates for surface-enhanced Raman scattering *Appl. Phys. Lett* **78**, pp. 802–804

[120] Cecchini M. P., Turek V. A., Paget J., Kornyshev A. A. and Edel J. B. (2012) Self-assembled nanoparticle arrays for multiphase trace analyte detection *Nat. Mater.* **12**, pp.165–171

[121] Liu X. J., Zhao L. A., Shen H., Xu H. X. and Lu L. H. (2011) Ordered gold nanoparticle arrays as surface-enhanced Raman spectroscopy substrates for label-free detection of nitroexplosives *Talanta* **83**, pp.1023–1029

[122] Hatab N. A., Hsueh C. H., Gaddis A. L., Retterer S. T., Li J. H., Eres G., Zhang Z. Y. and Gu B. H. (2010) Free-Standing Optical Gold Bowtie Nanoantenna with Variable Gap Size for Enhanced Raman Spectroscopy *Nano Lett.* **10**, pp.4952–4955

[123] Wei H. and Xu H. X. (2013) Hot spots in different metal nanostructures for plasmon-enhanced Raman spectroscopy *Nanoscale* **5**, pp.10794-10805

[124] Li X. L., Zhang Y. Z., Shen Z. X. and Fan H. J. (2012) Highly Ordered Arrays of Particle-in-Bowl Plasmonic Nanostructures for Surface-Enhanced Raman Scattering *Small* **8** (16), pp. 2548–2554

[125] Wang J. et al. (2012) Silver nanostructure arrays abundant in sub-5 nm gaps as highly Raman-enhancing substrates *Applied Surface Science* **258**, pp. 3519– 3523

[126] Chang A. S. P. *et al.* (2011) Nanopillars array for surface enhanced Raman scattering *Proc. SPIE* **8024**, Advanced Environmental, Chemical, and Biological Sensing Technologies VIII, 80240I

[127] Kim K. H., Baek Y. K., Jeon H. J., Srinivasarao M. and Jung H. T. (2012) Cylindrical posts of Ag/SiO2/Au multi-segment layer patterns for highly efficient surface enhanced Raman scattering *Nanotechnology* **23**, 315302

[128] Yue W. S., Wang Z. H., Yang Y., Chen L. Q., Syed A., Wong K. C. and Wang X. B. (2012) Electron-beam lithography of gold nanostructures for surface-enhanced Raman scattering *J. Micromech. Microeng.* **22**, 125007 (9pp)

[129] Jeon T. Y., Park S. G., Lee S. Y., Jeon H. C. and Yang S. M. (2013) Shape Control of Ag Nanostructures for Practical SERS Substrates *Appl. Mater. Interfaces* **5**, pp. 243−248

[130] Jain P. K., Lee K. S., El-Sayed I. H. and El-Sayed M. A. (2006) Calculated Absorption and Scattering Properties of Gold Nanoparticles of Different Size, Shape, and Composition: Applications in Biological Imaging and Biomedicine *J. Phys. Chem. B* **110** (14), pp. 7238–7248

[131] Catchpole K. R. and Polman A. (2008) Design principles for particle plasmon enhanced solar cells *Appl. Phys. Lett.* **93**, 191113

[132] Bohren C. F. & Huffman D. R. (2008) *Absorption and Scattering of Light by Small Particles* (Wiley, 2008).

[133] Sönnichsen C., Franzl T., Wilk T., von Plessen G., Feldmann J., Wilson O. and Mulvaney P. (2002) Drastic Reduction of Plasmon Damping in Gold Nanorods *Phys. Rev. Lett.* **88**, 077402

[134] *http://www.amolf.nl/nanophotovoltaics*

[135] *http://docs.lumerical.com/en/fdtd/solar_plasmonic.html*

[136] Atwater H. A. and Polman A. (2010) Plasmonics for improved photovoltaic devices *Nature Materials* **9**, pp.205–213

[137] Adamovic N. and Schmid U. (2011) Potential of plasmonics in photovoltaic solar cells *e & i Elektrotechnik und Informationstechnik* **128** (10), pp. 342-347

[138] Stratakis E. and Kymakis E. (2013) Nanoparticle-based plasmonic organic photovoltaic devices *Materials Today* **16** (4), pp. 133‑146

[139] David D., Philippe T., Ludovic E., Florent M., Jean J. S., Francois F. and Gerard M. (2009) Improving light absorption in organic solar cells by plasmonic contribution *Solar Energy Materials & Solar Cells* **93**, pp.1377–1382

[140] Spyropoulos G. D., Stylianakis M., Stratakis E. and Kymakis E. (2010) Plasmonic organic photovoltaics doped with metal nanoparticles *Photonics and Nanostructures–Fundamentals and Applications* **9**, pp. 184–189

[141] *https://www1.hitachigst.com/hdd/research/storage/pm/index.html*

[142] Yang X. M., Xiao S. G., Wu W., Xu Y., Mountfield K. and Rottmayer R. (2007) Challenges in 1 Teradot/in^2 dot patterning using electron beam lithography for bit-patterned media *Journal of Vacuum Science & Technology B* **25**, pp. 2202-2209

[143] Rath S., Heilig M., Port H. and Wrachtrup J. (2007) Periodic Organic Nano dot Patterns for Optical Memory *Nano Lett.* **7**, (12), pp. 3845-3848

[144] Chen X. Z., Li Q., Chen X., Guo X., Ge H. X. , Liu Y. and Shen Q. D. (2013) Nano-Imprinted Ferroelectric Polymer Nano dot Arrays for High Density Data Storage *Adv. Funct. Mater.* **23**, pp.3124–3129

[145] Joannopoulos J. D., Villeneuve P. R. and Fan S. (1997) Photonic crystals: putting a new twist on light *Nature* **386**, pp. 143-149

[146] Chris Mack (2007) Fundamental Principles of Optical Lithography: The Science of Microfabrication. © 2007 John Wiley & Sons, Ltd. ISBN: 978-0-470-01893-4

[147] Scotten W. J. (2000) Photolithography (a chapter for inclusion in a text book on silicon integrated circuit process technology). IC Knowledge LLC

[148] Waser R. (2012) Nanoelectronics and Information Technology: Advanced Electronic Materials and Novel Devices, Chapter 9, ISBN: 978-3-527-40927-3

[149] Technology Backgrounder: Immersion lithography (2003) IC knowledge.com

[150] Chaudhari A. and Musa Ibrahim M. (2011) Electron Beam and X-Ray Lithography, ENEE 416

[151] http://www.ritsumei.ac.jp/~sugiyama/English/research.htm

[152] Alongkorn P. and Werayut S. (2012) Review on Micro- and Nanolithography Techniques and their Applications *Engineering Journal* **16** (1)

[153] Manfrinato V. R., Zhang L. H., Su D., Duan H. G., Hobbs R. G., Stach E. A. and Berggren K. K. (2013) Resolution Limits of Electron-Beam Lithography toward the Atomic Scale *Nano Lett.* **13**, pp. 1555−1558

[154] Landobasa Y. M. T., Liliana T., Dao H. Z., Qing Z. and Qihua X. (2013) Deep subwavelength fourfold rotationally symmetric split-ring-resonator metamaterials for highly sensitive and robust biosensing platform *SCIENTIFIC REPORTS* **3**, 2437

[155] Fabrice Donatini and Le Si Dang (2010) A single-step electron beam lithography of buried nanostructures using cathodoluminescence imaging and low temperature *Nanotechnology* **21**, 375303 (4pp)

[156] Sergey G., Vitaliy A. G., Joan V. C. and Christian D. (2010) Direct e-beam writing of dense and high aspect ratio nanostructures in thick layers of PMMA for electroplating *Nanotechnology* **21**, 295303 (8pp)

[157] http://m.jeolusa.com/PRODUCTS/ElectronOptics/ScanningElectronMicroscopesSEM/SEM-FIB/JIB-4501MultiBeam/tabid/1132/Default.aspx

[158] Reyntjens S, Puers R (2001) A review of focused ion beam applications in microsystem technology. *J. Micromech. Microeng.* **11**, pp.287-300

[159] Kim C. S., S. H. Ahn, Jang D. Y. (2008) Review: Developments in micro/nanoscale fabrication by focused ion beams *Vacuum* **86**, 1014e1035

[160] Bharat Bhushan B. (2010) Springer Handbook of Nanotechnology, *Springer-Verlag Berlin Heidelberg 2010*

[161] Dickreuter S., Gleixner J., Kolloch A., Boneberg J., Scheer E. and Leiderer P. (2013) Mapping of plasmonic resonances in nanotriangles Beilstein J. Nanotechnol. 4, pp.588–602.

[162] Lee S. H., Bantz K. C., Lindquist N. C., Sang-Hyun Oh S. H. and Haynes C. L. (2009) Self-Assembled Plasmonic Nanohole Arrays Langmuir 25 (23), pp. 13685–13693

[163] Yu Q., Huang H. W., Chen R., Yang H. S., Peng X. S. and Ye Z. Z. (2011) Filtration-assembling colloidal crystal templates for ordered macroporous nanoparticle films J. Mater. Chem., 2011, 21, 18089–18094

[164] Burgos N., Paulis M. and Montes M. (2003) Preparation of Al2O3/Al monoliths by anodisation of aluminium as structured catalytic supports. *J. Mater. Chem.*, **13**, pp. 1458–1467

[165] Gerrard E. J. P., Nurshahidah A. and Derek F. (2011) Progress in Nano-Engineered Anodic Aluminum Oxide Membrane Development *Materials* **4**, pp.487-526

[166] Raquel P., Pilar F., Eugenia M. F., Josep F. B., Josep P. and Lluis F. M. (2011) F8BT nanopillars from porous anodic alumina *Phys. Status Solidi A* **208** (6), pp. 1422–1425

[167] Nagaura T., Takeuchi F., Yamauchi Y., Wada K., Inoue S. (2008) Fabrication of ordered Ni nanocones using a porous anodic alumina template Electrochemistry Communications 10 681–685

[168] Binnig G. and Rohrer H. (1982) Scanning tunnelling microscopy. *Helv. Phys. Acta,* **55** (6), pp. 26–735.

[169] Binnig G., Quate C. F. and Gerber C. (1986) Atomic force microscope *Phys. Rev. Lett.*, **56** (9), pp. 930.

[170] Jung B., Jo W., Gwon M. J., Lee E. and Kim D. W. (2010) Scanning probe lithography for fabrication of Ti metal nano dot arrays *Ultramicroscopy* **110**, pp. 737–740

[171] Lee W. K., Chen S. H., Chilkoti A. and Zauscher S. (2007) Fabrication of Gold Nanowires by Electric-Field-Induced Scanning Probe Lithography and In Situ Chemical Development small 3 (2), pp. 249 – 254

[172] Alexander B. T., Lev C., Tanya K., Tatyana A. B., Gilad H., Alexander V. and Israel R. (2011) Tunable Localized Plasmon Transducers Prepared by Thermal Dewetting of Percolated Evaporated Gold Films *J. Phys. Chem. C,* **115** (50), pp. 24642-24652

[173] Sun H. T., Yu M. P., Wang G. K., Sun X. and Lian J. (2012) Temperature-Dependent Morphology Evolution and Surface Plasmon Absorption of Ultrathin Gold Island Films *J. Phys. Chem. C* **116** (16), pp. 9000–9008

[174] Anantatmula R. P., Johnson A. A., Gupta S. P. and Horylev R. J. (1975) The gold-silicon phase diagram *Journal of Electronic Materials* **4** (3), pp. 445-463

[175] Okamoto H., and Massalski T. B. (1983) The Au−Si (Gold-Silicon) system, *Bulletin of Alloy Phase Diagrams* **4** (2), pp. 190-198

[176] Xun S., Song X., Wang L., Grass M. E., Liu Z., Battaglia V. S. and Liu G. (2011) The Effects of Native Oxide Surface Layer on the Electrochemical Performance of Si Nanoparticle-Based Electrodes *Journal of The Electrochemical Society* **158** (12), pp. 1260-1266

[177] Miura T., Niwano M., Shoji D. and Miyamoto N. (1996) Kinetics of oxidation on hydrogen-terminated Si(100) and (111) surfaces stored in air *J. Appl. Phys.* **79** , 4373

[178] Jaccodine R. J. (1963) Surface Energy of Germanium and Silicon *J. Electrochem. Soc.* **110** (6), pp. 524-527

[179] Shchipalov Y. K. (2000) Surface Energy of Crystalline and Vitreous Silica *Glass and Ceramics* **57** (11-12), pp. 8-11

[180] Tanya K., Devora H., Mila G., Alexander V. and Israel R. (2009) Morphology and Refractive Index Sensitivity of Gold Island Films *Chem. Mater.* **21** (24), pp. 5875-5885

[181] Kim B., Tripp S. L. and Wei A. (2001) Self-Organization of Large Gold Nanoparticle Arrays *J. Am. Chem. Soc.***123** (32), pp. 7955–7956

[182] Zhang X. M., Zhang J. H., Wang H., Hao Y.D., Zhang X., Wang T. Q., Wang Y. N., Zhao R., Zhang H. and Yang B. (2010) Thermal-Induced Surface Plasmon Band Shift of Gold Nanoparticle Monolayer: Morphology and Refractive Index Sensitivity *Nanotechnology* **21**, 465702, pp. 1-11

[183] Yoshino M, Osawa H and Yamanaka A 2011 Rapid fabrication of an ordered nano-dot array by the combination of nano-plastic forming and annealing methods *J. Micromech. Microeng.* **21** 125017

[184] Yoshino M, Aravindan S, Kinouchi Y and Matsumura T 2008 Critical depth of hard brittle materials on nano plastic forming *J. Adv. Mech. Des. Syst. Manuf.* **2** 59–70

[185] Li Z., Yoshino M. and Yamanaka A. (2012) Fabrication of three dimensional ordered nano dot array structures by a thermal dewetting method *Nanotechnology* **23**, 485303

[186] Phuc T. D., Yoshino M., Yamanaka A. and Yamamoto T. (2014) Effects of Morphology of Nanodots on Localized Surface Plasmon Resonance Property *Int. J. of Automation Technology* **8** (1), pp. 74-82

APPENDIX A

Supplementary data

Diameter of nano dot array after annealing (nm), gold film thickness is 8 nm					
	600°C	**700°C**	**800°C**	**900°C**	**1000°C**
5 min	41.6	41.1	36.5	34.2	35.3
10 min	42.6	41.1	35.9	32.8	34.0
15 min	42.7	40.4	35.0	33.4	34.1
20 min	42.1	39.4	34.3	32.3	32.0
30 min	41.6	41.0	35.3	31.8	33.0
60 min	42.7	39.1	34.6	32.6	34.0
90 min	40.9	39.7	35.0	31.4	33.0
120 min	40.2	39.0	34.8	31.2	32.0
Standard deviation of dot diameter					
	600°C	**700°C**	**800°C**	**900°C**	**1000°C**
5 min	18.2	20.3	18.1	13.8	15.2
10 min	19.1	20.3	18.7	12.2	16.3
15 min	18.6	19.8	18.5	12.9	18.5
20 min	16.8	18.5	17.0	11.8	18.0
30 min	23.6	20.5	23.4	11.3	11.7
60 min	21.9	19.0	21.6	11.3	12.7
90 min	23.8	19.7	23.3	10.9	15.3
120 min	19.8	19.2	19.6	10.5	17.1

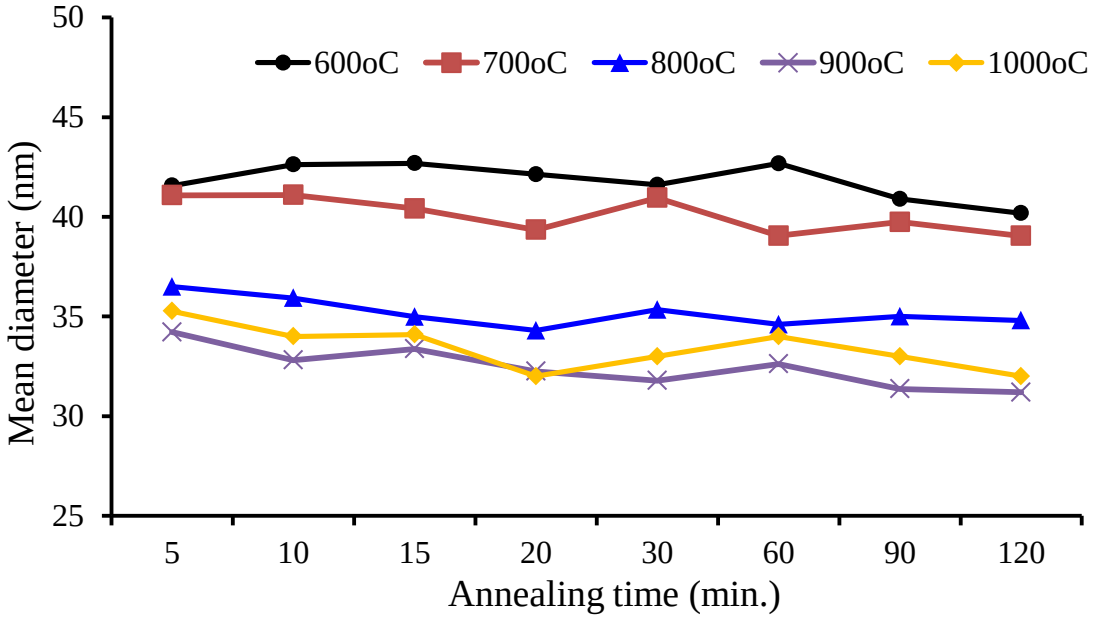

Figure A1: Variation of mean diameter of nano dots for different annealing conditions

APPENDIX B

List of Publications

Journal papers

1. T. D. Phuc, A. Yamanaka and M. Yoshino, "High Throughput Method to Fabricate Ordered Nano dot array on Various Plastic Films," Journal of Key Engineering Materials, Vol.523-524, pp. 633-638, (2012).
2. T. D. Phuc, M. Yoshino, A. Yamanaka and T. Yamamoto, "Effects of Morphology of Nanodots on Localized Surface Plasmon Resonance Property", Int. J. of Automation Technology, Vol .8, No. 1, pp. 74-82, (2014).
3. T. D. Phuc, M. Terano and M. Yoshino, "Fabrication of an ordered nano dot array by thermal dewetting on a patterned substrate", Manufacturing Letter, (2014) (Accepted for publication).

Conference papers

1. T. D. Phuc, A. Yamanaka and M. Yoshino, "Study on Nano Dots Formation by Thermal Dewetting and Transfer to Plastic Films," Proceeding of Conference of the Japan Society for Precision Engineering 2012, (JSPE 2012).
2. T. D. Phuc, M. Yoshino, A. Yamanaka and T. Yamamoto, "Fabrication of Gold Nano dots on Plastic Films for Bio-sensing", Procedia CIRP, Vol.5, pp.47-52, 2013.
3. T. D. Phuc, A. Yamanaka and M. Yoshino, "Novel manufacturing process with high throughput to fabricate ordered metal nano dot array on various plastic films" Proceeding of The 5th AUN/SEED-Net Regional Conference in Mechanical and Aerospace Technology, Bangkok, Thailand.
4. M. Yoshino, T. D. Phuc and T. Yamamoto, "High throughput manufacturing process of a nano dot array on a plastic film," Proceeding of Conference of the Japan Society for Precision Engineering 2013, (JSPE 2013).

Patent

1. T. D. Phuc, A. Yamanaka and M. Yoshino (2012) New Process for Fabrication of an Ordered Gold Nano Dot Array on a Plastic Film. Japan 2011-278 (11T232), (pending).